Budapest Neutron Centre
Centre for Energy Research

Neutron Radiography and Tomography

László Szentmiklósi, Zoltán Kis
Central European Training School on Neutron Techniques, Budapest, Hungary

Budapest Neutron Centre, Budapest, Hungary
szentm@bnc.hu

Nuclear Analysis and Radiography Department
Centre for Energy Research, Budapest, Hungary
szentmiklosi.laszlo@ek-cer.hu

BNC
Budapest Neutron Centre

BUDAPEST RESEARCH REACTOR
1959 2019
60 YEARS OF RESEARCH & INNOVATION

Neutron-matter interactions

	Particle		*Wave*
Charge	: 0		
Mass	$m = 1{,}67 \cdot 10^{-24}$ g		
"Radius"	$r_0 = 6 \cdot 10^{-16}$ m	Wave length	$\lambda = \frac{h}{m \cdot v}$
Spin	: 1/2	Wave number	$k = \frac{2\pi}{\lambda}$
Magn. Moment	$\mu = -1{,}9\,\mu_N$		
Momentum	$\vec{p} = m \cdot \vec{v}$	Momentum	$\vec{p} = \frac{h \cdot \vec{k}}{2\pi} = \hbar \cdot \vec{k}$
Energy	$E = \frac{m}{2} v^2$	Energy	$E = \frac{h^2}{2m\lambda^2} = \frac{\hbar^2 \cdot k^2}{2m}$
(v = velocity)		(h = Plank´s constant)	

$$E = k_B T = \frac{mv^2}{2} = \frac{\hbar^2 k^2}{2m}$$

Neutrons interact with the condensed matter:

- Induce nuclear reactions (capture, fission)
- Scattering (elastic, inelastic)
- Reflection
- Unaffected neutrons pass through the sample

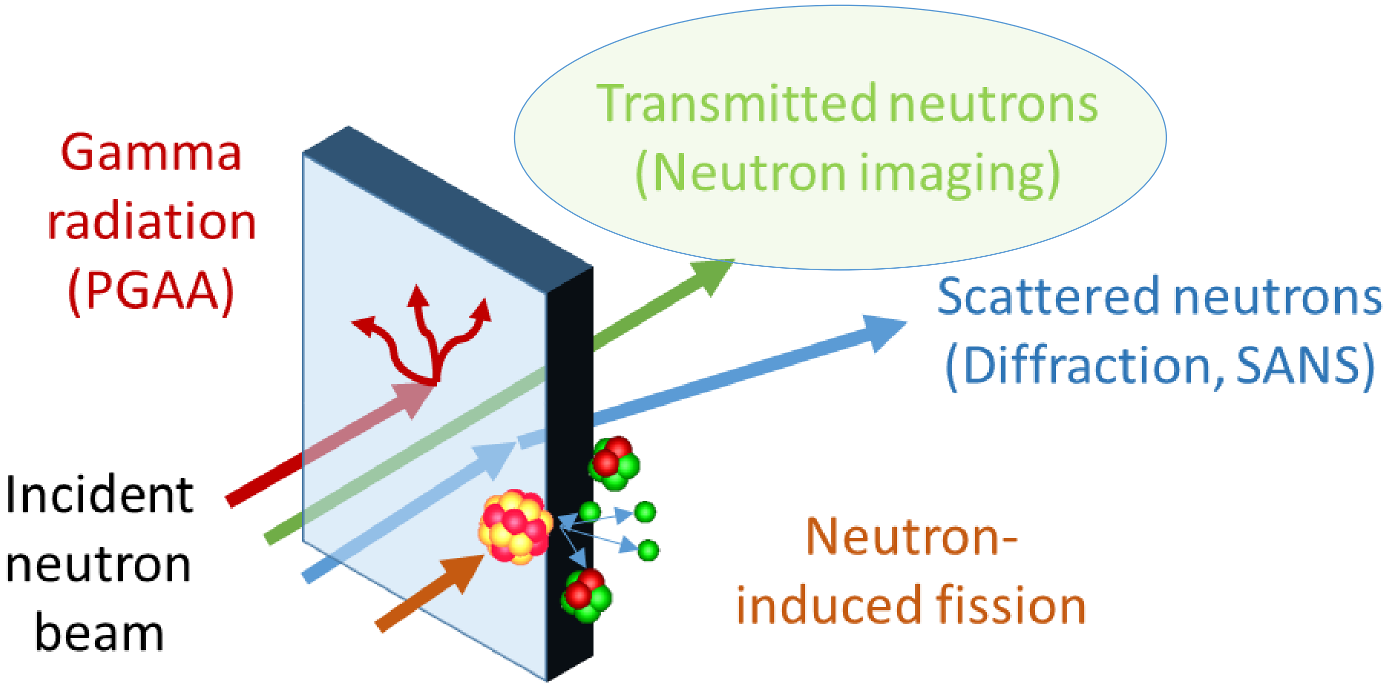

Principle of the radiography

- Radiography = „Draw with radiation”
- Radiography is a direct imaging technique, where the 2D visual representation of an object is obtained nondestructively by detecting the modification of an incident beam as it passes through the matter
- **Transforms invisible radiation into visible images**

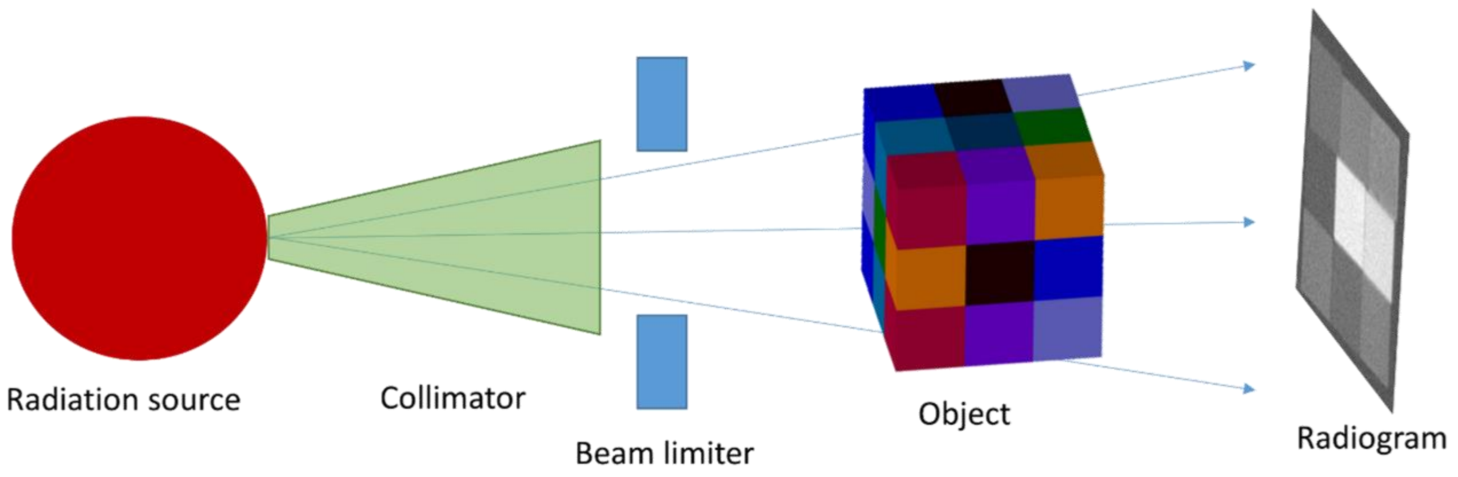

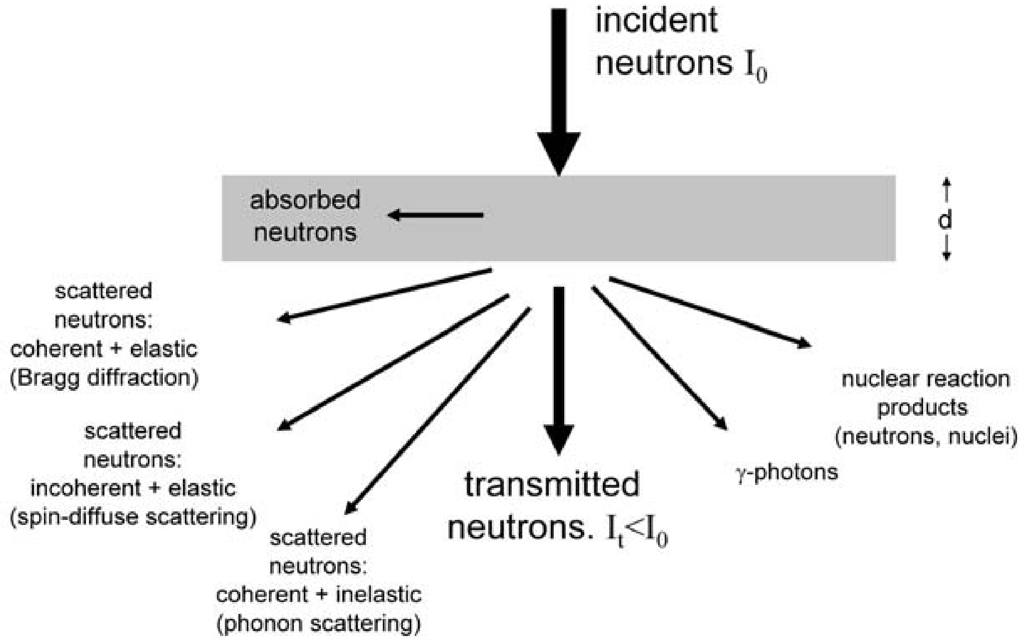

Attenuation (μ) of the neutron beam depends on:

- absorption (σ_{abs})
- scattering (σ_s)

$$\mu^{tot} = N_V(\sigma_{abs} + \sigma_s) = N_V \sigma^{tot}$$

N_V : number of atoms per unit volume

Physics behind the radiography

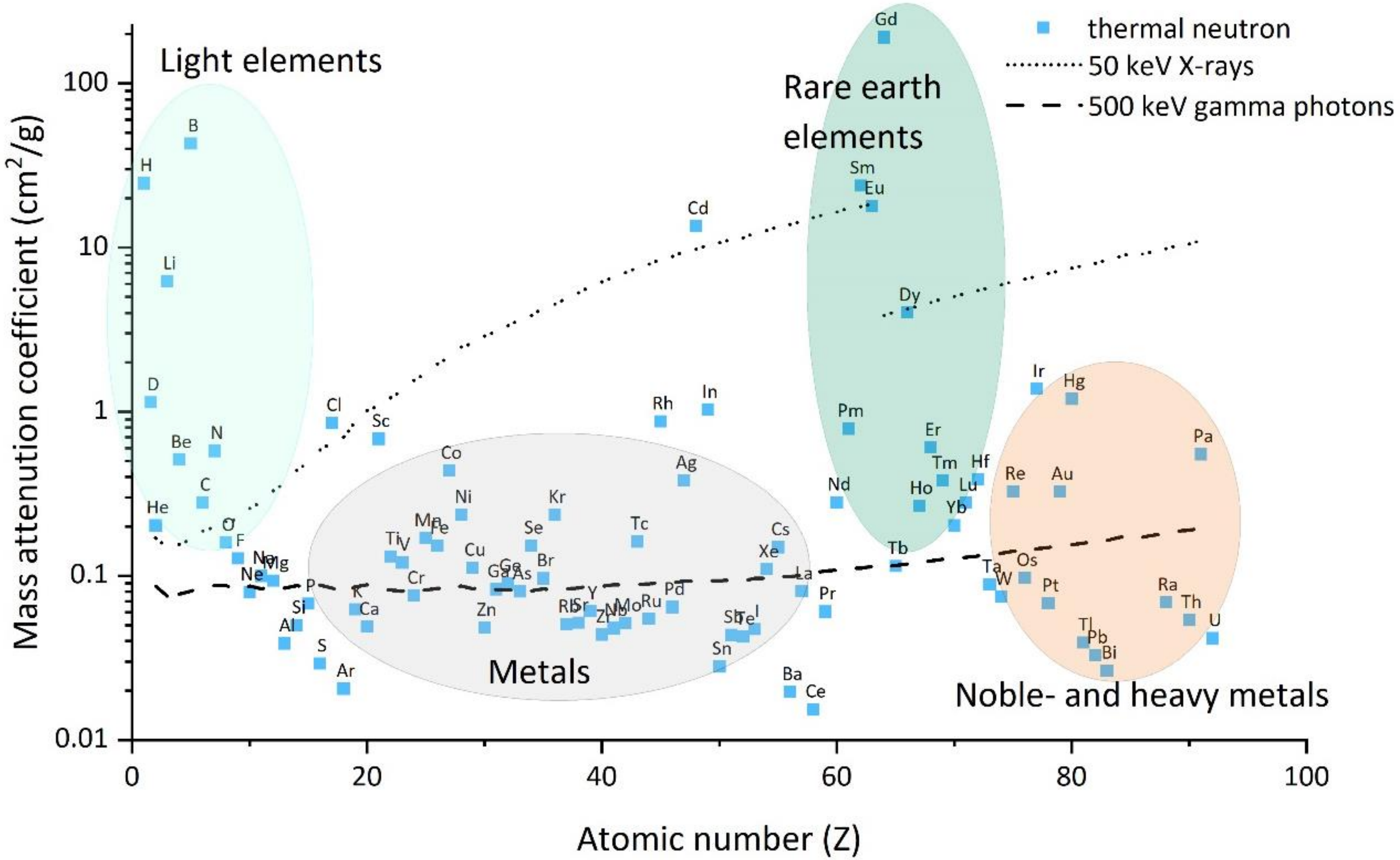

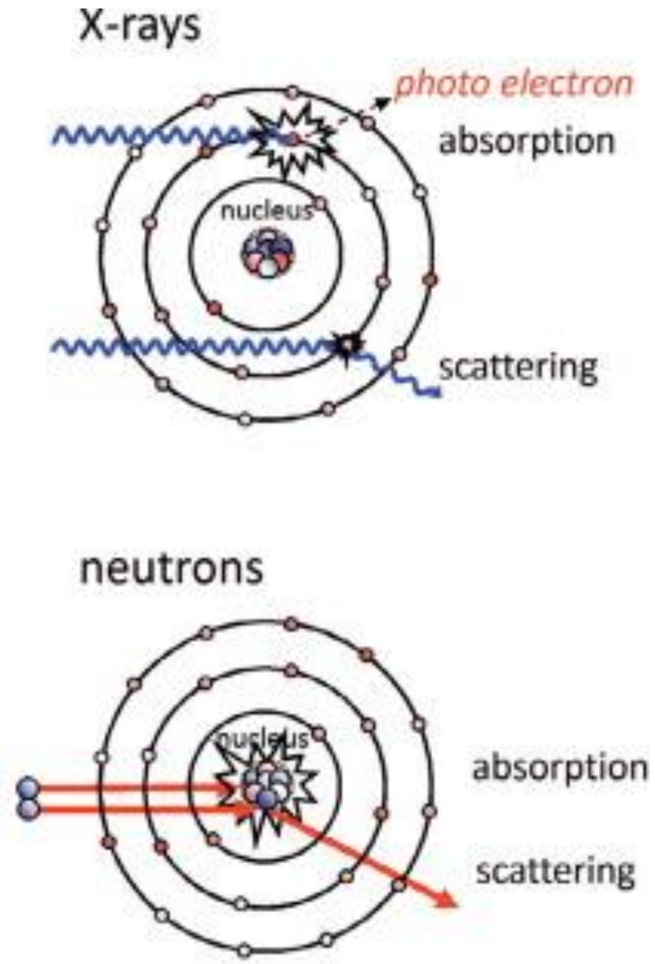

Attenuation coefficient (note the logarithmic scale) of elements for thermal neutrons (separate dots - black), for 1 MeV gamma-ray (dotted line), for 150 kV X-ray (solid line) and for 60 kV X-ray (dashed line)

Contrasts

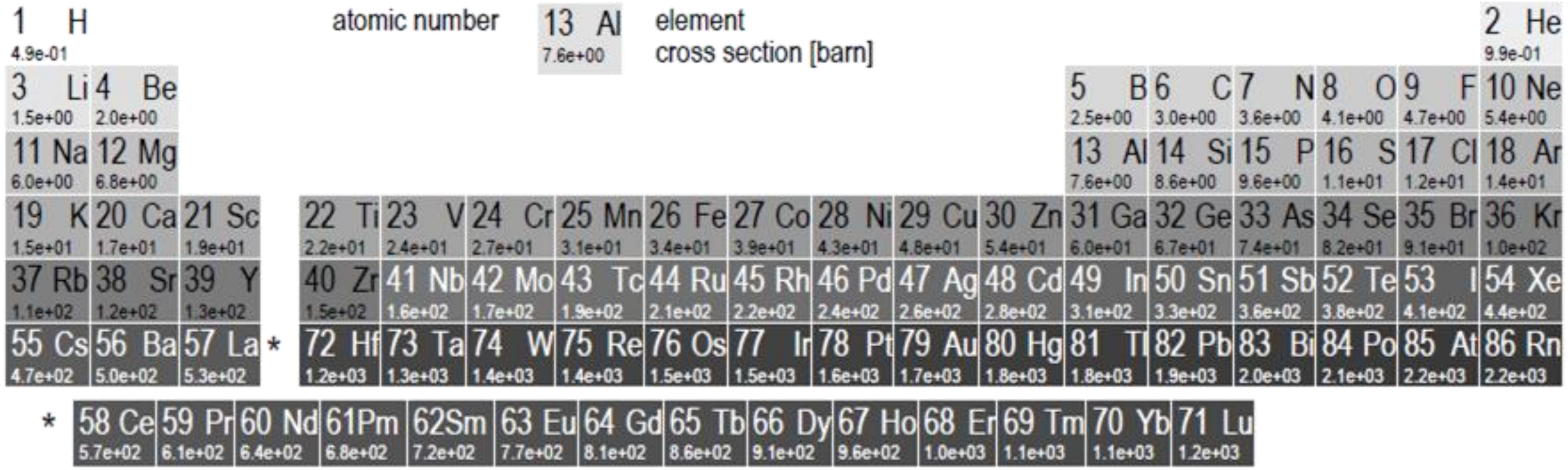

Total microscopic cross section σ [barn] for photons with an energy of 100 keV (the interaction takes place with the electron shell)

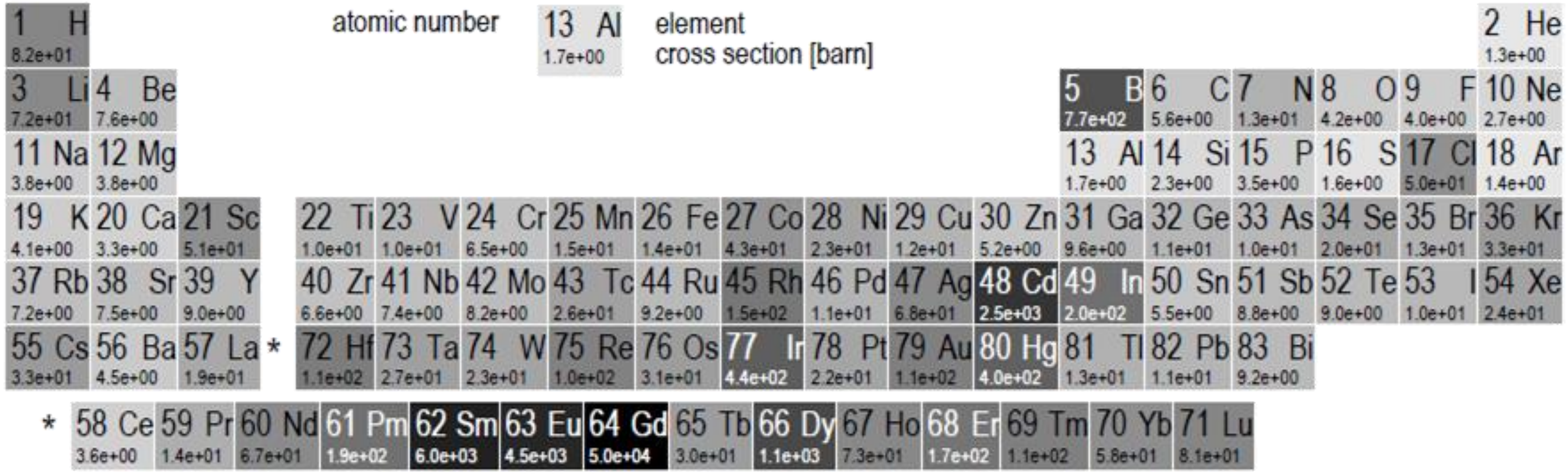

Total microscopic cross section σ [barn] for neutrons with an energy of 25 meV (the interaction takes place with the atomic nucleus)

Phenomenological formalism

- Mass attenuation coefficient (m^2/kg):

  $$\mu_m = \mu/\rho,$$

  ρ: sample density (kg/m^3),

  μ: linear attenuation coefficient (1/m)

  It has the same value for the solid, liquid or gaseous state of a given element.

- Mass-thickness (kg/m^2):

  $$d_m = \rho \times d$$

  d: sample thickness (m)

- Beer-Lambert law

  valid for a point detector and a well-collimated, thin pencil beam without buildup effect

$$\frac{I_{tr}}{I_0} = \exp\left(-\mu^{tot} \cdot d\right) = \exp\left(-\mu_m^{tot} \cdot d_m\right)$$

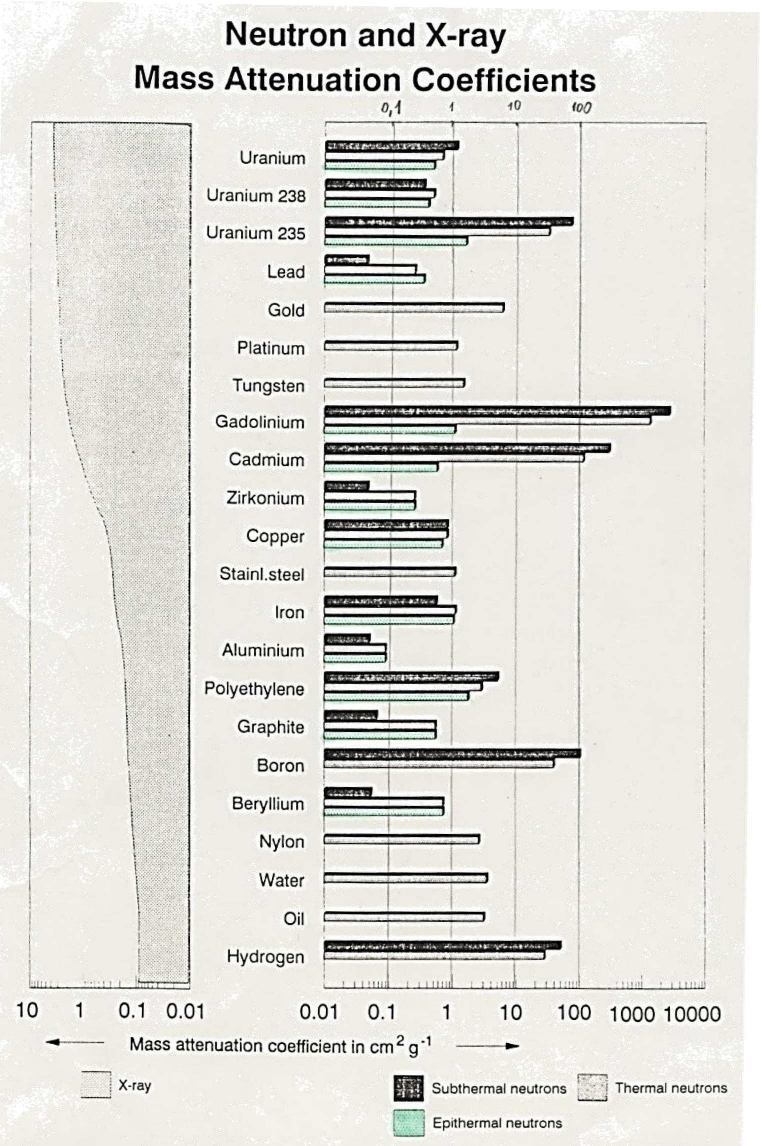

Figure 5.3. Mass attenuation coefficients for X-rays and neutrons of different energies (e.g. epithermal, thermal and subthermal) [32]

Chronology of neutron radiography

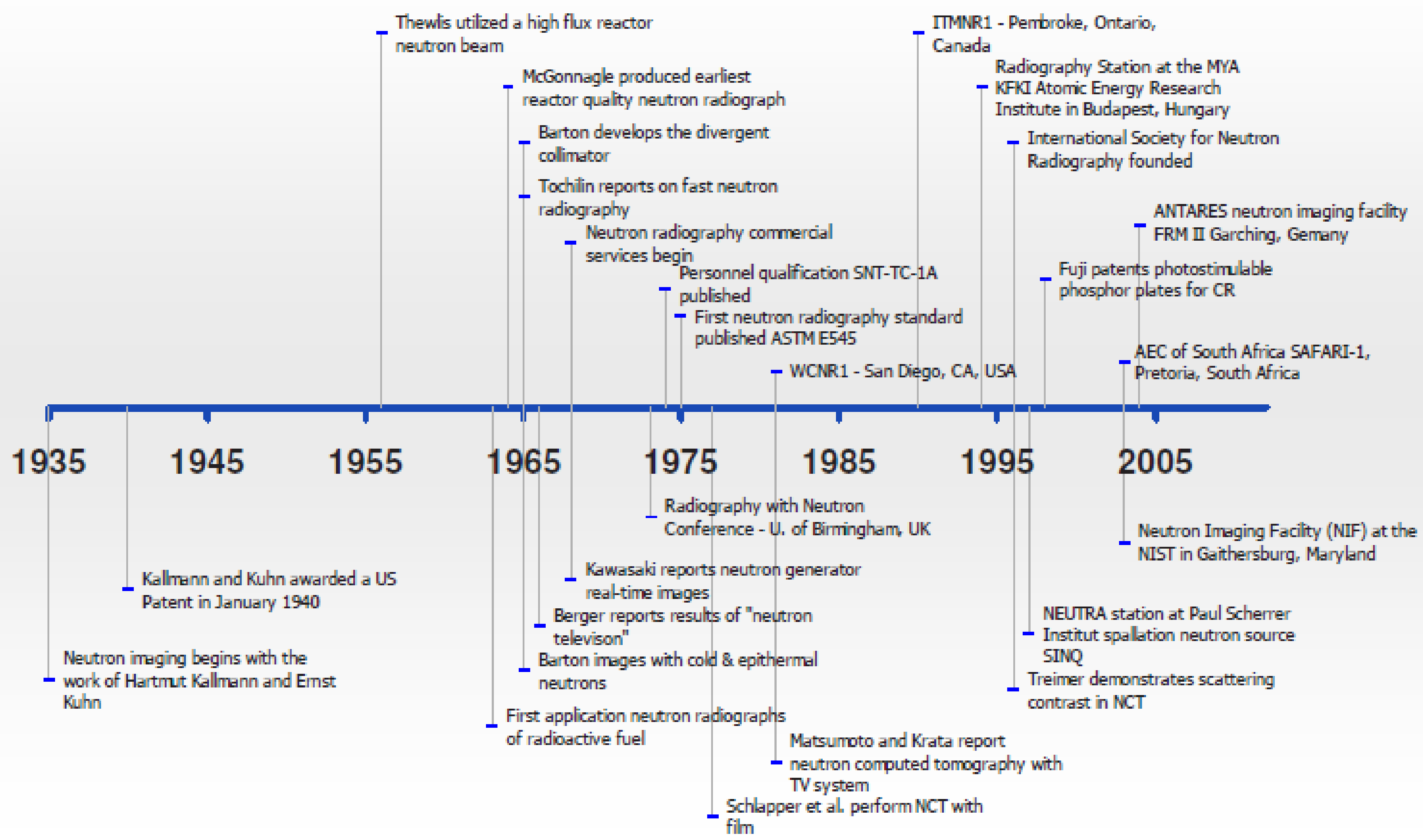

J.S. Brenizer / Physics Procedia 43 (2013) 10 – 20

Classification of neutrons

Neutrons	Energy range	Wavelength [Å]	Velocity [m/s]
ultra cold	≤ 300 neV	≥ 500	≤ 8
very cold	300 neV - 0.12 meV	52.2 – 26.1	7.5 – 152
cold	**0.12 meV - 12 meV**	**26.1 – 2.6**	**152 – 1515**
thermal	**12 meV - 100 meV**	**2.6 - 0.9**	**1515 - 4374**
epithermal	100 meV - 1eV	0.9 - 0.28	4374 - 13.8 10^3
intermediate	1eV - 0.8MeV		
fast	> 0.8MeV		

Neutron sources for imaging

- Research reactor (ILL, FRM-II, BNC, ...)
- Spallation sources (ISIS, SINQ, SNS,...)
- Radioactive nuclides (Cf, Ra-Be, Sb-Be)
- Accelerator sources (D-D, D-T reactions)

Source type	*nuclear reactor*	*neutron generator*	*spallation source*	*radio isotope*
Reaction	fission	D-T fusion	spallation by protons	gamma-n-reaction
used material	U-235	deuterium, tritium	high mass nuclides	Sb, Be
gain: primary neutron intensity [1/s]	1.00E+16	4.00E+11	1.00E+15	1.00E+08
beam intensity[cm-2 s-1]	10^6 to 10^9	10^5	10^6 to n*10^7	10^3
neutron energy	fast, thermal and cold	fast, thermal	fast, thermal and cold	24 keV, thermal
limitation of use	burn up	life time tube	target life time	half life Sb-124
typical operation cycle	1 month	1000 h	1 year	0,5 year
costs of the facility	high	medium	very high	low

Components of a neutron imaging facility

1. Source 2. Moderator 3. Cold source (optional)
4. Collimator 5. Radiation filters 6. Flight tube
7. Sample manipulator 8. Detector 9. Shielding+beam dump
10. Door 11. Shutters 12. Beam Limiters

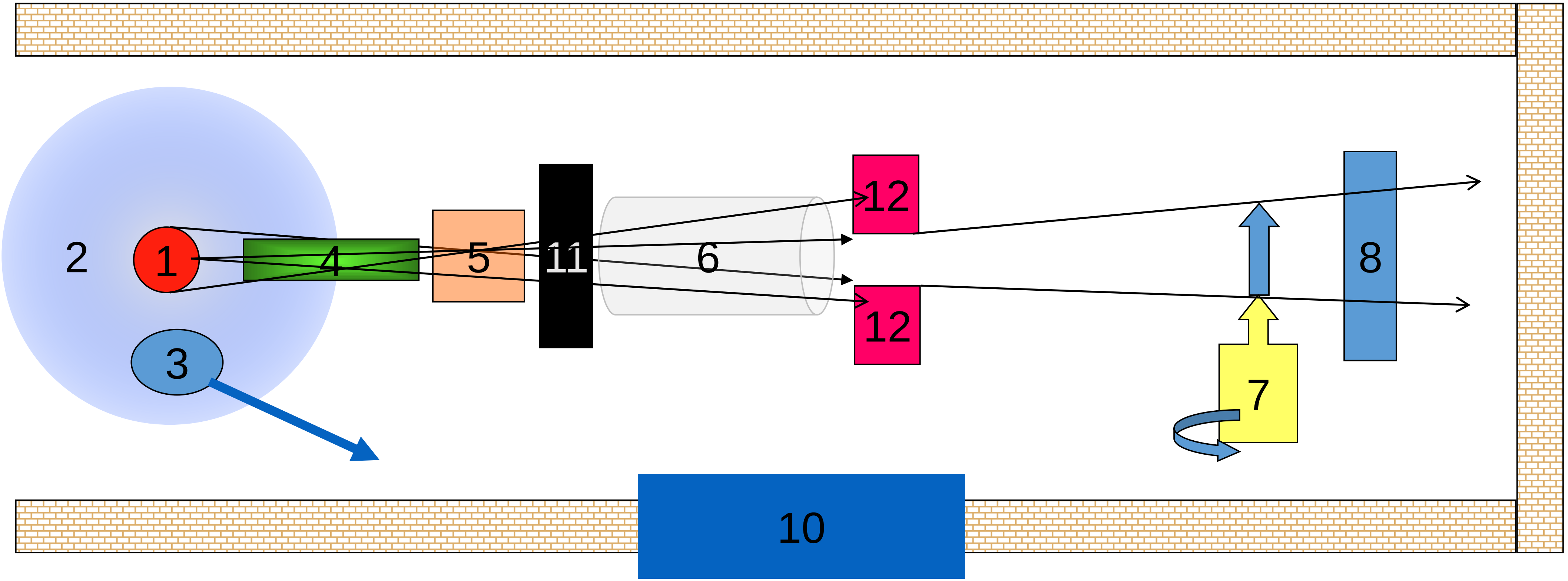

Geometry of the collimation

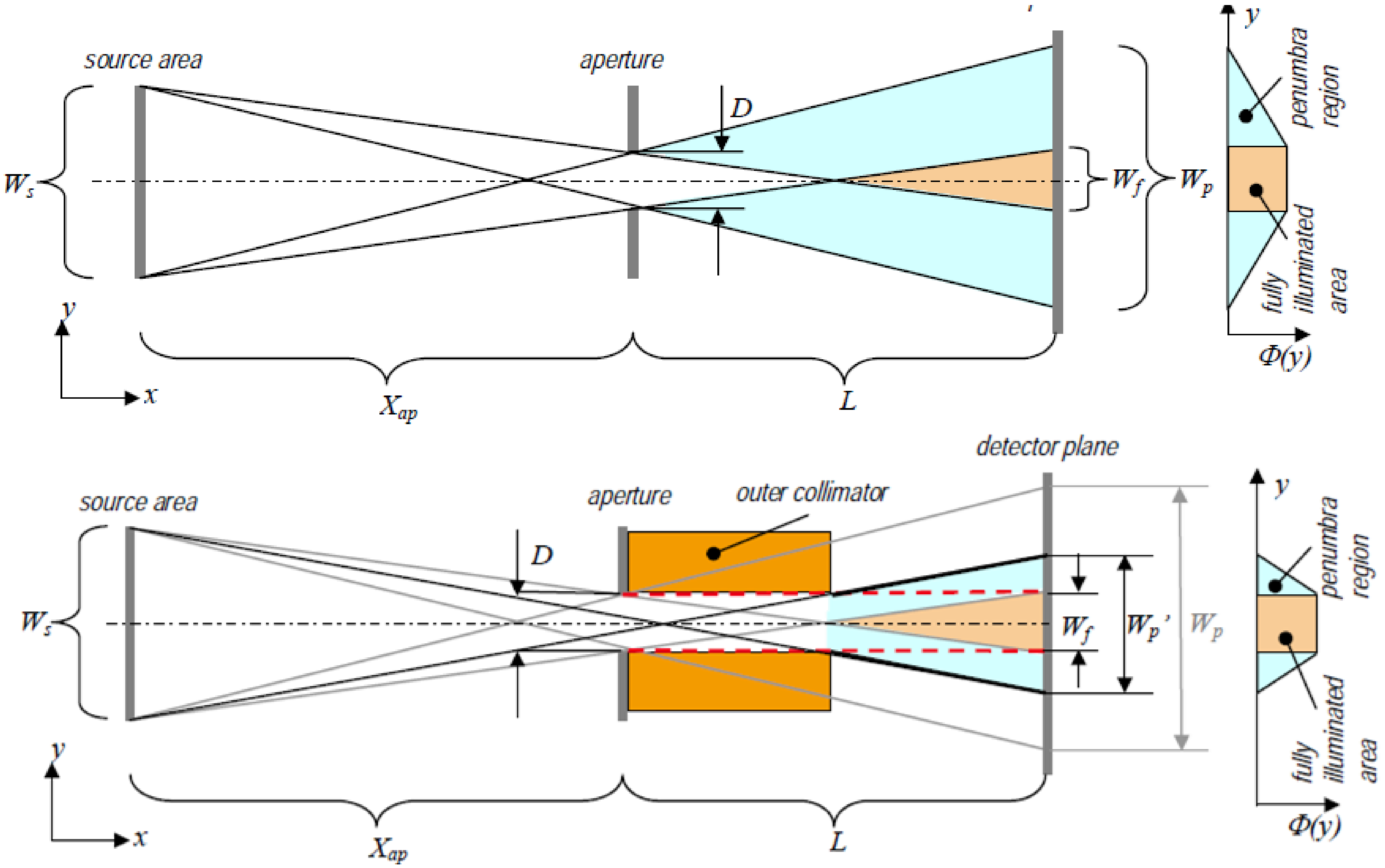

Collimator ratio: L/D

The collimator forms a shaped and directional beam out of the neutron source (e.g. reactor)

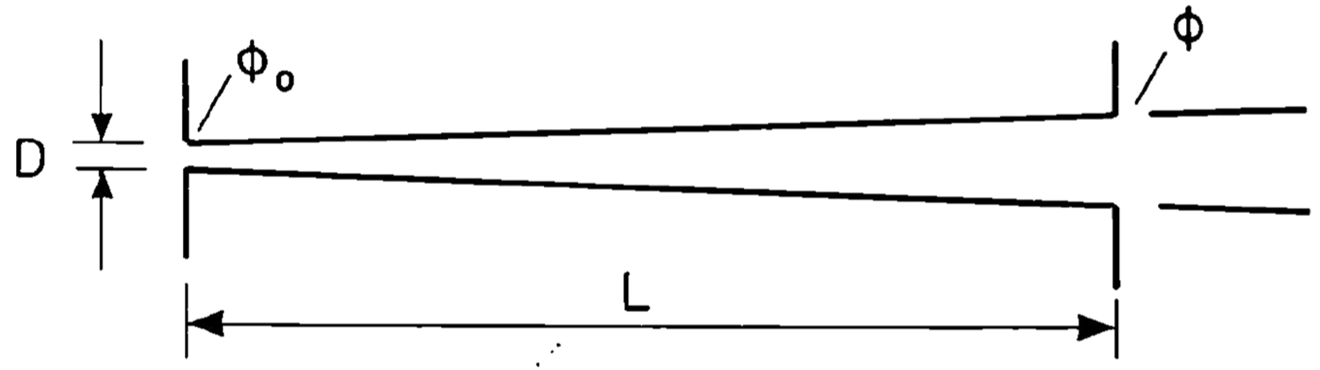

$$\Phi = \frac{\Phi_0 A}{4\pi L^2}$$

$$A = \frac{\pi D^2}{4}$$

$$\frac{\Phi_0}{\Phi} = \frac{incoming\ flux}{outcoming\ flux} = 16\left(\frac{L}{D}\right)^2$$

Centre for Energy Research

Beam formation

Budapest Neutron Centre

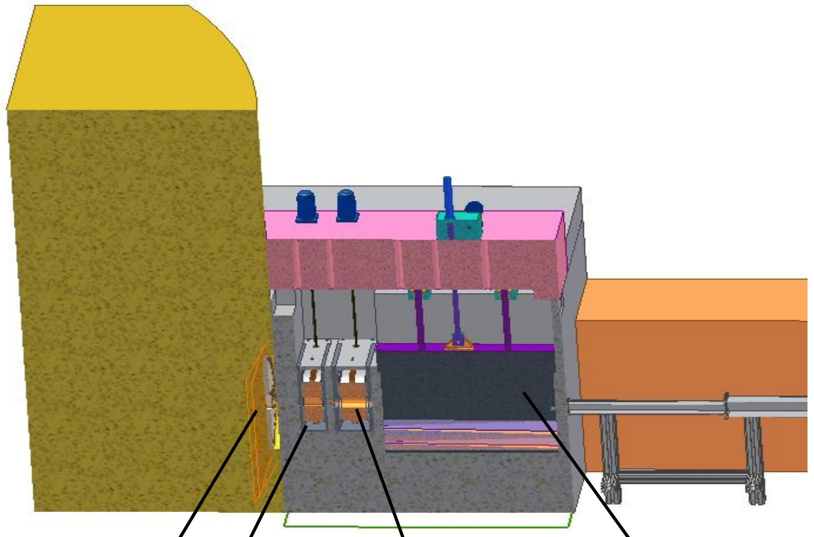

pre-collimator filter diaphragm Outer-collimator

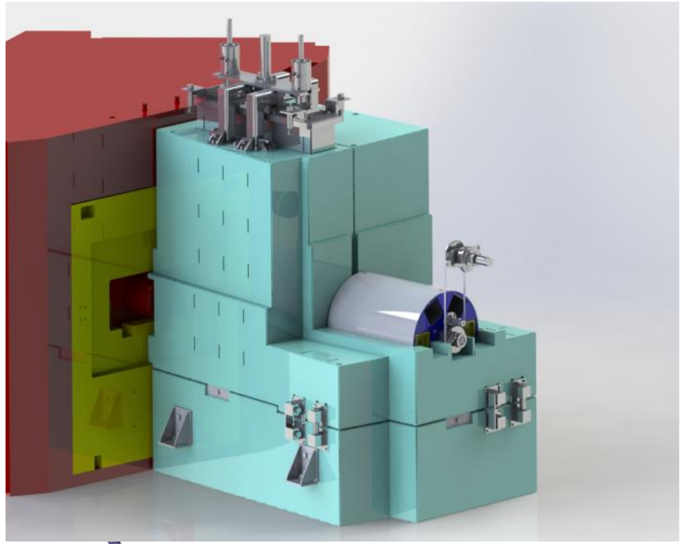

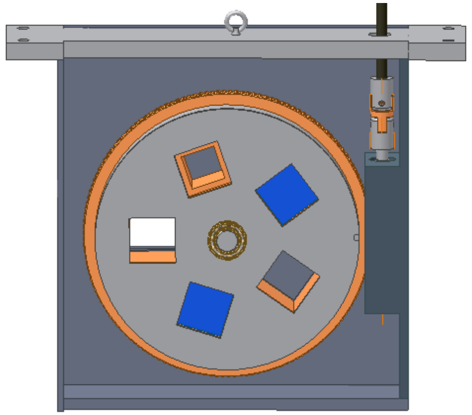

Filters

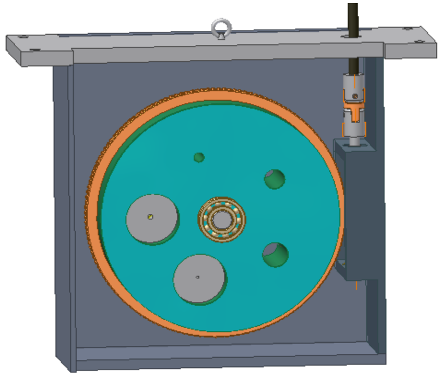

Pinhole collimators

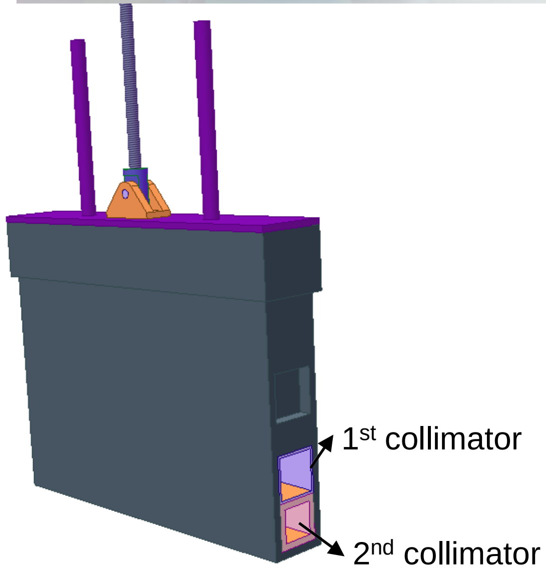

Outer-collimator

Monochromatization (optional)

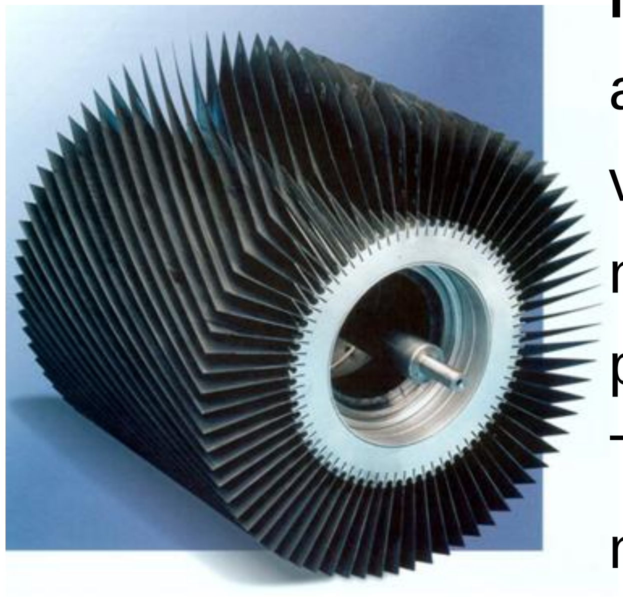

Neutron Velocity Selector

a device that allows neutrons of defined velocity to pass while absorbing all other neutrons, used for the purpose of producing a monochromatic neutron beam. The blades are coated with a strongly neutron-absorbing material

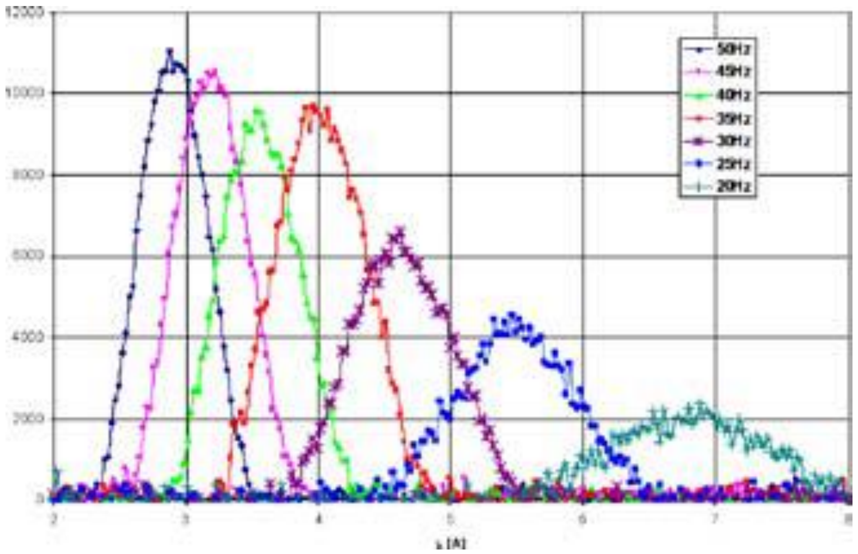

Double crystal monochromator

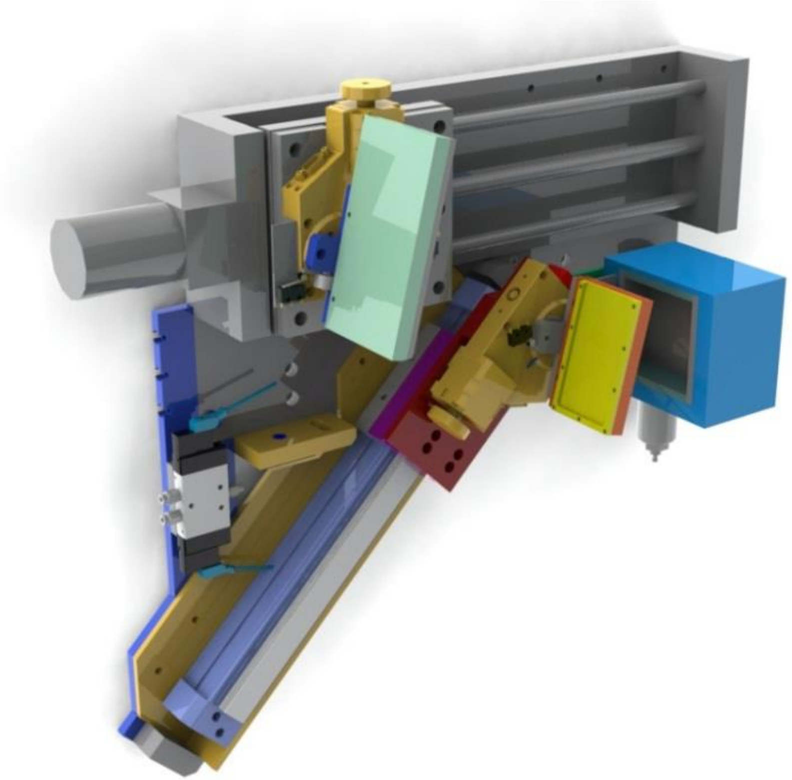

E. Calzada, ANTARES II, FRM II, Garching

Pyrolytic graphite (002) crystals

- Mosaicity 0.7°
- Δλ/λ = 1% .. 3%
- Wavelength band: 2.7 … 6.5Å

Flight tube with beam limiters

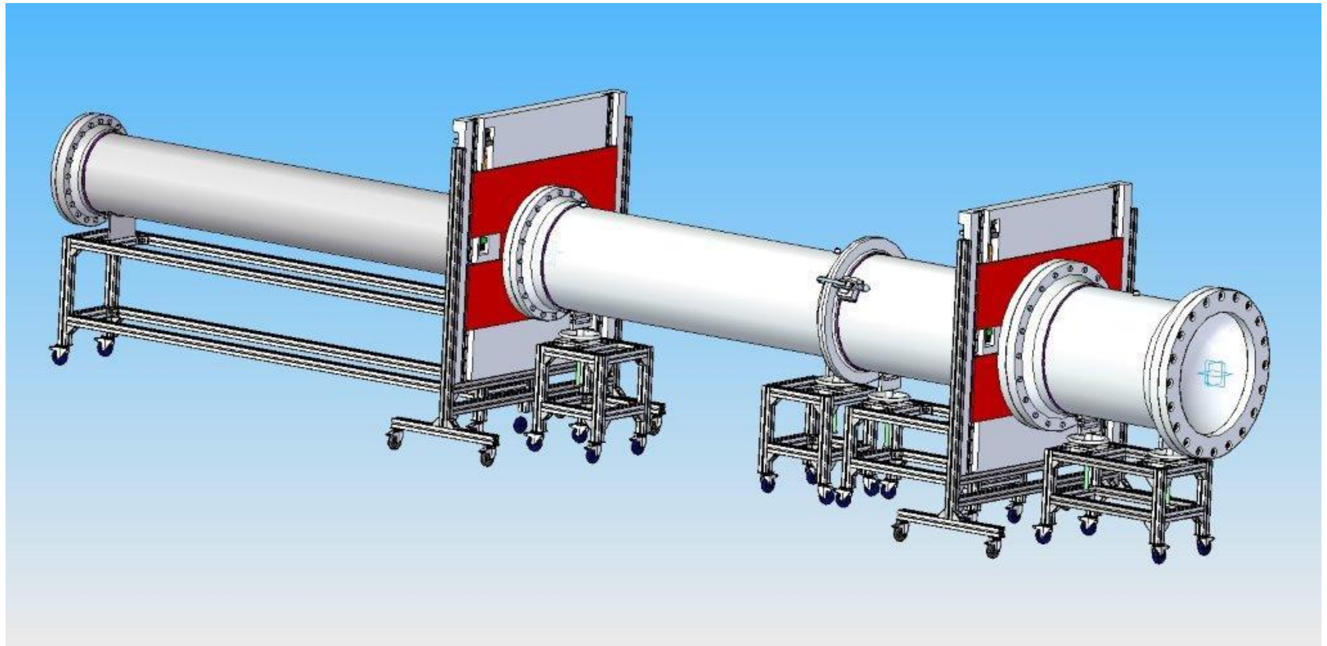

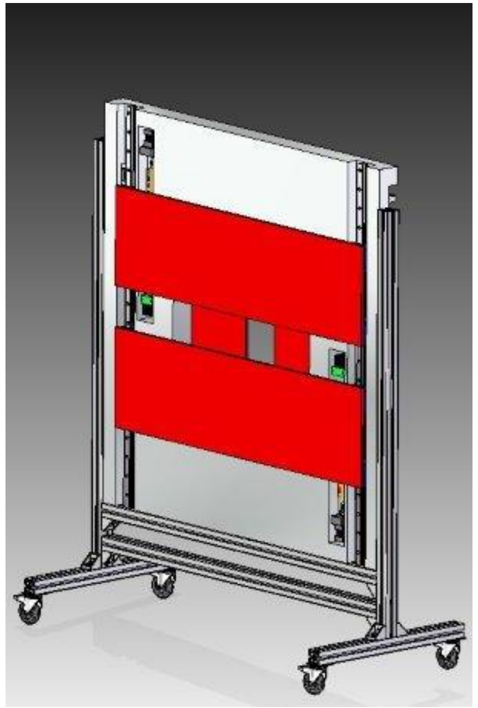

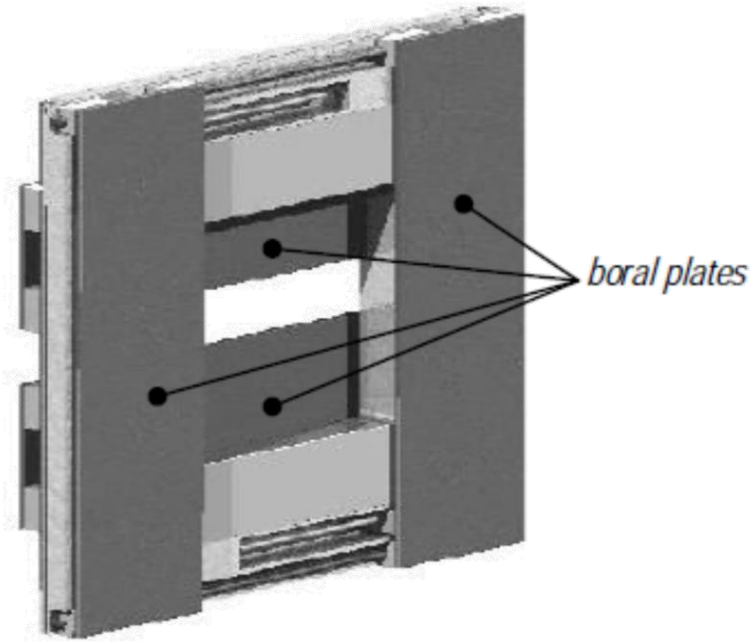

Vacuum, or He gas
to reduce
the loss of neutrons

Beam collimation (flight tube case)

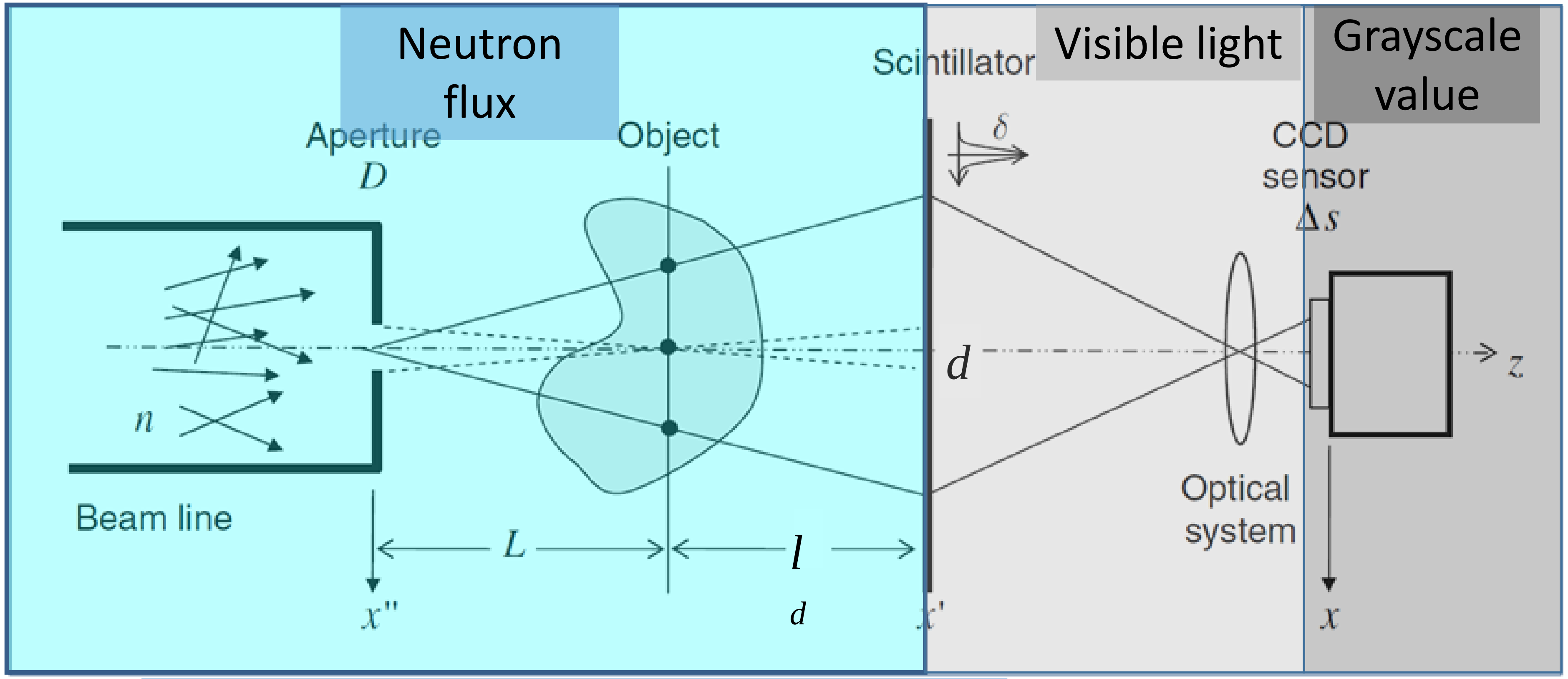

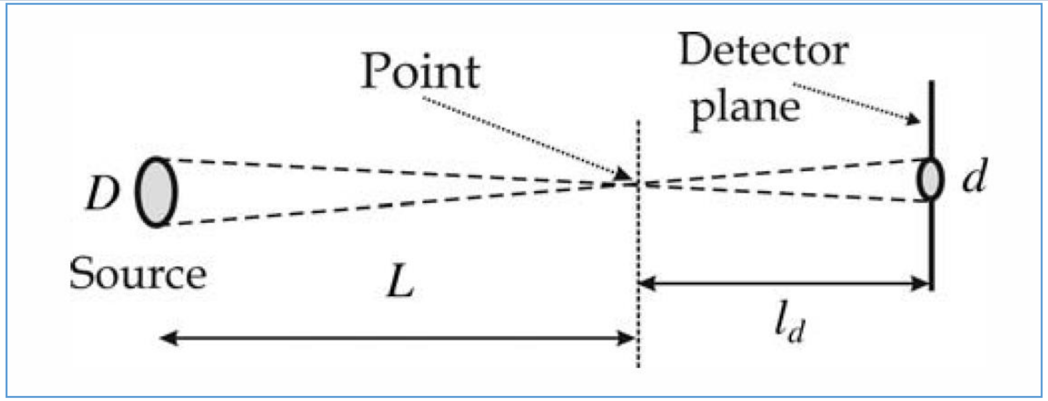

$$\frac{L}{D} = \frac{l_d}{d}$$

How close the beam geometry is to the ideal point-source configuration?

A larger L/D ratio provides better image resolution because image blur (*d*) is smaller.

Beam collimation (neutron guide)

Neutron guide

The definition of L/D for a simple flight tube is no longer valid.

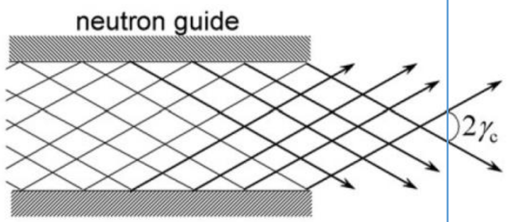

Beam div ~ γ_c
tot. refl. angle for Ni-nat:

γ_c = *1.73×10^{-3} rad/Å or 0.1°/Å*

$$\frac{L}{D} = \frac{1}{\tan[2\gamma_c(\lambda)]}$$

Energy dependent!

Flight tube

Collimators should be positioned in the flight tube

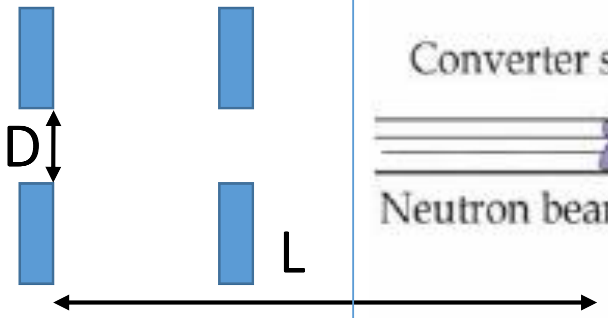

Collimators:

- shaping field of view
- less flux
- improving L/D

Sample & Tomograph

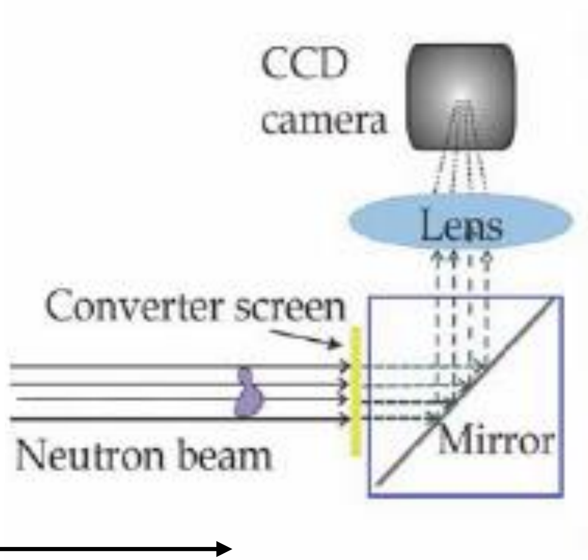

Neutrons hit the screen (e.g. 2:1 mixture of $ZnS/^6LiF$)

↓

Conversion into visible light

↓

That is collected on the CCD of a camera

Light-proof box containing mirror and CCD optics and camera

Neutron Periscope @ FRM II

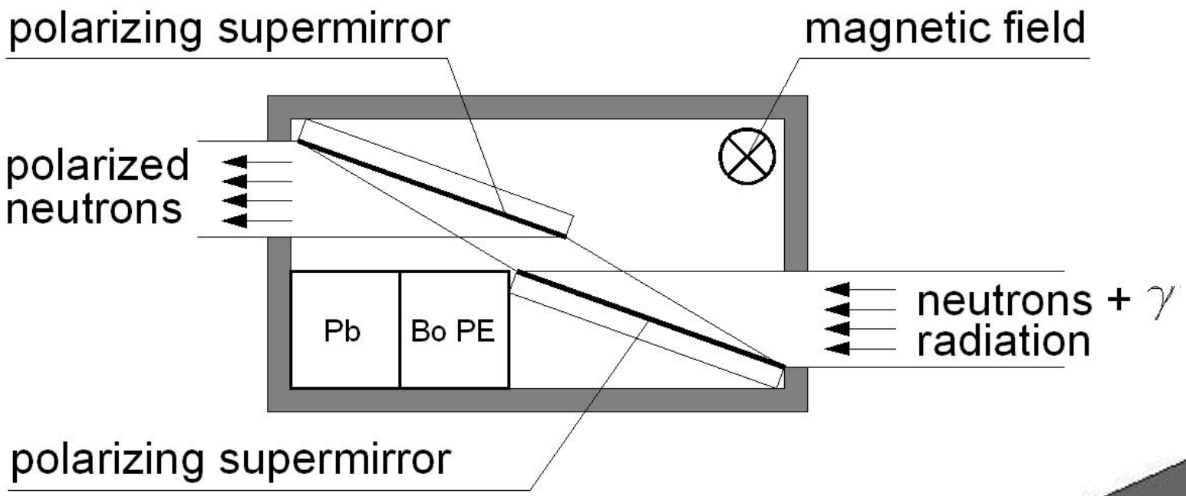

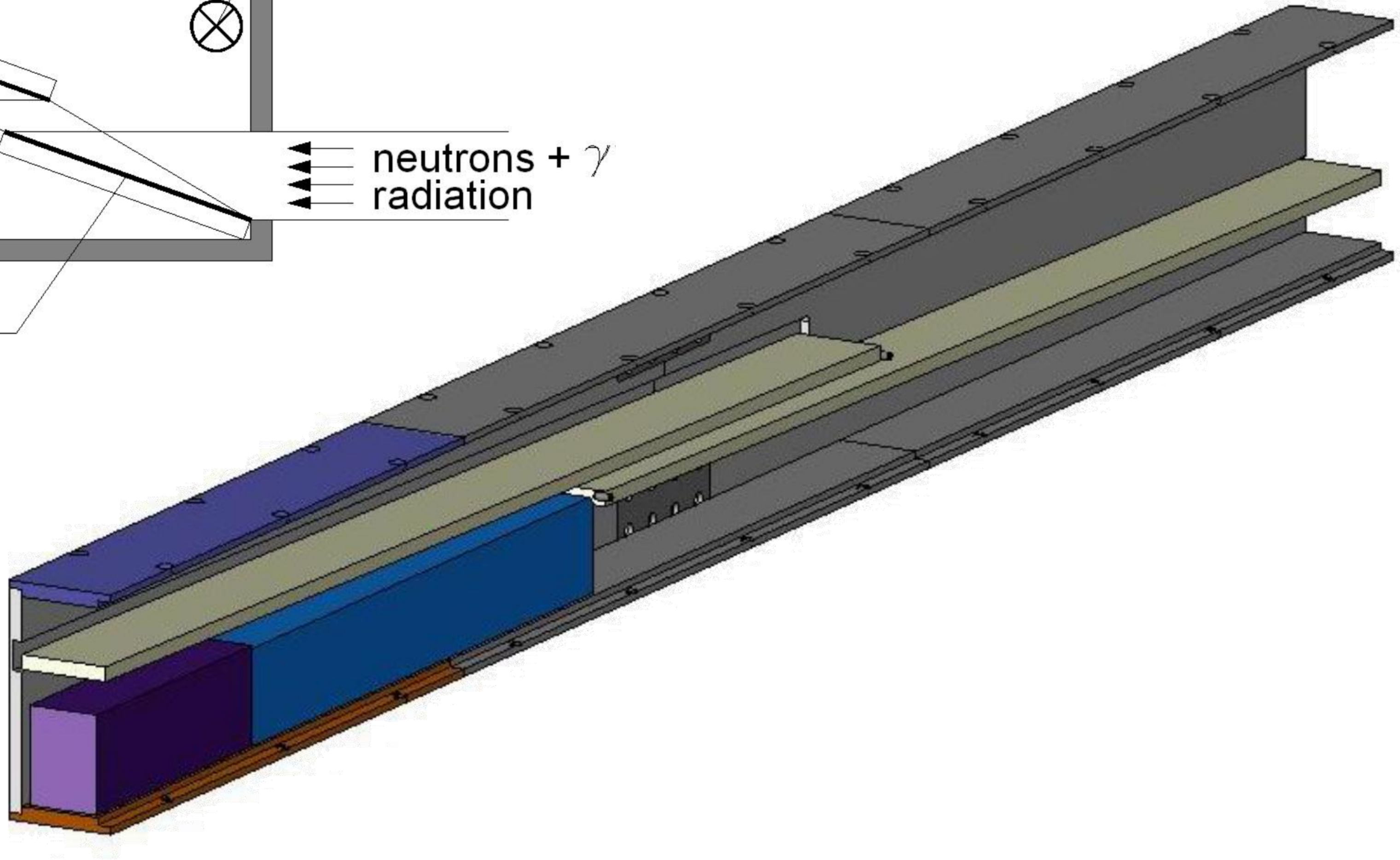

Impact of the beam quality on the image

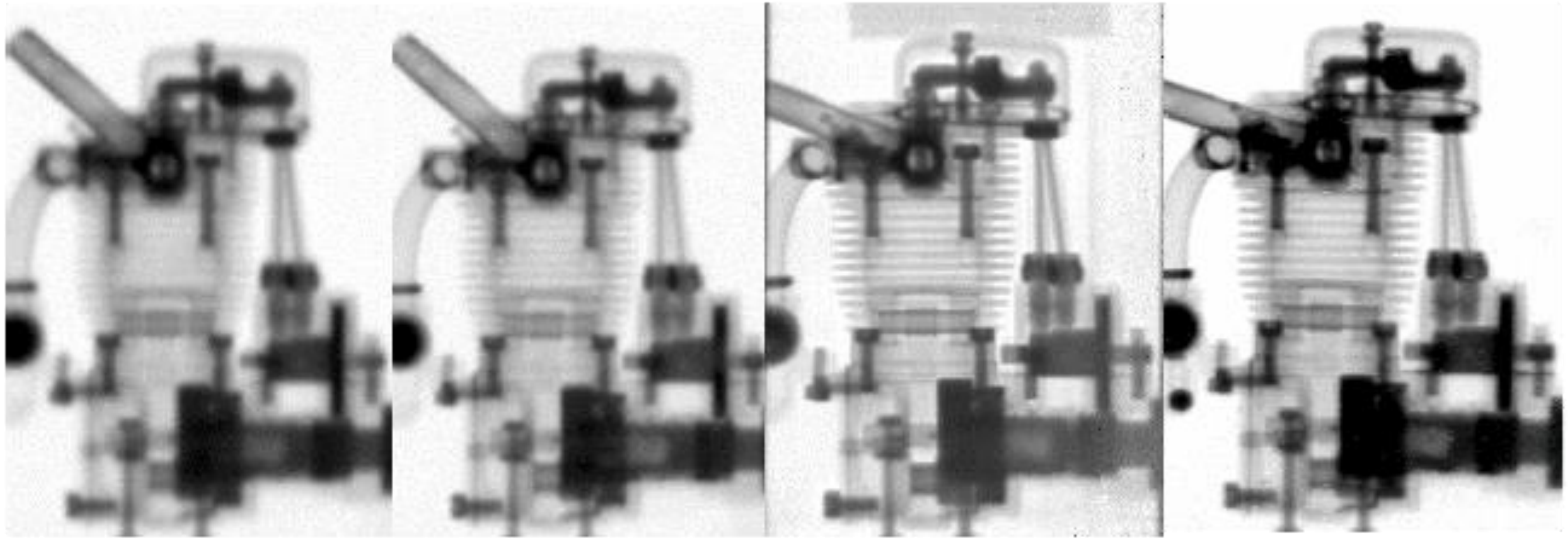

L/D=71 L/D=115 L/D=320 L/D>500.

Radiographs of a small motor taken at different beam positions with different L/D ratios.

The radiographs were taken at a cold guide, a thermal guide, a cold guide with a consecutive 15 mm pinhole and 4.8 m flight tube and at a classical 20 mm pinhole and 10 m flight tube arrangement.

Neutron flux as function of the beam

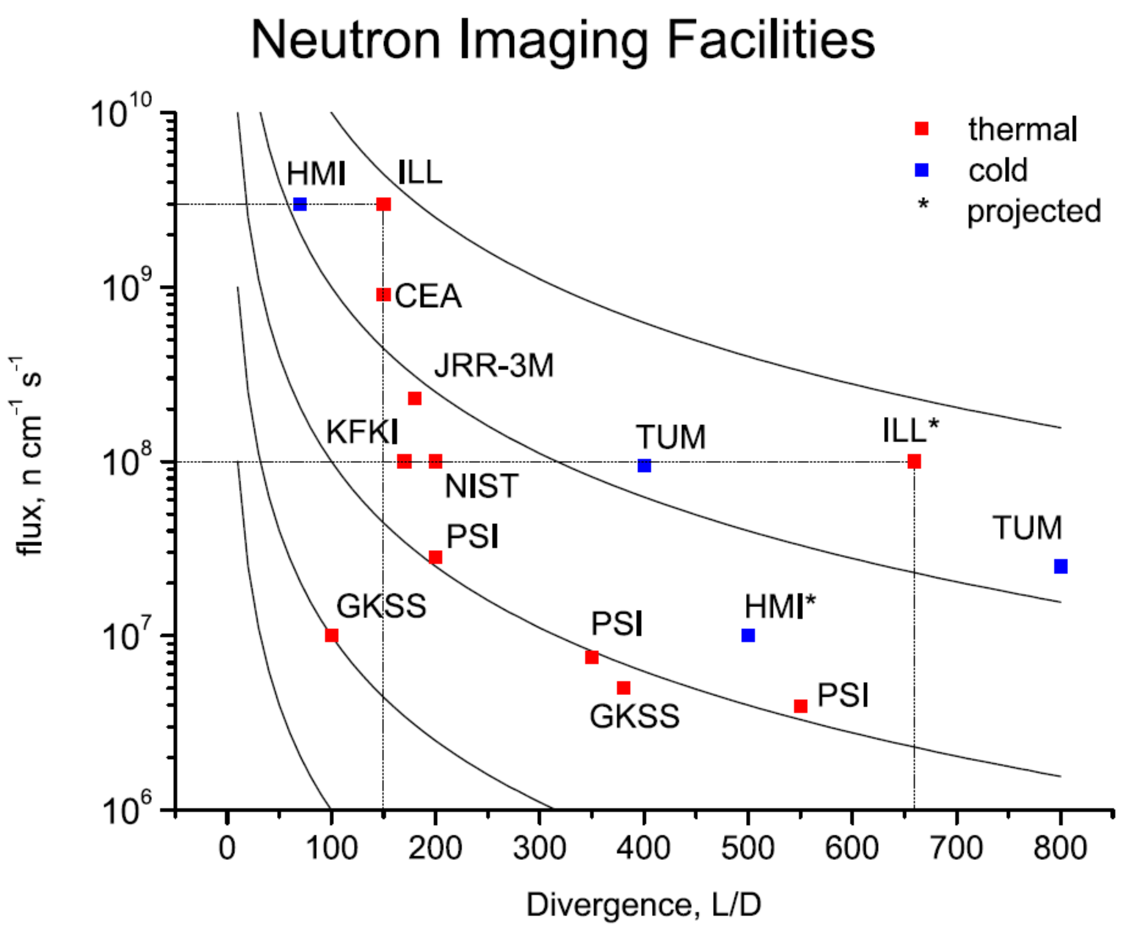

The curved lines represent constant values of the neutron flux per solid angle.

From PhD. Thesis of A .Van Overberghe

Better homogeneity of guided beams

Beam profile of guided beams always have horizontal and veritcal stripe structure
More homogenous beam can be obtained with a scatterer - N. Kardjilov (HMI Berlin)

Without graphite | 5mm graphite | 10mm graphite

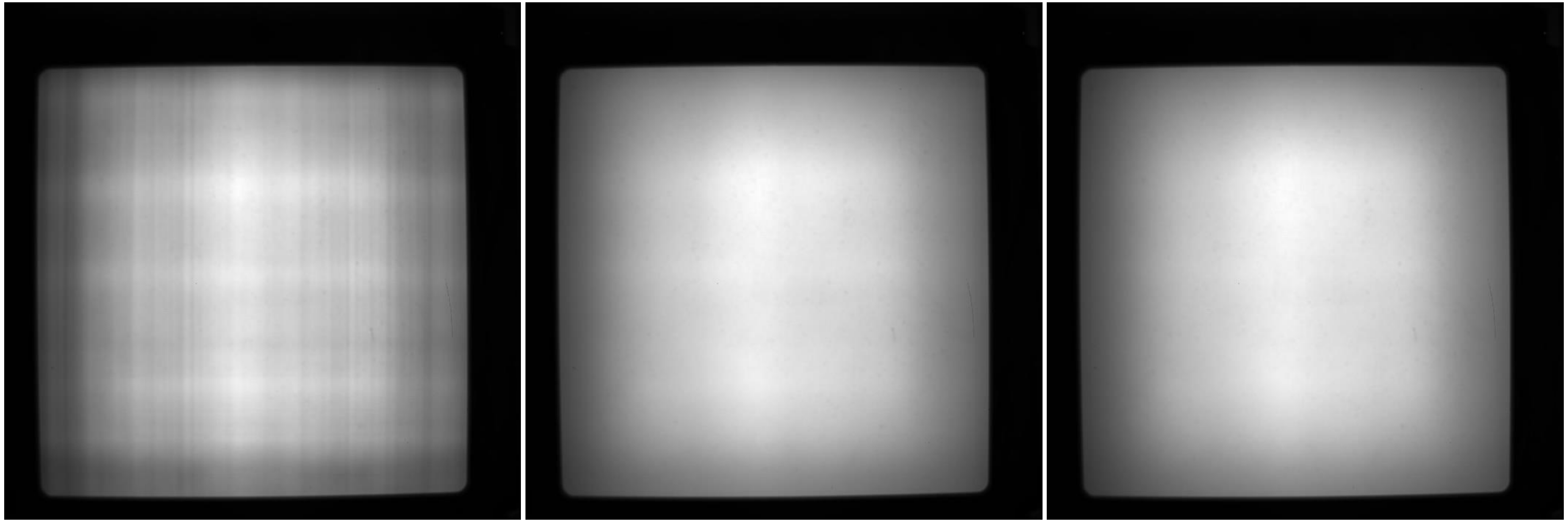

Intensity: 100 % | 95 % | 82 %

Sample manipulator(s)

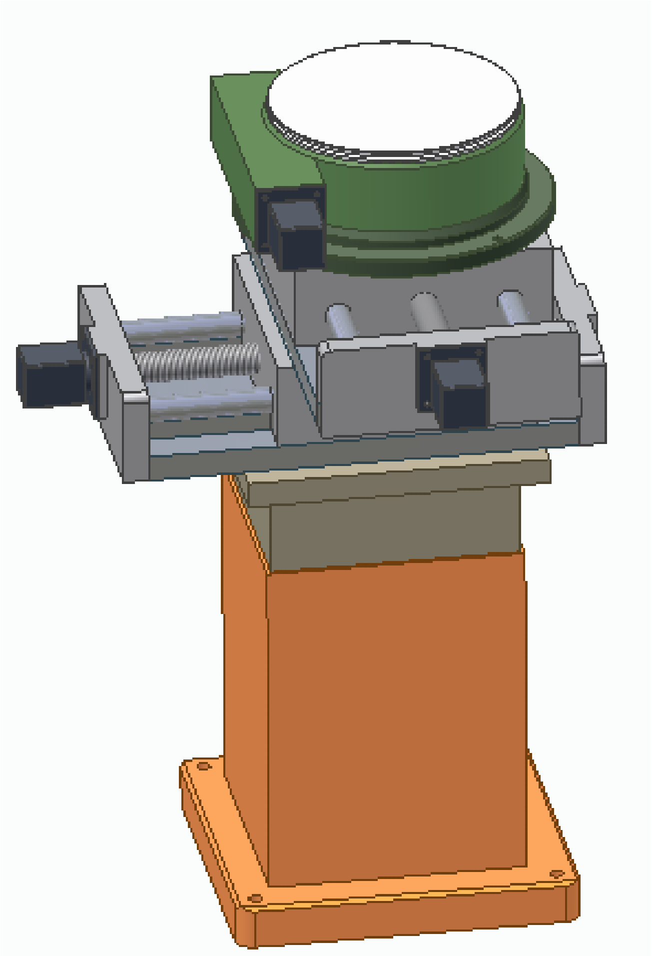

Heavy-load sample manipulator
(up to few hundred kg)

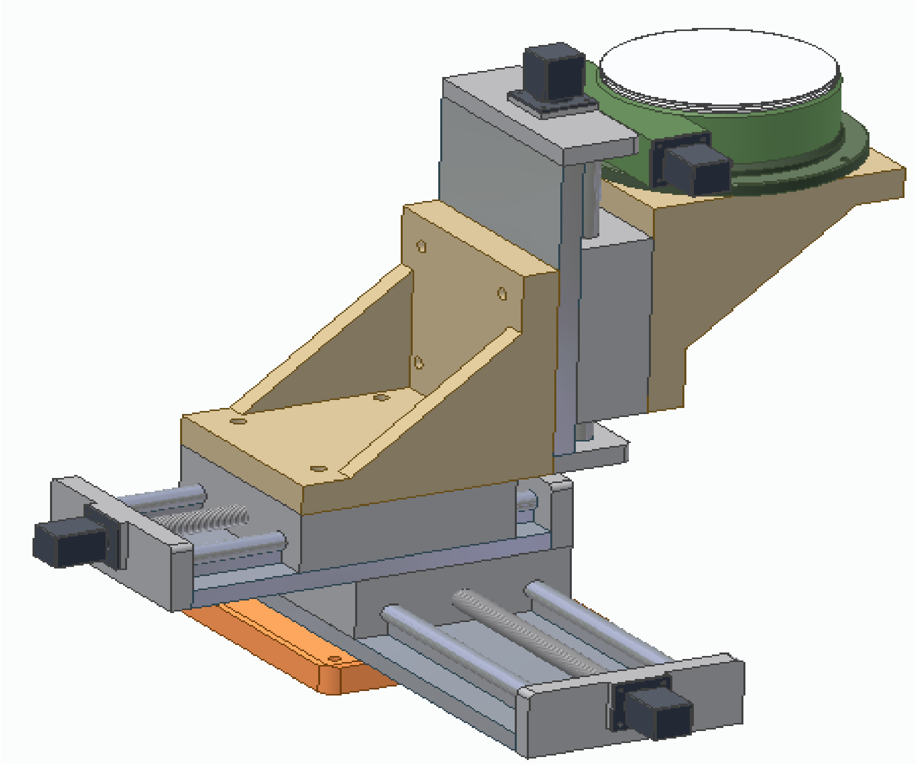

small sample table (few kg)

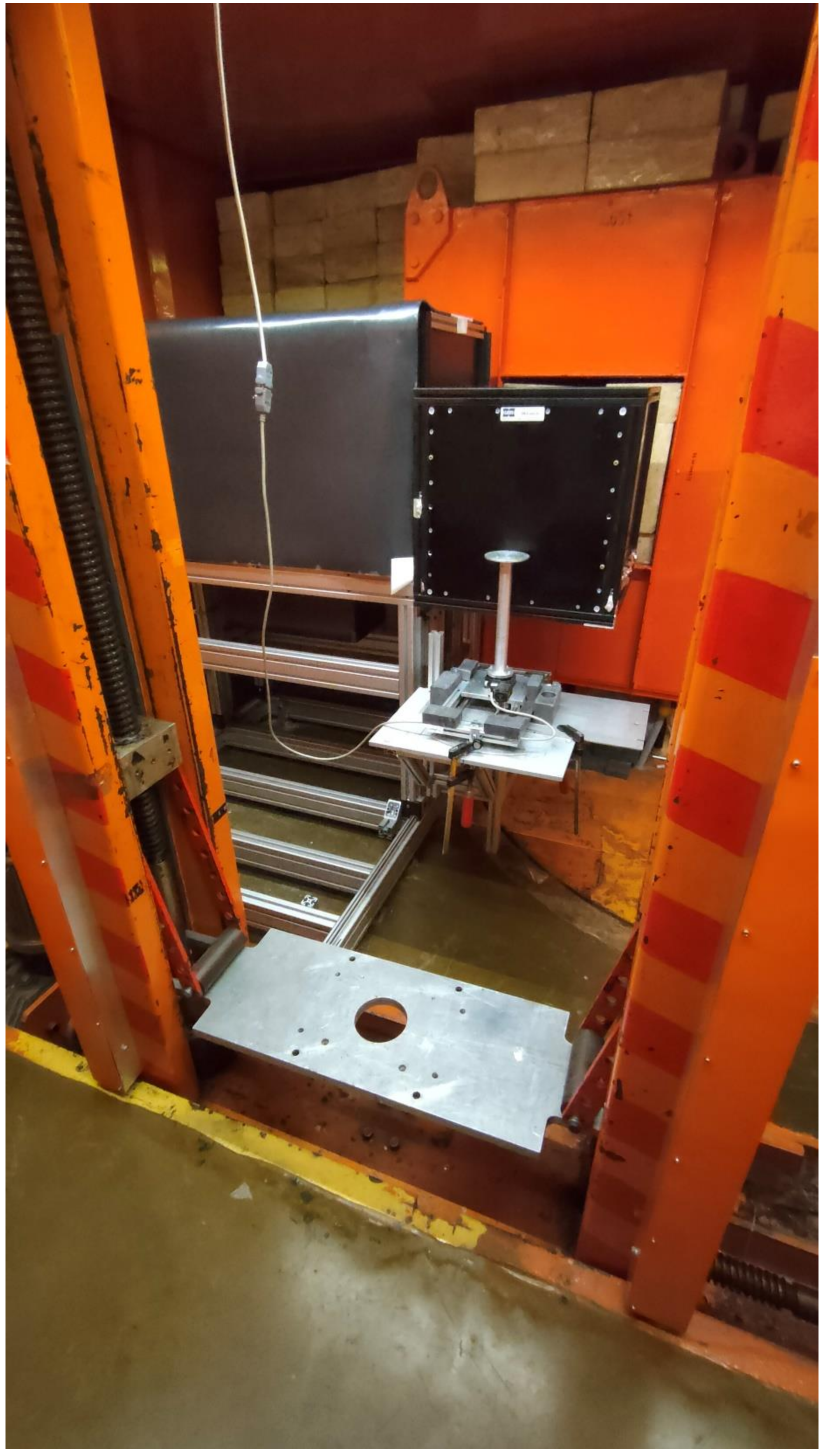

- No direct neutron detection possible
- A secondary nuclear process is needed:

  capture, fission, collision
- Main neutron imaging processes are using:
  - scintillation
  - photo-luminiscence by secondary particles +β, γ
  - nuclear track detection
  - chemical excitation
  - charge collection in semi-conductors

Performance parameters of neutron imaging detectors

- Spatial resolution
- Time resolution
- Signal-to-Noise Ratio
- Dynamic Range
- Read-out behaviour
- Sensitivity, efficiency
- Stationarity
- Trigger options

To be optimized for the specific problem!

E. Lehmann

Digital imaging

The **result** of (digital) radiography:

- 2D image with linear scale (e.g. black/white)

  Integrating all layers of the object in beam direction suitable for image post-processing

- Data set as matrix of pixel values containing intensity information

  Suitable for quantitative evaluation of the sample content

The **limitation** of neutron radiography:

- **Spatial resolution** (finally given by the detection process)

  But also limited by the beam collimation, the pixel size and optical systems

- Frame rate (exposure time and readout time)

  Limited by the beam intensity, the detector sensitivity and the electronic readout

- Sample size (by the transmission properties of the sample material)

  Can be overcome with fast neutrons …

CCD or sCMOS camera with a scintillator

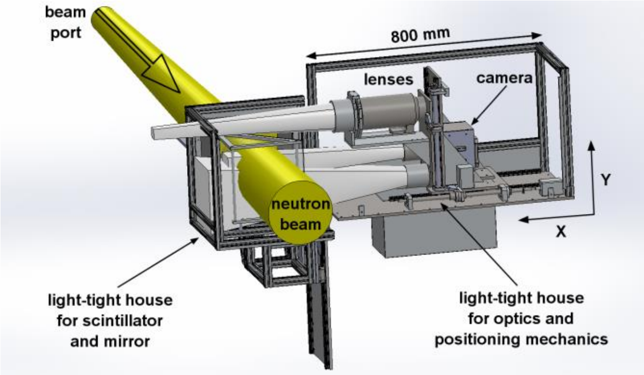

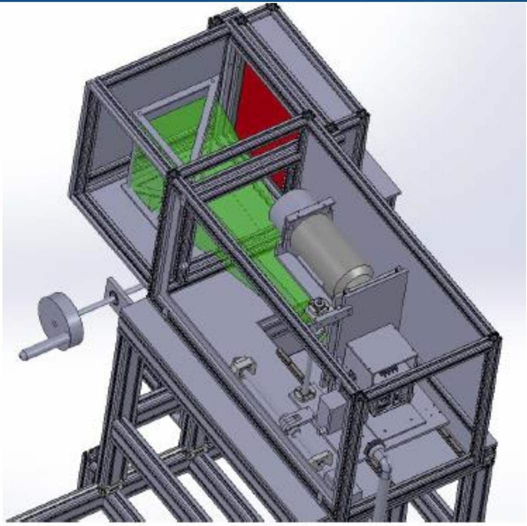

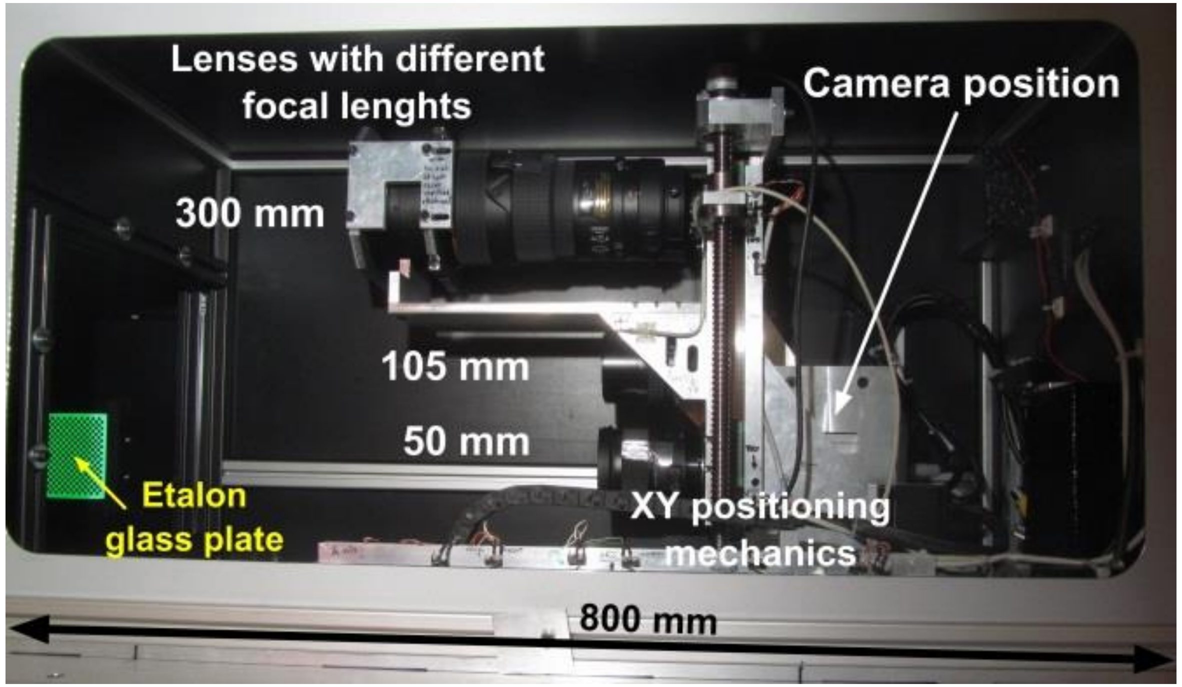

The digital image detector of RAD

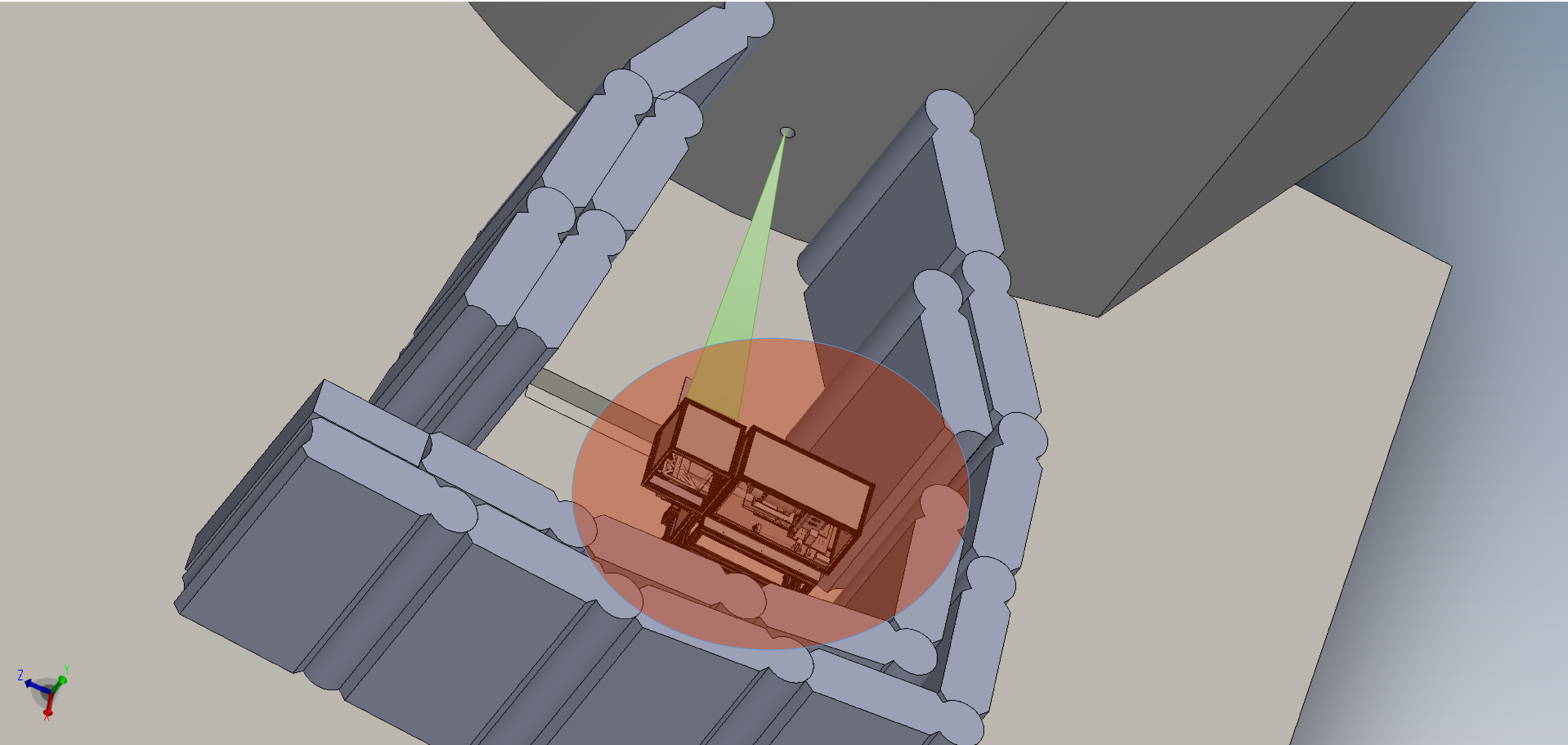

Components of a scintillator-based digital

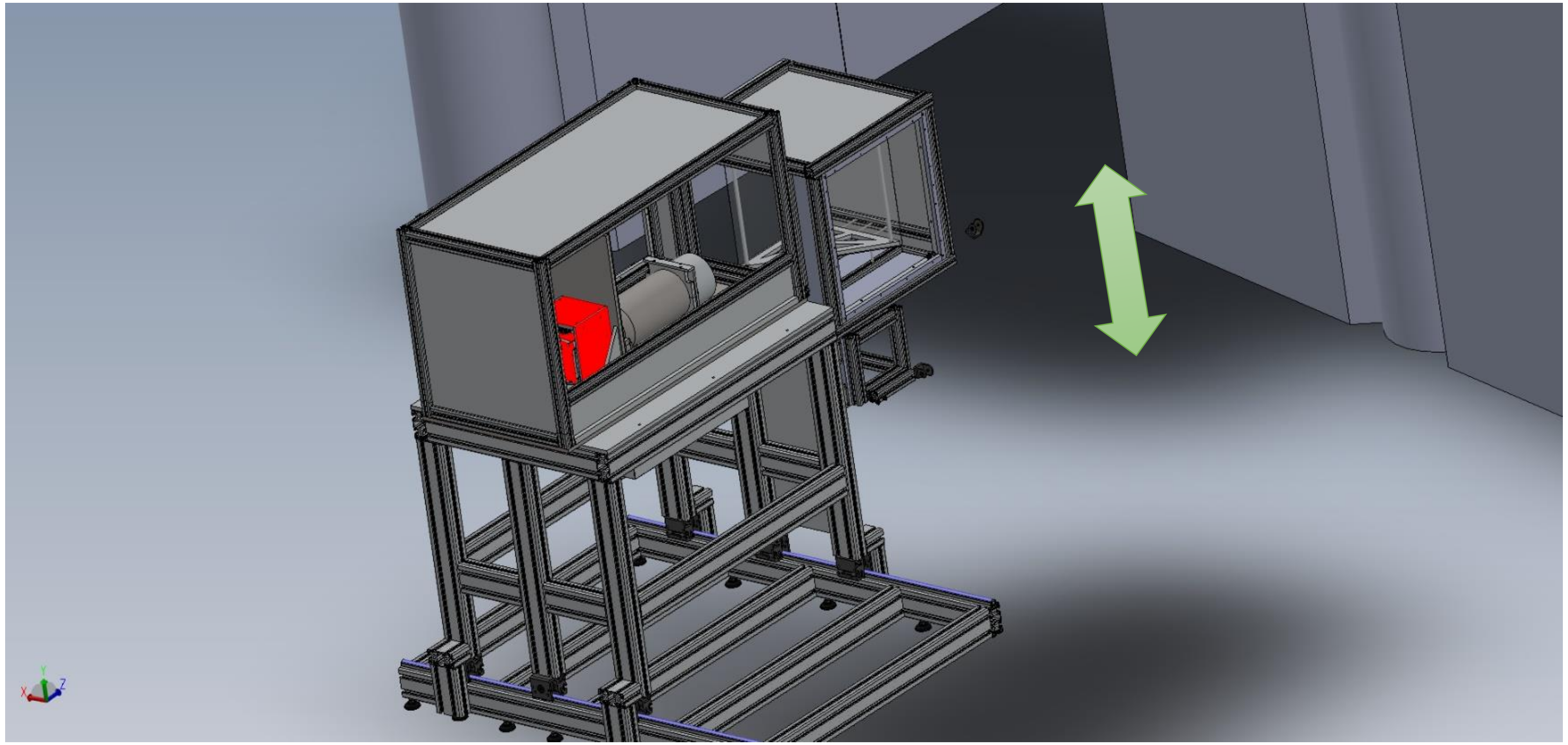

Light-tight box
Sample platform
Scintillator
Mirror
Exchangeable optics
CCD or sCMOS camera

- The impinging neutrons are converted to visible light using a ^{6}LiF/ZnS or Gadox scintillator layer
- The light is reflected out of the neutron beam direction with a mirror
- Collected with optical lenses and detected with a pixelized CCD or sCMOS camera
- Stored as a grayscale image with 16-bit depth (e.g., TIFF)

Optics for CCD/sCMOS camera

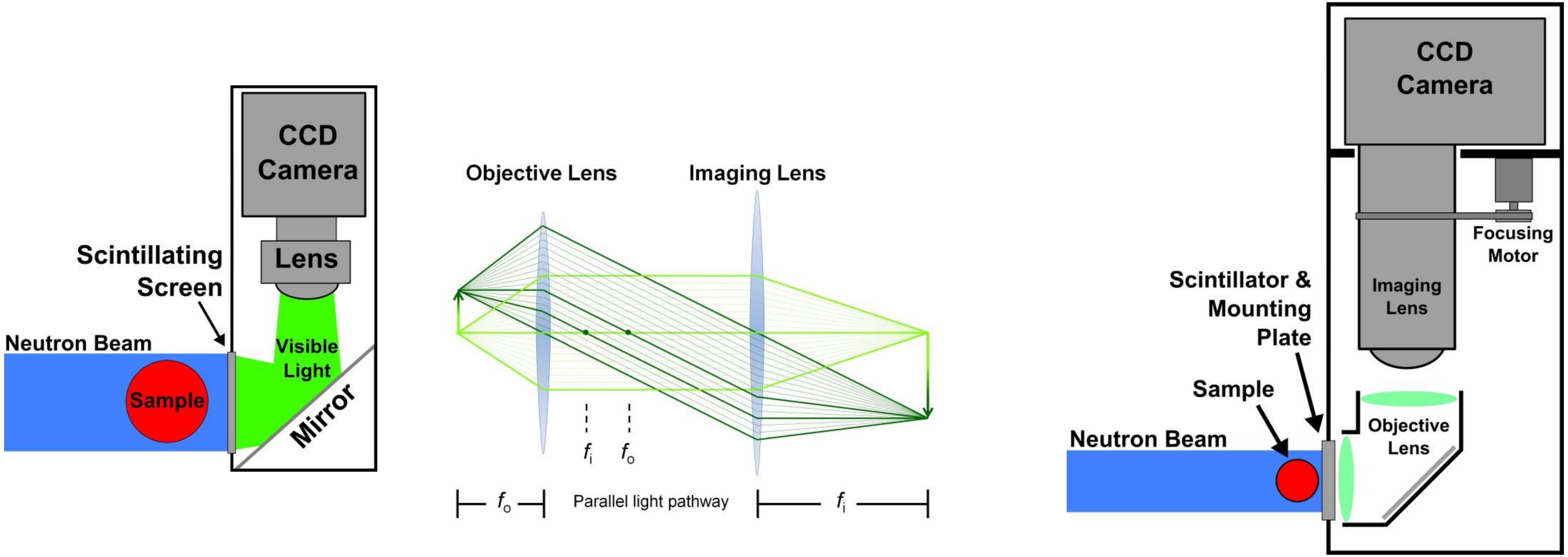

Table 2. Magnification (M), effective pixel size (P_{eff}), Field of View (FOV) and neutron flux of several objective/imaging lens combinations with three available pinhole diameters.

				Neutron flux (n/s/pixel)		
Obj. Lens/Img. Lens	*M*	P_{eff} (μm)	*FOV (mm)*	*D = 3 cm*	*D = 2 cm*	*D = 1 cm*
105 mm / 50 mm	2.10	6.429	13.2 × 13.2	9.9	6.6	2.4
200 mm / 100 mm	2.00	6.750	13.8 × 13.8	10.9	7.3	2.6
200 mm / 50 mm	4.00	3.375	6.9 × 6.9	2.7	1.8	0.7

S. H. Williams et al, J. of Instrumentation (2012)

Microchannel plate

- microchannel plate is an emerging method that is a digital semiconductor detector array with very small pixel sizes
- MediPix collaboration (CERN -> Nova Scientific, WidePix)
- 5 micron channels spaced on 6 micron centers
- pixel detector readout chip working in single photon counting mode
- resolution about 100 μm, 30 frames per second

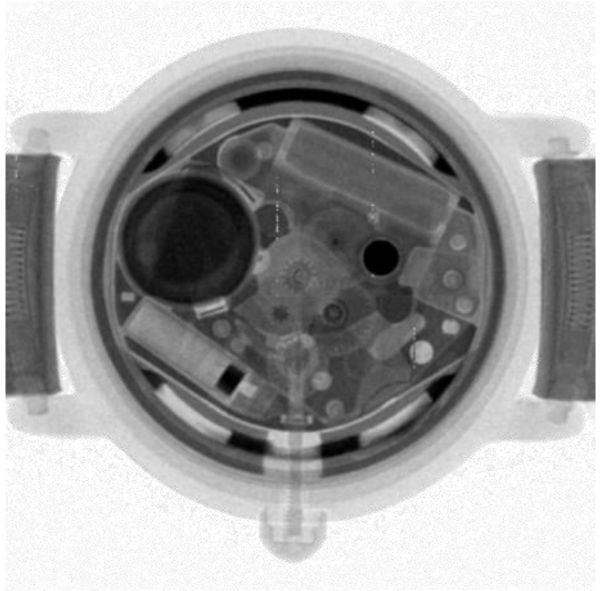

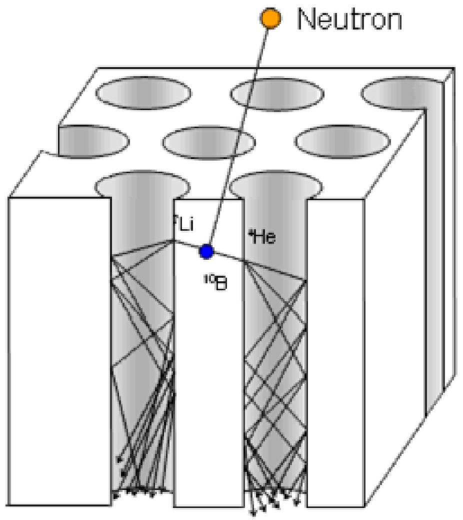

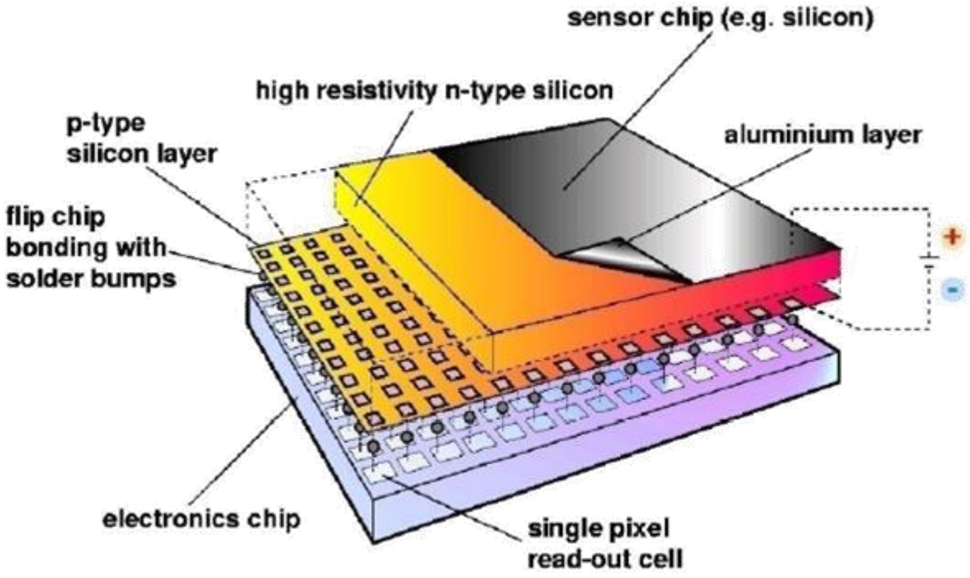

Spatial resolution of the system

Light from a point source passing through the lens interferes with itself (diffraction from a circular aperture) creating a ring-shape diffraction pattern, known as the **Airy pattern**. The Airy pattern is observable in the far field:

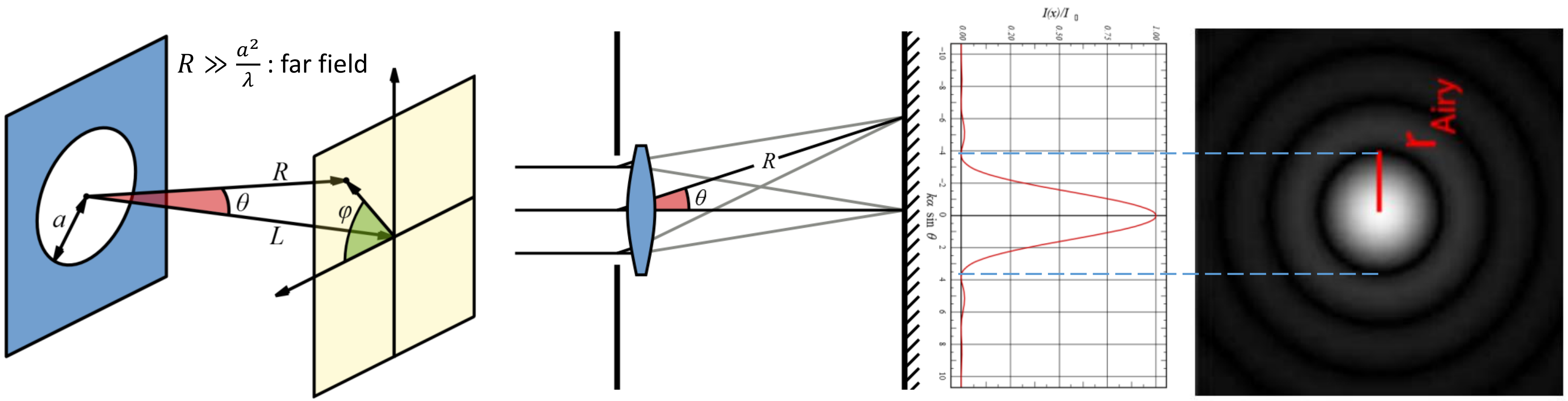

Rayleigh criterion (the **angular resolution** of an optical system, ***Θ***):

Two point sources are regarded as just resolved when the principal diffraction maximum of one image coincides with the first minimum of the other.

at r_{Airy}: $\sin\Theta = 1.22\frac{\lambda}{a}$

Θ, angle of observation

λ, wavelength

a, is the diameter of the entrance pupil of the aperture or lens

Energiatudományi Kutatóközpont

The spatial resolution of an imaging system

- Methods to measure the spatial resolution in 2D:
  - Gd Siemens Star test pattern:
    - labeled spoke periods of concentric rings
    - The pattern gives a qualitative measurement of resolution capability of the system
  - Measurements based on a sharp Gd foil edge:
    - Distance across the Edge Spread Function (ESF) as defined from 10% to 90% of full intensity
    - Full width at half maximum (FWHM) of the Gaussian peak fit to the Line-Spread Function (LSF)
    - Inverse of the spatial frequency when Modulation Transfer Function (MTF) = 10%
- Spatial resolution in 3D: pile of Ti spheres

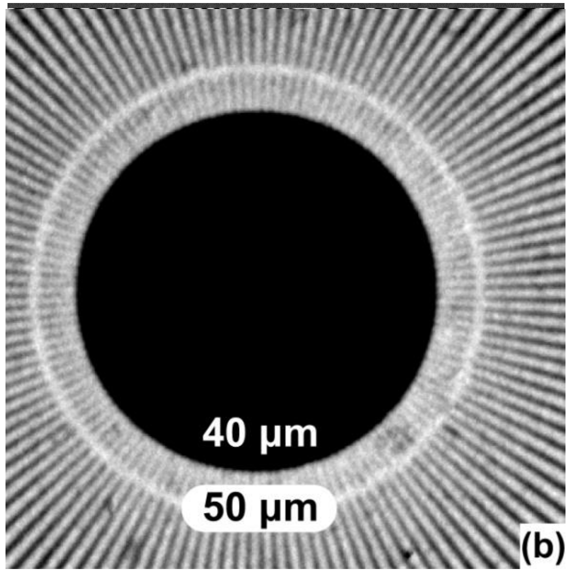

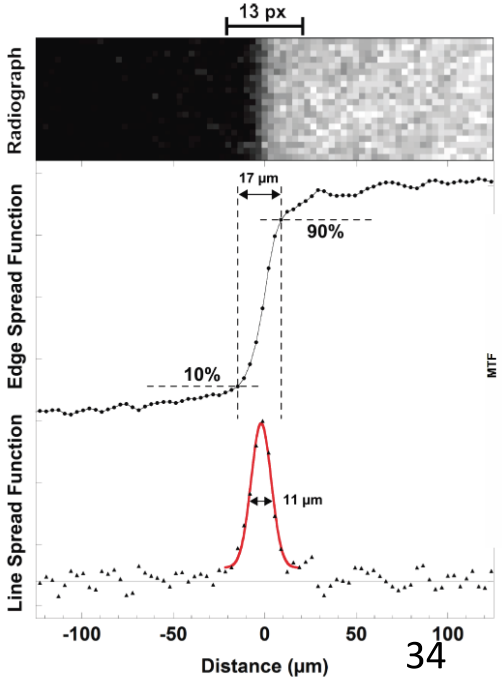

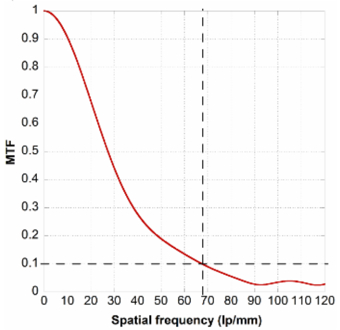

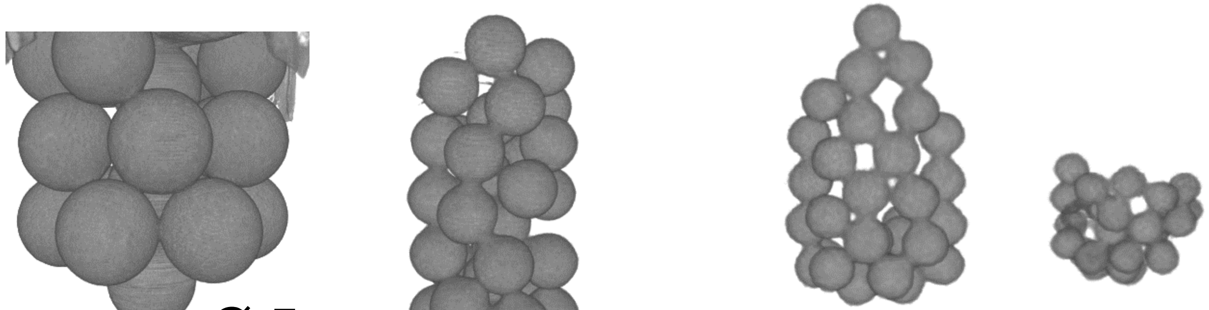

Ø 5mm Ø 2mm Ø 1mm Ø 0.7mm

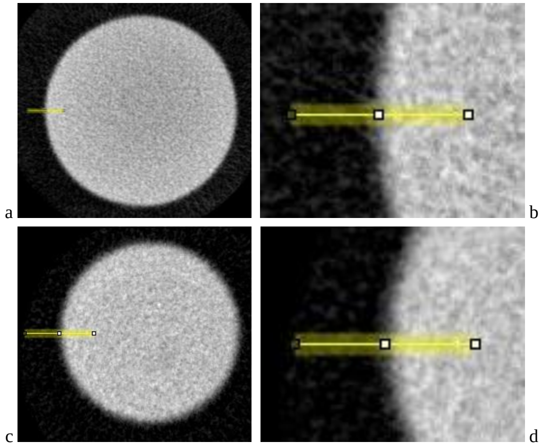

Spatial resolution of the system (10%-90%)

Example: CCD camera + optics + $^{6}LiF/ZnS(Ag)$ scint. in different thicknesses

- The spatial resolution is measured by a sharp edge of a 25-μm-thick Gadolinium foil placed directly on the aluminum plate of the scintillator
- ESF was determined from a line profile perpendicular across the edge
- Spatial resolution was determined by calculating the mean value of the 10%–90% responses

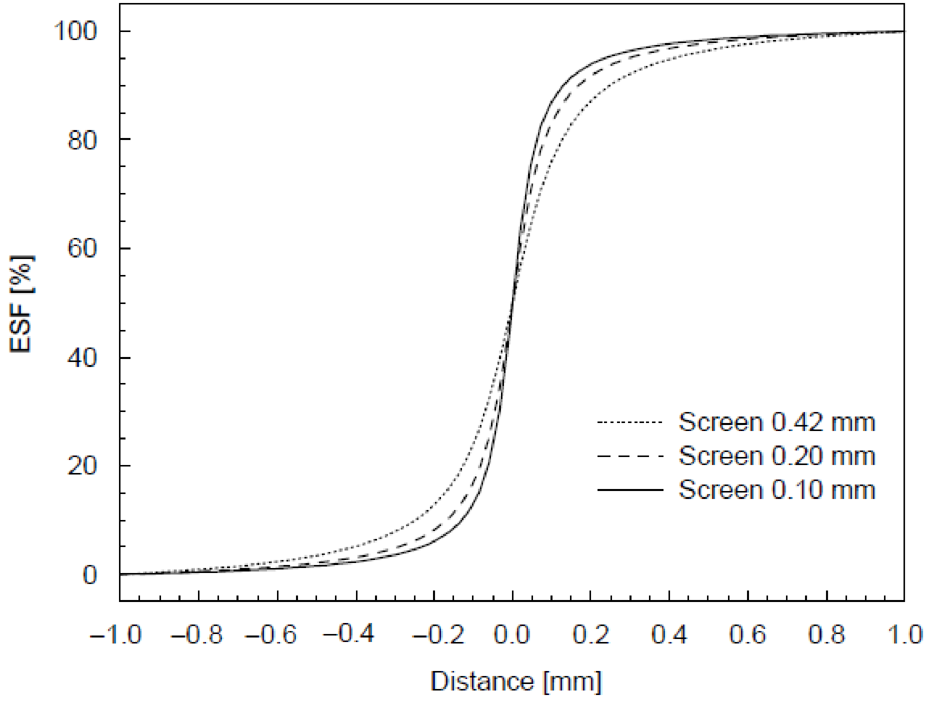

Fig. 1. ESF of three converter screens with different thickness.

Spatial resolution and relative efficiency of the detection system using $^{6}LiF/ZnS:Ag$ scintillators with various thicknesses

Thickness (mm)	Resolution (mm)	Relative efficiency (%)
0.42	0.54±0.02	100
0.20	0.34±0.01	85
0.10	0.24±0.01	64

Spatial resolution vs. scintillator thickness

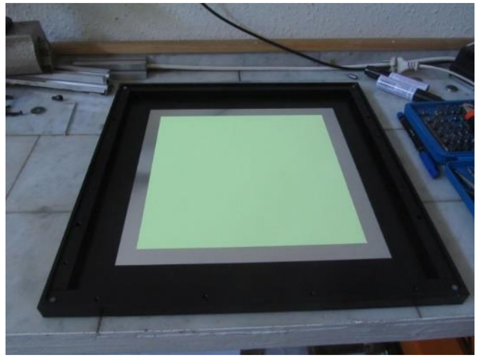

S. Baechler et al. / Nuclear Instruments and Methods in Physics Research A 491 (2002) 481–491

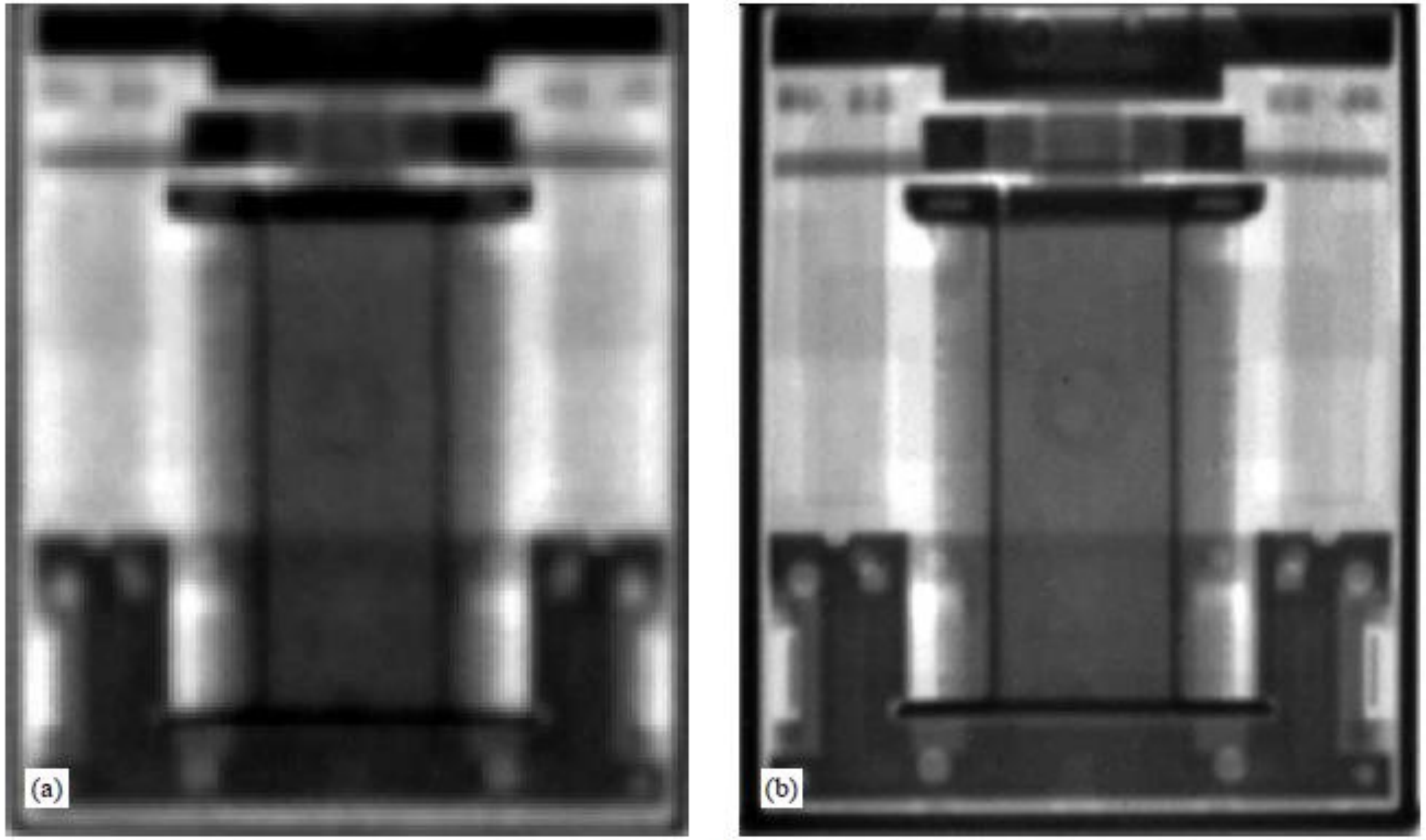

Fig. 3. Radiographs of a relay, $24 \times 30\,mm^2$, taken with (a) 0.40-mm-thick converter; and (b) 0.10-mm-thick converter.

Several exchangeable scintillator screens to properly detect neutrons and X-rays
Thickness: compromise between exposure time and spatial resolution

Math of 3D data reconstruction

Tomography is an extension of radiography, where the 3D visualization of the object is achieved using computational algorithms from a series of radiographic projections acquired as the object is rotated in small angular increments.

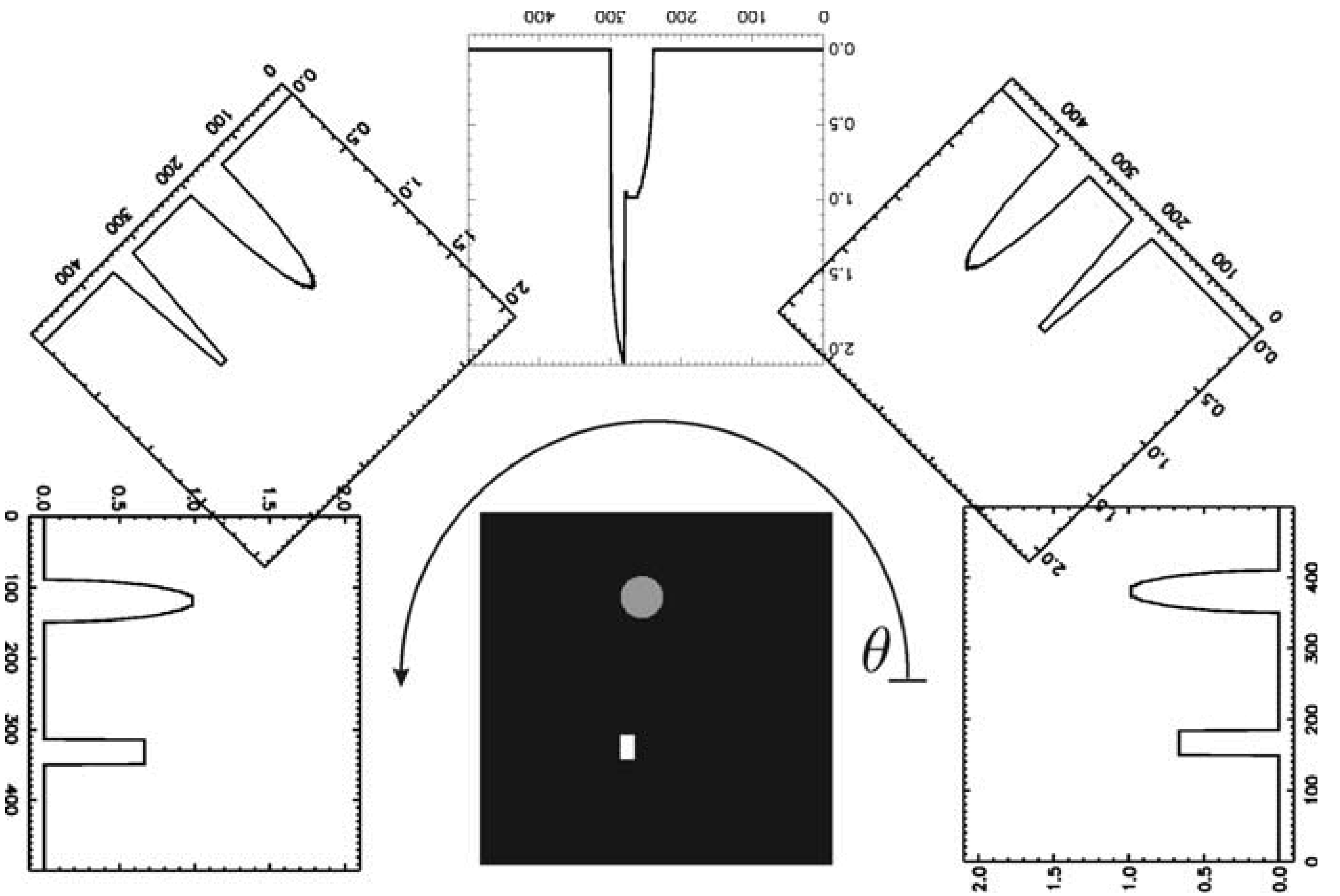

Centre for Energy Research

Corrections and projections (Radon

Budapest Neutron Centre

Intensity detected:

- $I_{openbeam}$, $I_{darkbeam}$, $I_{transmitted}$
- projections have to be corrected for:
  - inhomogeneity of the beam and the detector
  - dark current of the camera
- neutron flux transmitted → grayscale

$$\frac{I_{tr}}{I_0} = \frac{I_{transmitted} - I_{darkbeam}}{I_{openbeam} - I_{darkbeam}}$$

  - real sample = Σ (small, homogeneous samples)

$$\frac{I_{tr}}{I_0} = e^{-\int_{beam\ path} \mu^{tot}(x,y)ds}$$

Projections (Radon transform):

- line integrals of the attenuation coefficient $\mu(x,y)$
- perpendicular to t (along s) taken at angle Θ
- through a slice

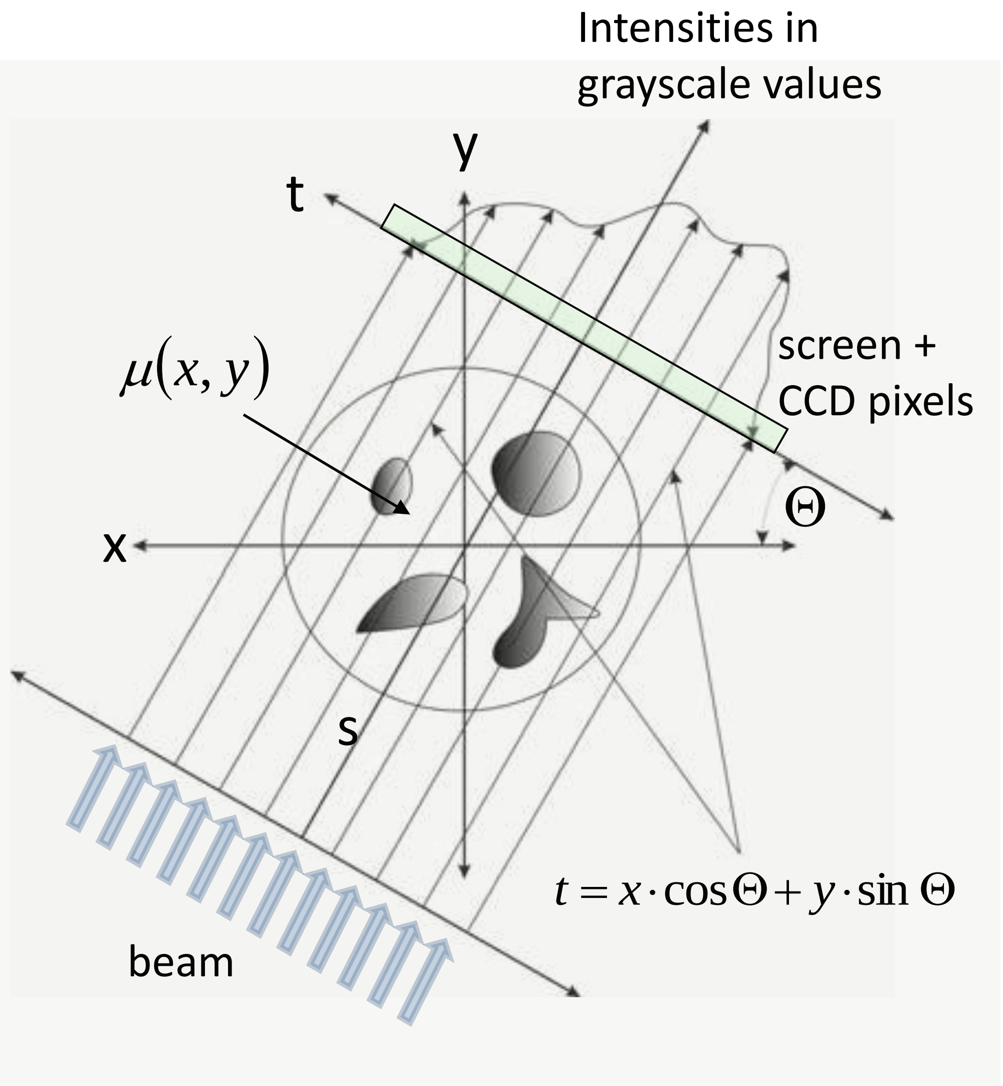

$$P_\Theta(t) = -\ln\frac{I_{tr}(\Theta,t)}{I_0(\Theta,t)} = \int_{line} \mu(x,y)ds =$$

$$= \int_{-\infty}^{\infty}\int_{-\infty}^{\infty} \mu(x,y)\cdot\delta(t - x\cos\Theta - y\sin\Theta)dxdy$$

Fourier slice theorem

The 1D Fourier Transform of a parallel projection $P_\theta(t)$ of a distribution $\mu(x,y)$, taken under an angle θ

=

a single line (a slice) within the 2D Fourier Transform of the distribution $\mu(x,y)$ that encloses the angle θ with the u-axis.

2D pixel detector of the neutron tomograph

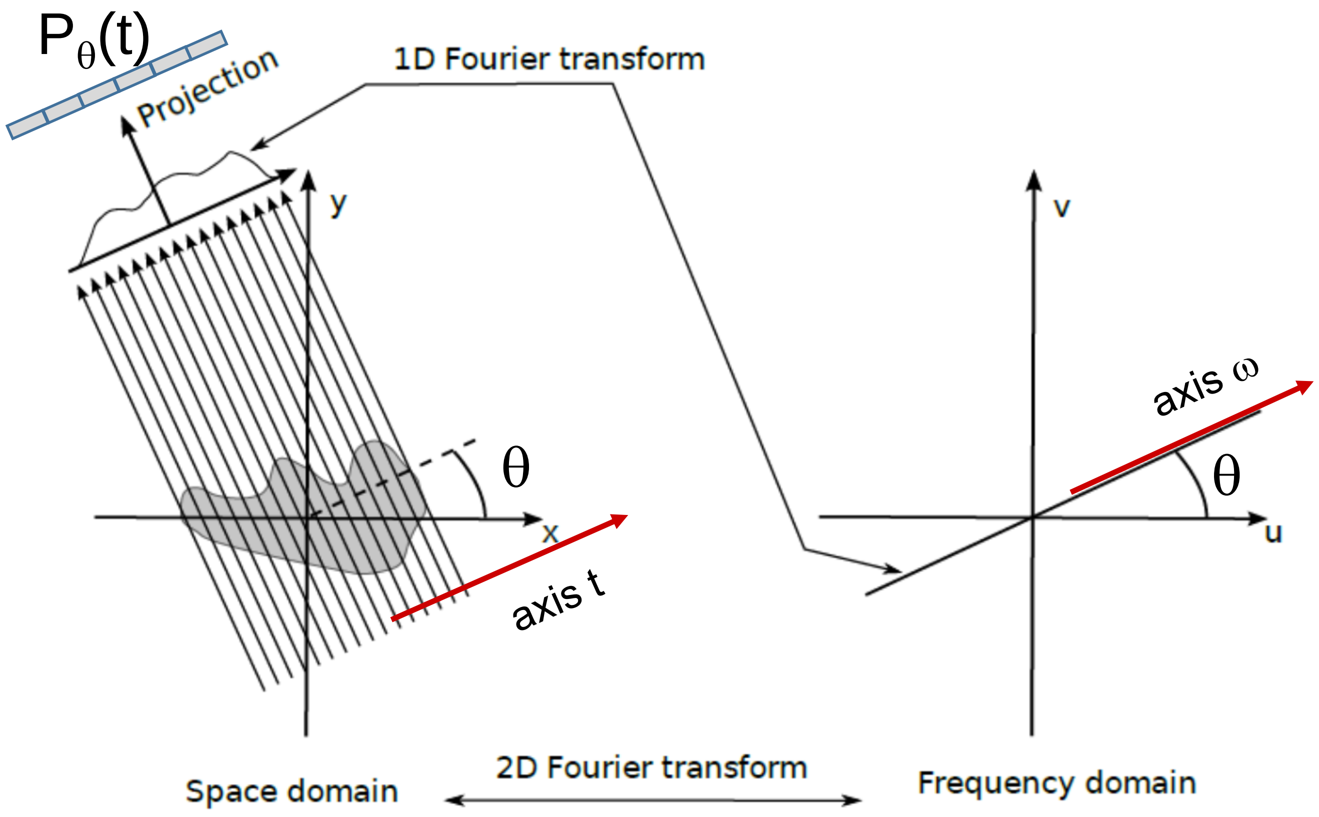

Filling up the frequency domain: measurement at multiple angles

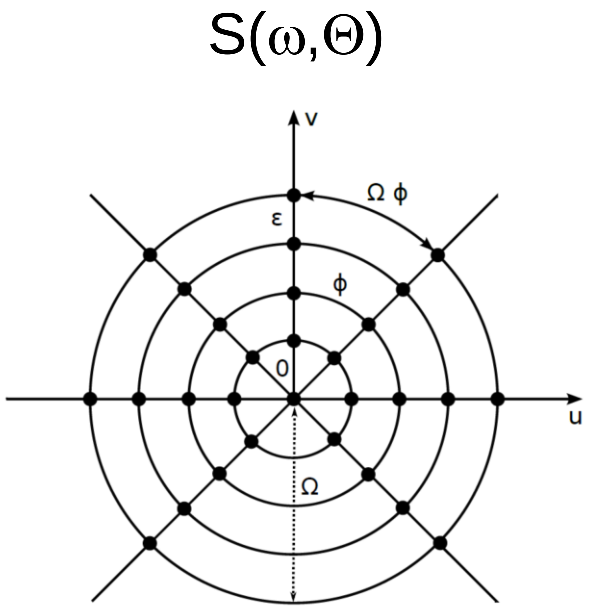

Image reconstruction step-by-step

Reverse transformation to the space domain:

- from interpolated mesh data
- inverse 2D Fourier transform

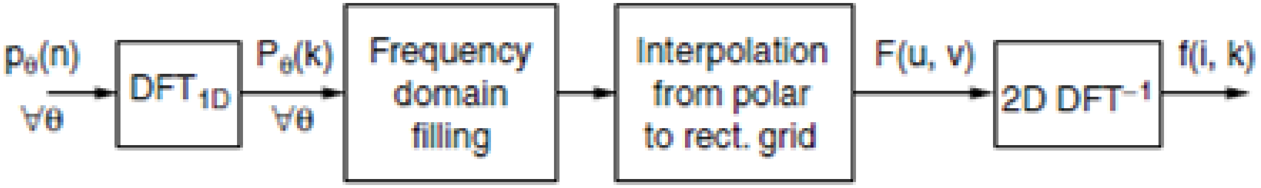

(a)

$S(\omega,\Theta) \rightarrow S(u,v)$

$$\mu(x,y) = \int_{-\infty}^{+\infty}\int_{-\infty}^{+\infty} S(u,v)\, e^{2\pi i(ux+vy)}\, du\, dv$$

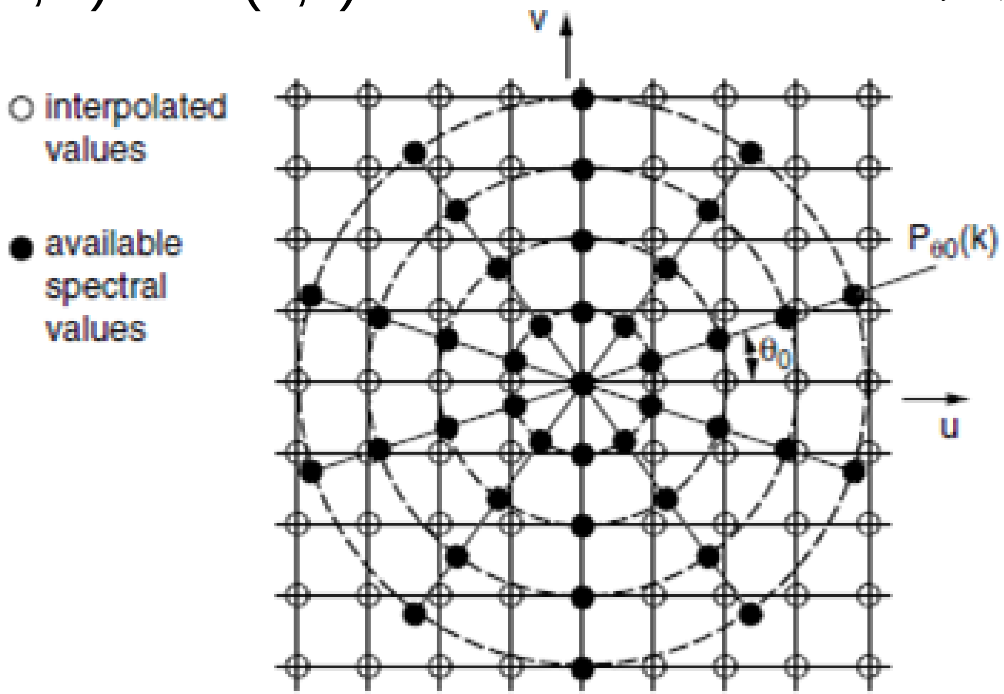

(b)

BUT:

- Direct reverse transformation is too slow
- Cannot measure infinite number of projections to fill up the Fourier space
- There is always noise, scattering
- We need filters: Filtered Backprojection (FBP)
- $S(\omega,\theta) \rightarrow S(u,v)$, and weight by $|\omega|$ (ramp filter)

Image processing in tomography

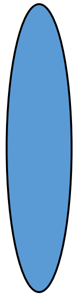

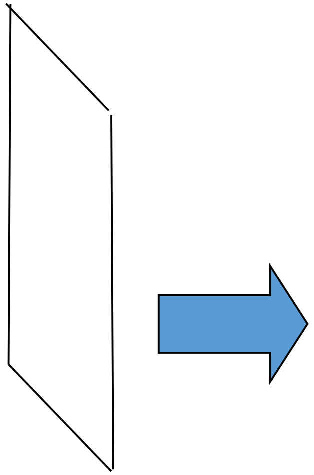

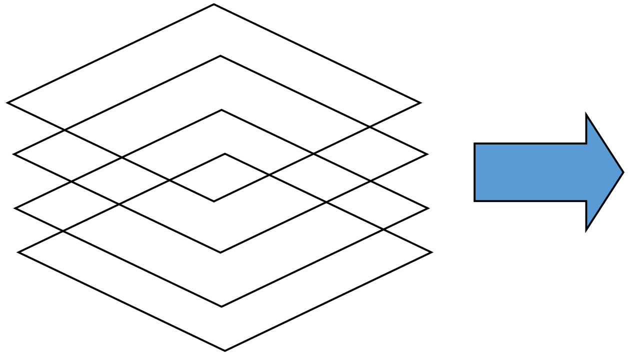

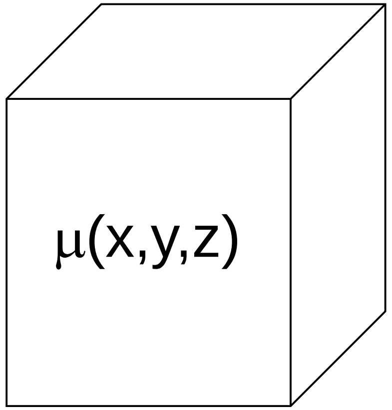

Object

$P_\theta(t)$
Projections at multiple angles

$\mu(x,y)$
Slices of the object

Visualization in the 3D space

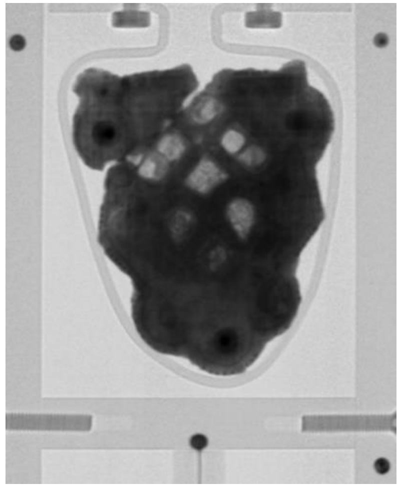

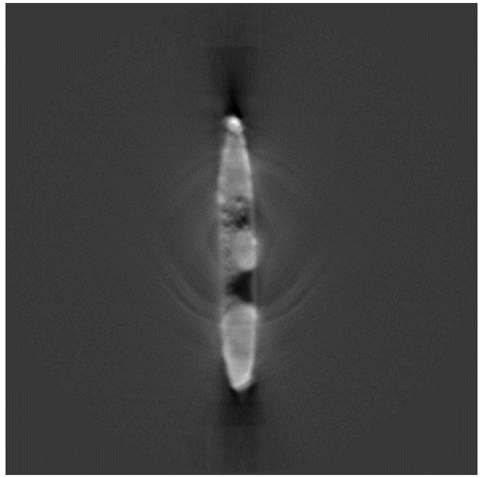

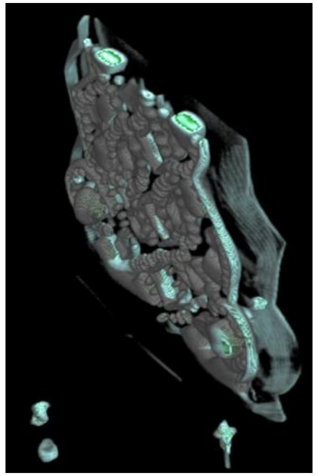

3D visualization with „Volume rendering”

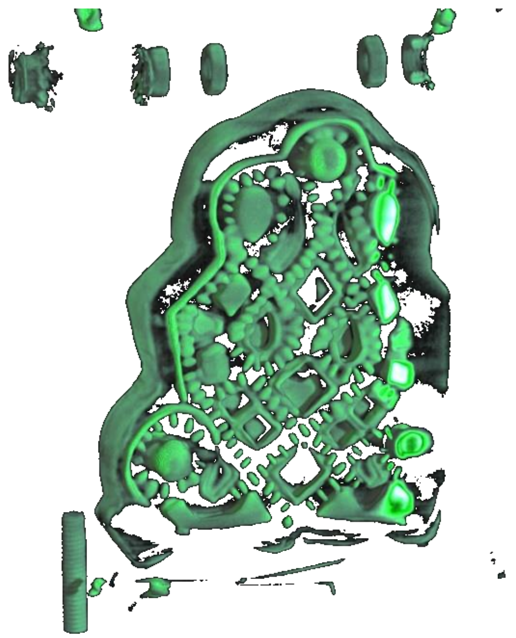

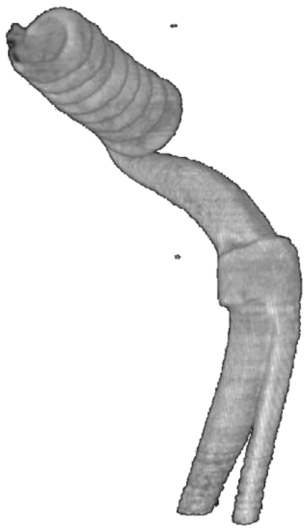

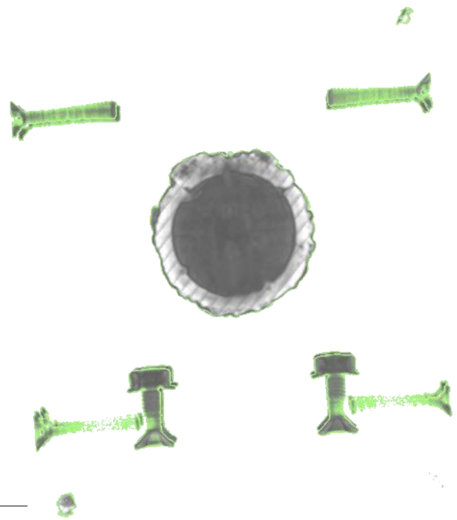

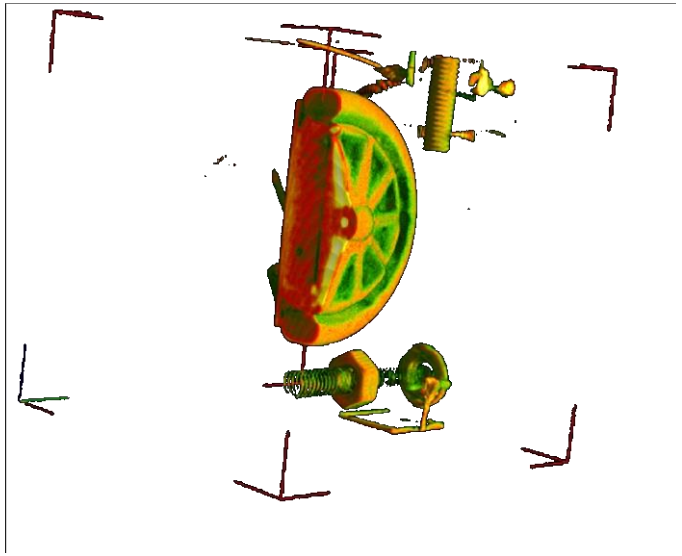

Disk fibula with garnet inlays

Merowingian style iron belt buckle

Data processing

Data processing can be a very labor- and computationally intense task

Image referencing

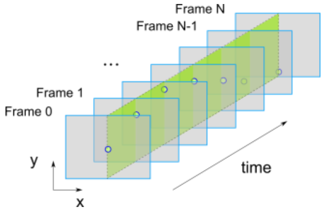

Minutes, hours

3D reconstruction

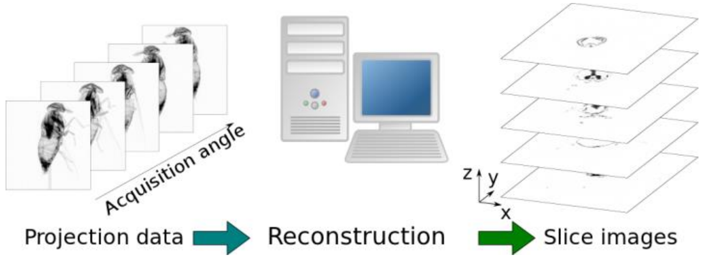

Minutes, hours

Image processing

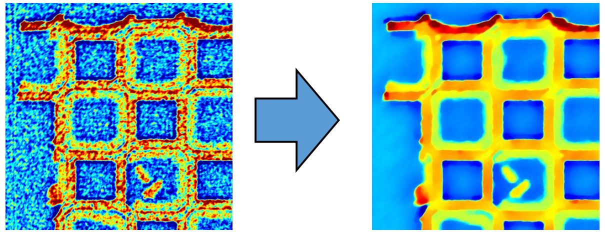

Hours

Visualization
Analysis

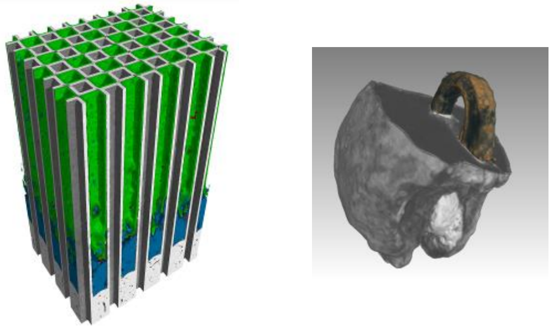

Hours, days

IAEA – PSI tomography contrast phantom

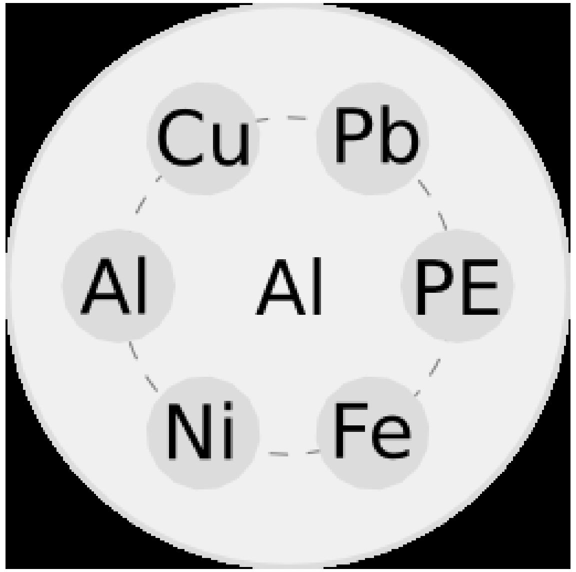

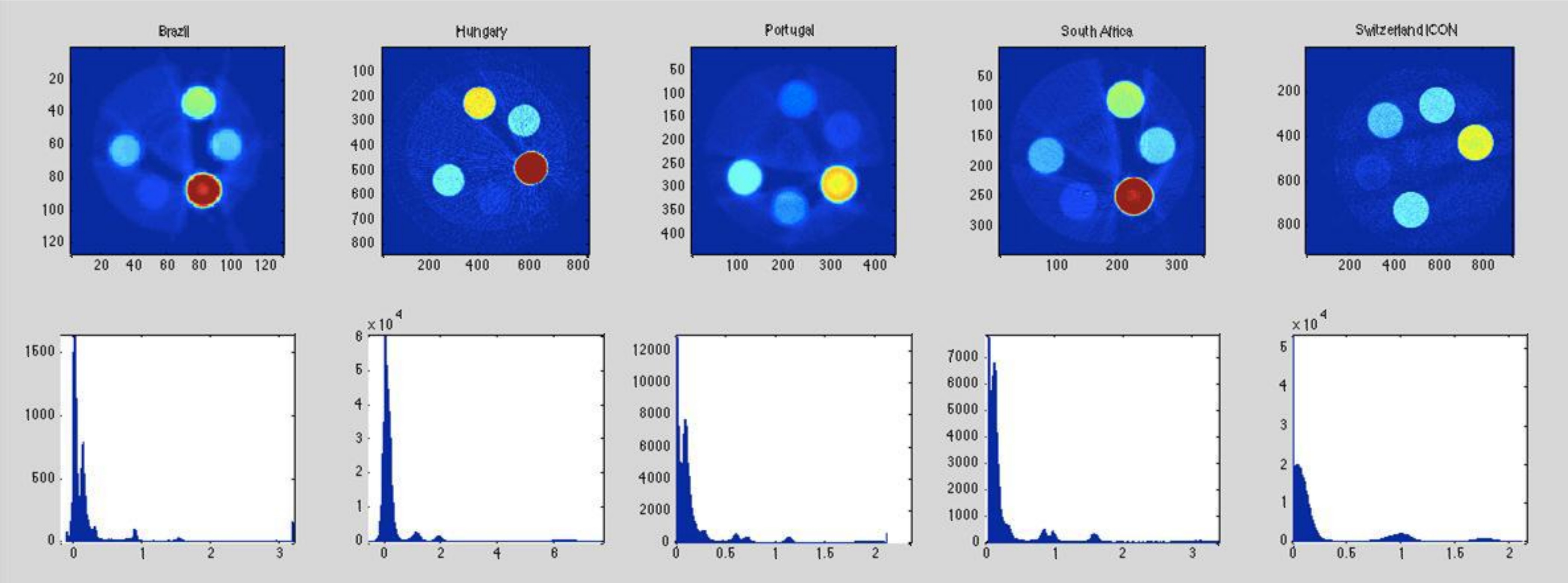

IAEA – PSI 3D resolution phantom

Iron blocks with Al placeholder sheets inbetween

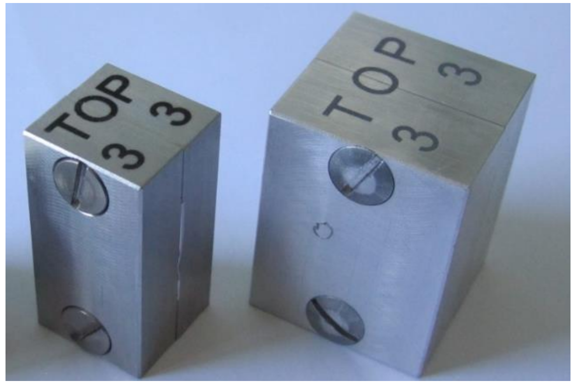

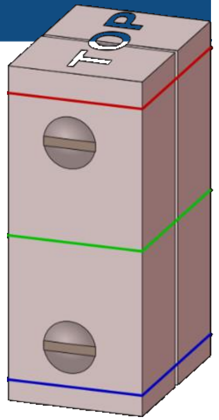

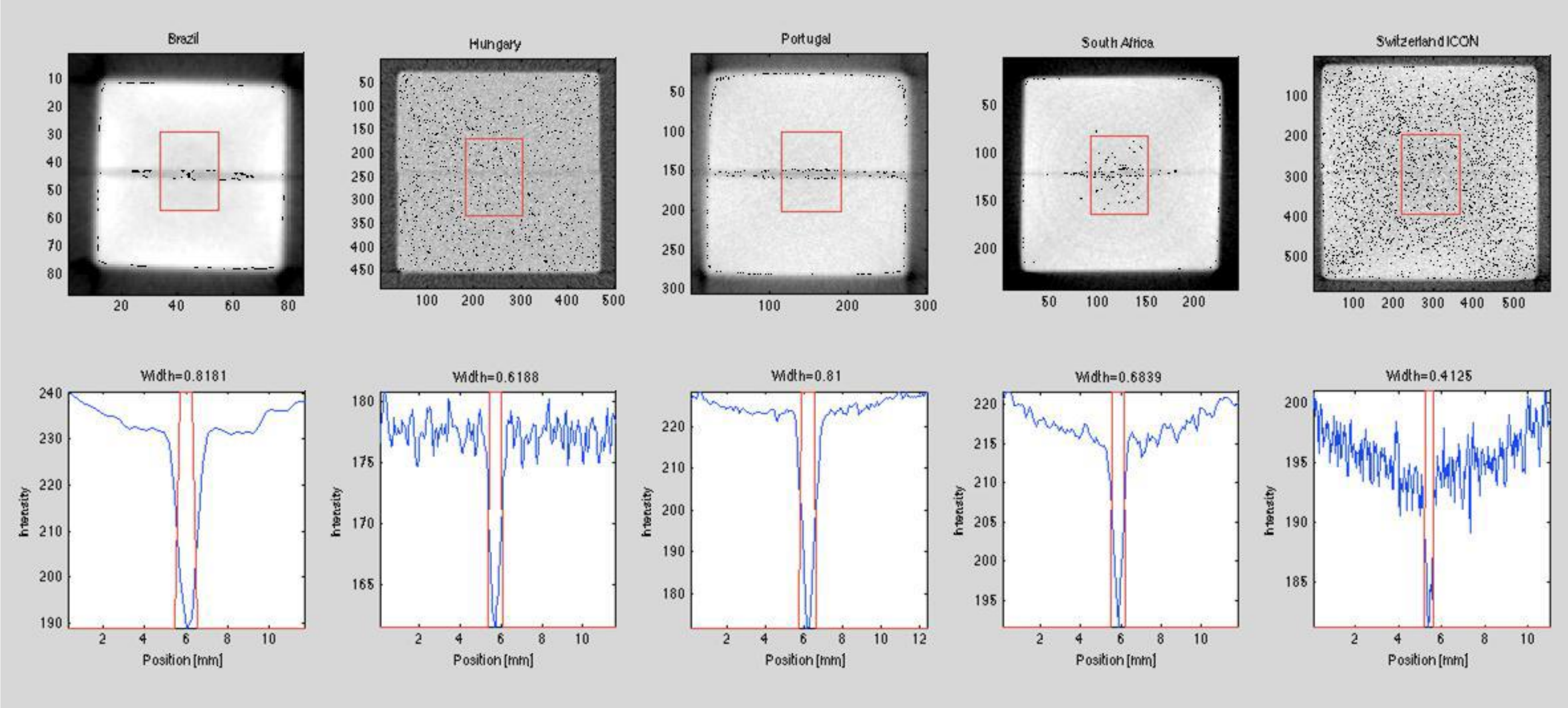

PSI 3D resolution phantom: pile of Ti spheres

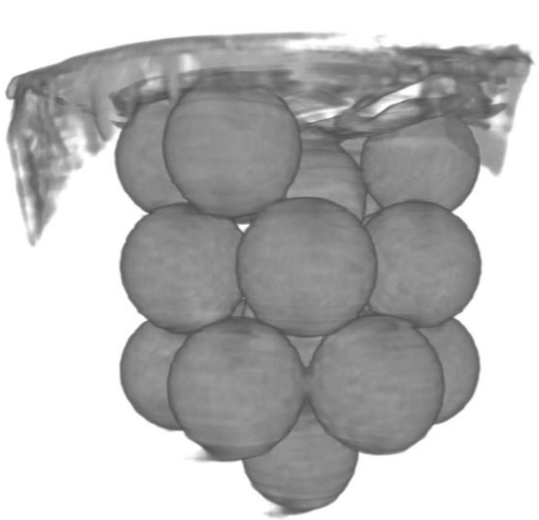

a: Ø4.997 mm

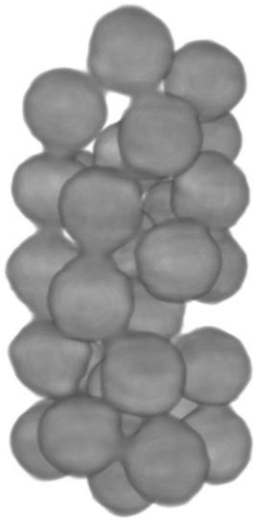

b: Ø2.09 mm

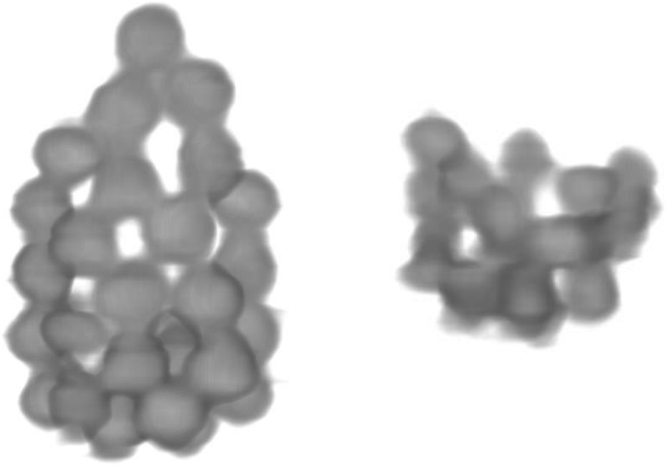

c: Ø1.00 mm and Ø0.704 mm

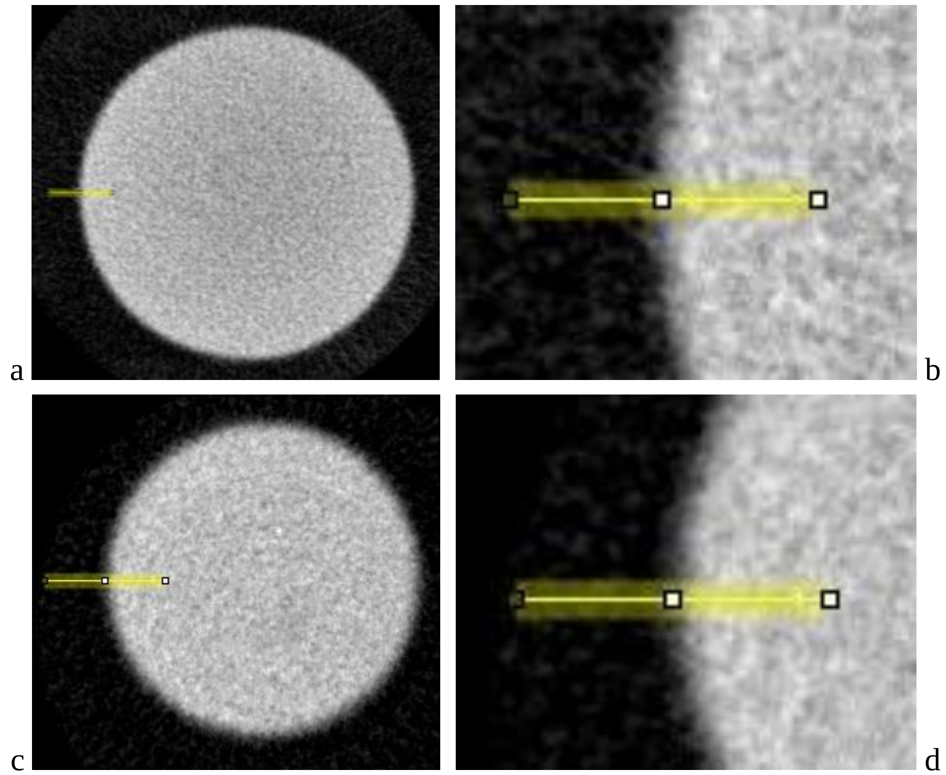

Budapest Neutron Centre
Centre for Energy Research

State-of-the-art European facilities

BNC
Budapest Neutron Centre

BUDAPEST RESEARCH REACTOR
1959 2019
60 YEARS OF RESEARCH & INNOVATION

RR application-oriented functions

Application	Number of RR involved	Involved / Operational, %	Number of countries
Education & Training	161	67	51
Neutron Activation Analysis	122	51	54
Radioisotope production	90	37	44
Neutron radiography	**68**	**28**	**40**
Material/fuel testing/irradiations	60	25	25
Neutron scattering	48	21	32
Nuclear Data Measurements	42	18	20
Gem coloration	36	15	22
Si doping	35	15	22
Geochronology	26	11	21
Neutron Therapy	20	8	13
Other	95	40	29

IAEA Research Reactor Database – D. Ridikas

Centre for Energy Research

Neutron imaging facilities around the world

Budapest Neutron Centre

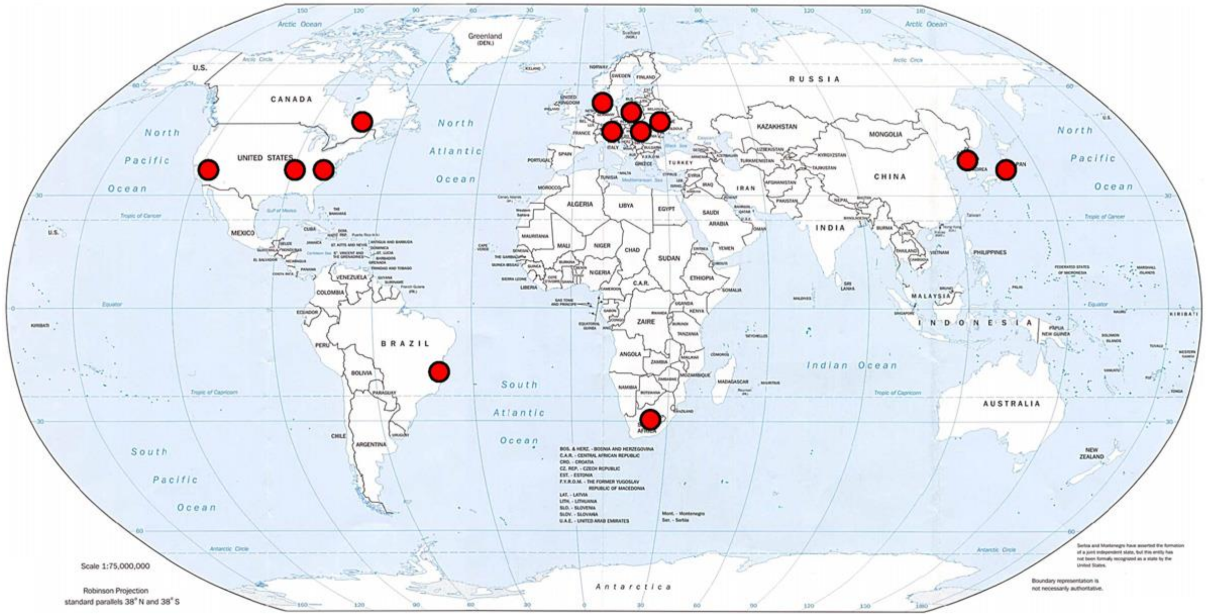

Table 2
Neutron imaging facilities with state-of-the-art properties and conditions (without claim for completeness); given parameters are raw values that can be varied only by changing beam conditions.

Country	Location	Institution	Facility	Neutron source	Thermal/cold flux ($cm^{-2}\,s^{-1}$)	*L*/*D* ratio	Field of view
Austria	Vienna	Atominstitut	Imaging beam line	TRIGA Mark-II, 250 kW	1.00E+05	125	90 mm diam.
Brazil	Sao Paulo	IPEN	Imaging beam line	IEA-R1M 5 MW	1.00E+06	110	25 cm diam.
Germany	Garching	TU Munich	ANTARES	FRM-II 25 MW	9.40E+07	400	32 cm diam.
Germany	Garching	TU Munich	NECTAR	FRM-II 25 MW	3.00E+07	150	20 cm diam.
Germany	Berlin	HZB	CONRAD	BER-II 10 MW	6.00E+06	500	10 cm × 10 cm
Hungary	Budapest	KFKI	Imaging beam line	WRS-M 10 MW	6.00E+05	100	25 cm diam.
Japan	Osaka	Kyoto University	Imaging beam line	MTR 5 MW	1.20E+06	100	16 cm diam.
Japan	Tokai	JAEA	Imaging beam line	JRRM-3M 20 MW MTR	2.60E+08	125	25 cm × 30 cm
Korea	Daejon	KAERI	Imaging beam line	HANARO 30 MW	1.00E+07	190	25 cm × 30 cm
Switzerland	Villigen	PSI	NEUTRA	SINQ spallation source	5.00E+06	550	40 cm diam.
Switzerland	Villigen	PSI	ICON	SINQ spallation source	1.00E+07	350	15 cm diam.
USA	Pennsylvania State University	University	Imaging beam line	TRIGA 2 MW	2.00E+06	100	23 cm diam.
USA	Gaithersburg	NIST	CNR	NBSR 20 MW	2.00E+07	500	25 cm diam.
USA	Sacramento	McCleallan RC	Imaging beam line	TRIGA 2 MW	2.00E+07	100	23 cm diam.
South Africa	Pelindaba	NECSA	SANRAD	SAFARI-1 20 MW	1.60E+06	150	36 cm diam.

E. Lehmann

NEUTRA @ PSI – Thermal neutrons

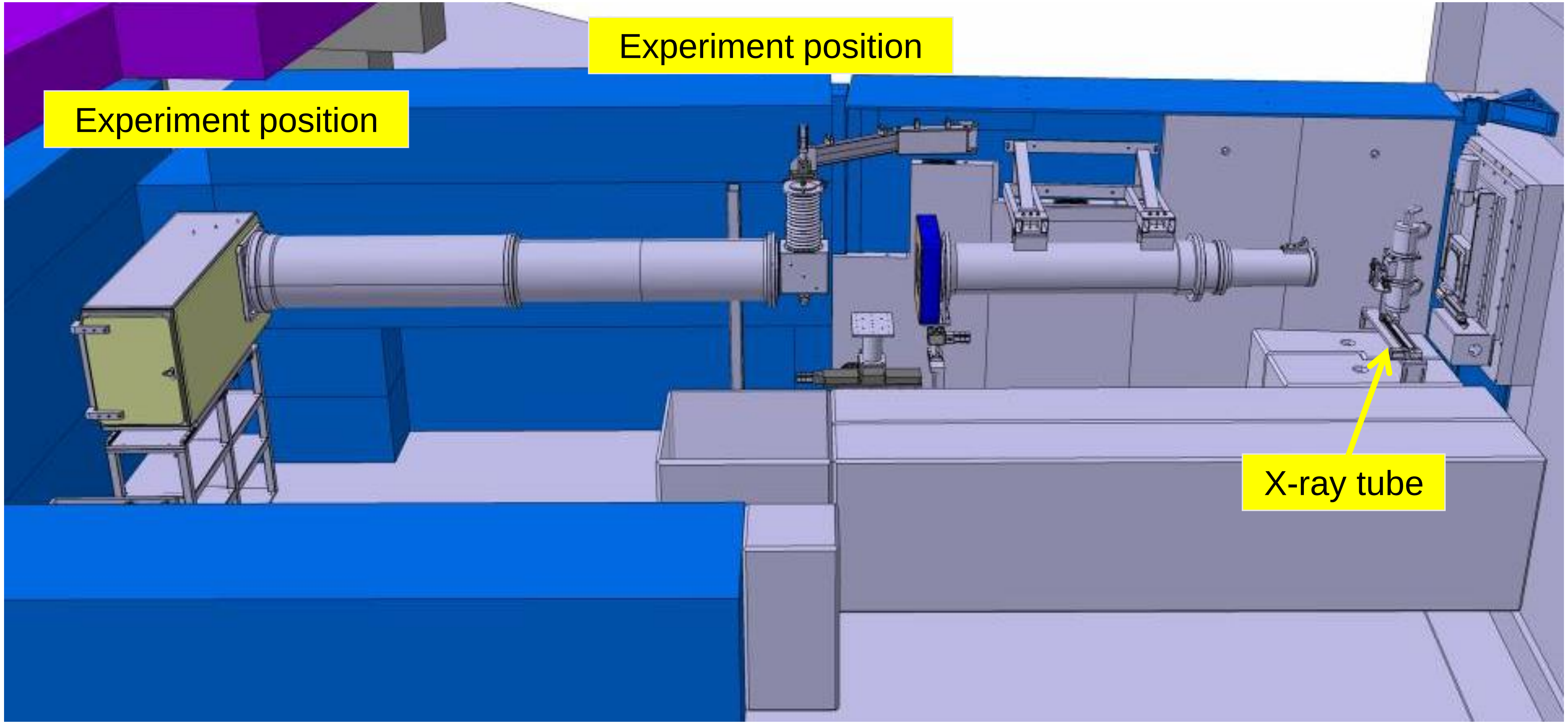

NEUTRA: NEUtron Transmission RAdiography

ICON @ PSI – Cold neutrons

ICON: Imaging with COld Neutrons
Extreme good resolution (25 μm) for small objects

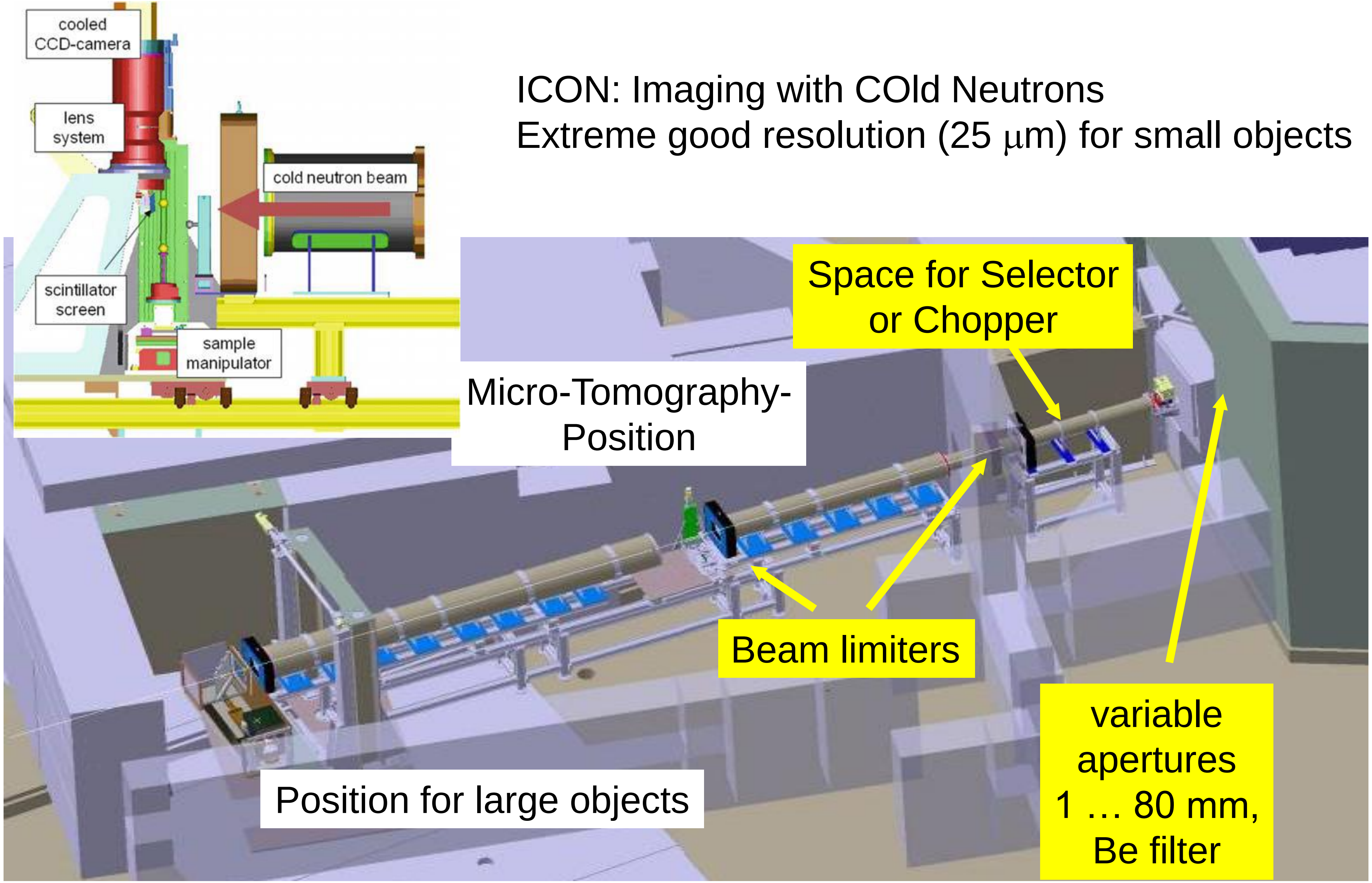

Antares II @ FRM-II

- Beam accessible along flight path
- More possibilities than ANTARES I
- Higher flexibility
- New & lighter shielding material
- Space for experiments & sample environment
- All components on rail system
- He-filled flight tubes,
- Highly flexible concept for moving, combining parts and removing parts from the flight tube

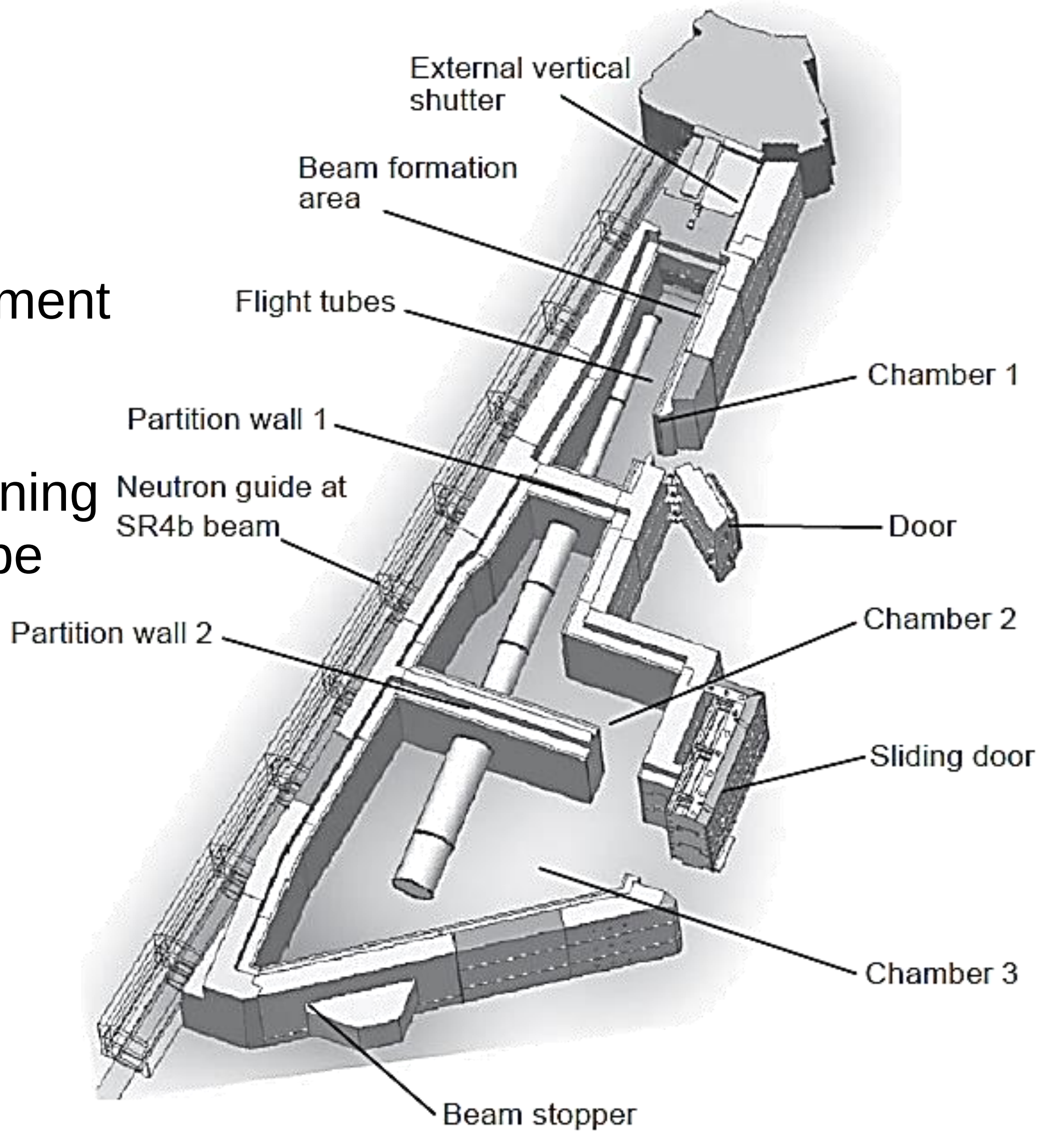

Fig. 5. View of ANTARES II with main components.

Fast neutron imaging with a uranium converter

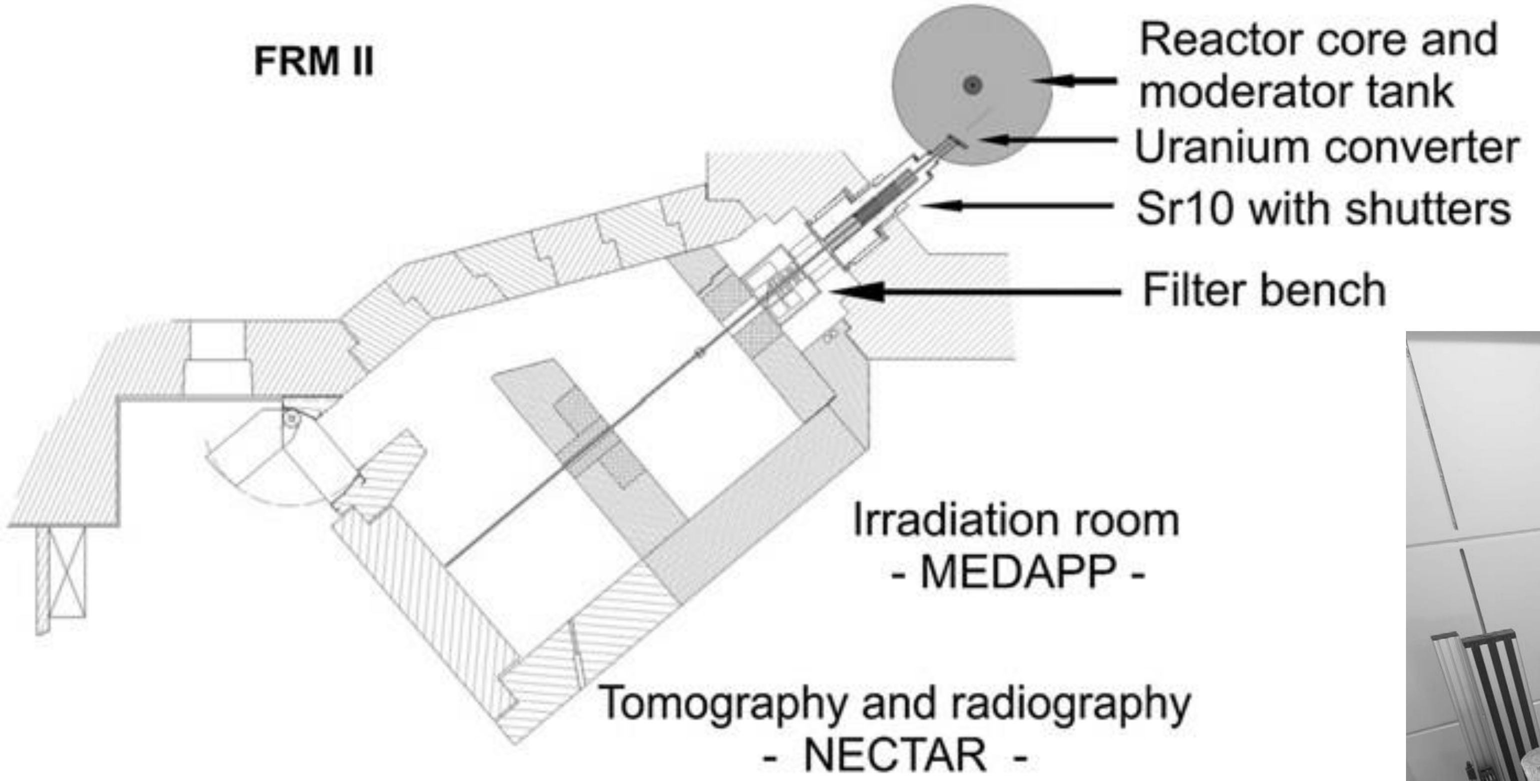

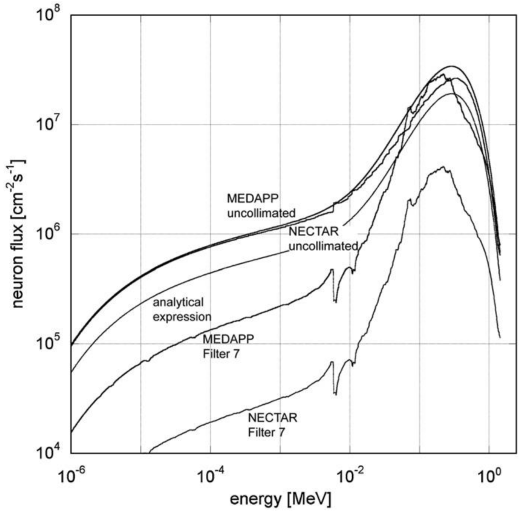

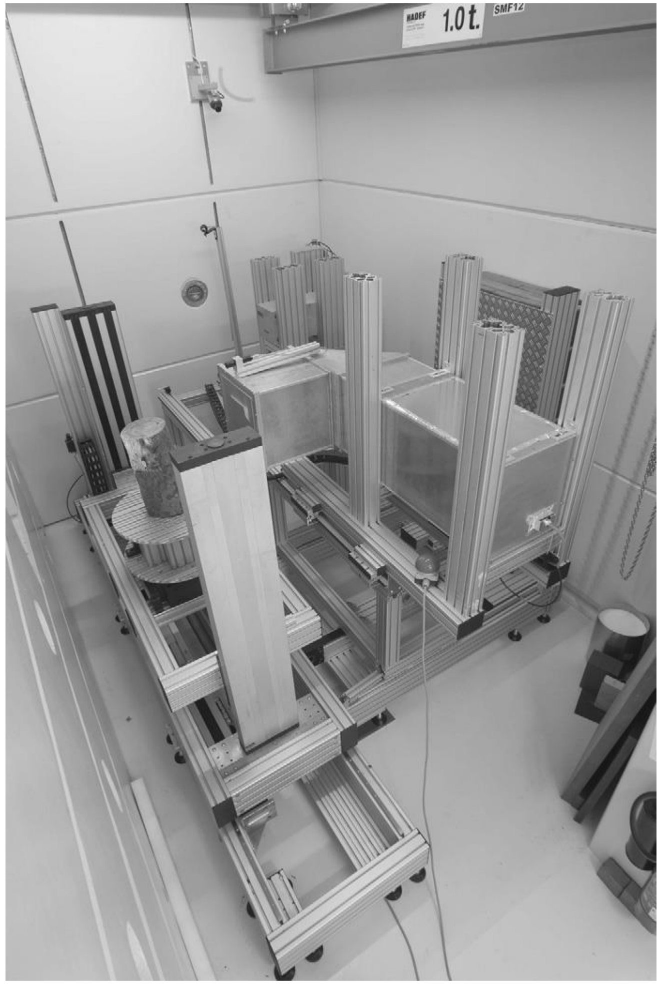

T. Bücherl (2011)

ILL NeXT: Neutron and X-ray Tomography

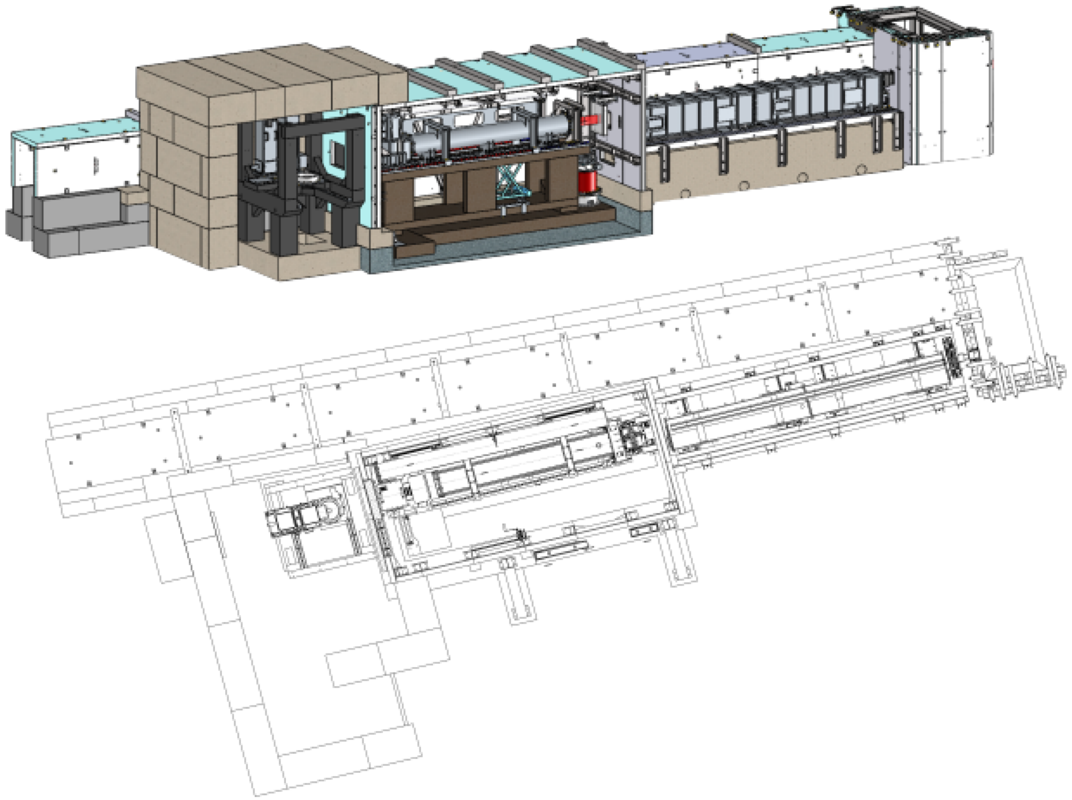

- Beamline D50
- 2D and 3D neutron imaging with a field of view of up to 170x170 mm^2, and real pixel resolution of 10 microns.
- Complementary 2D and 3D X-ray imaging with a field of view of 250x300 mm^2, and real pixel resolution of 5 microns.

ODIN @ ESS (from year ?)

- approved in 2013 as one of the three first instruments for construction at the European Spallation Source, Lund, Sweden
- unique combination of high flux and specific time structure (energy-selective imaging)
- Novel event-based imaging detectors not to waste valuable neutrons

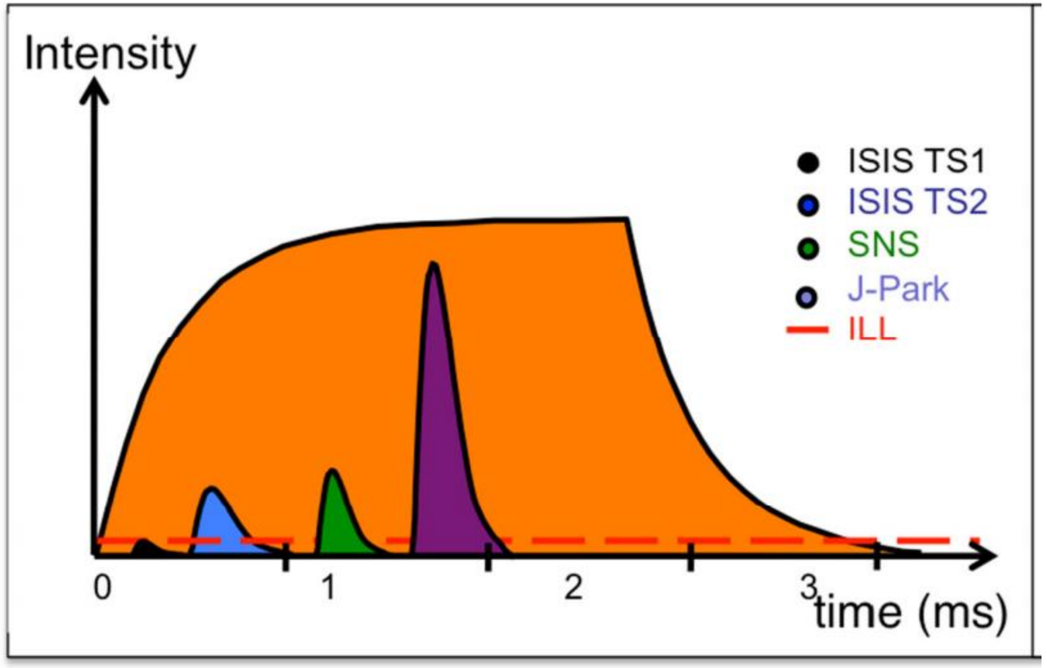

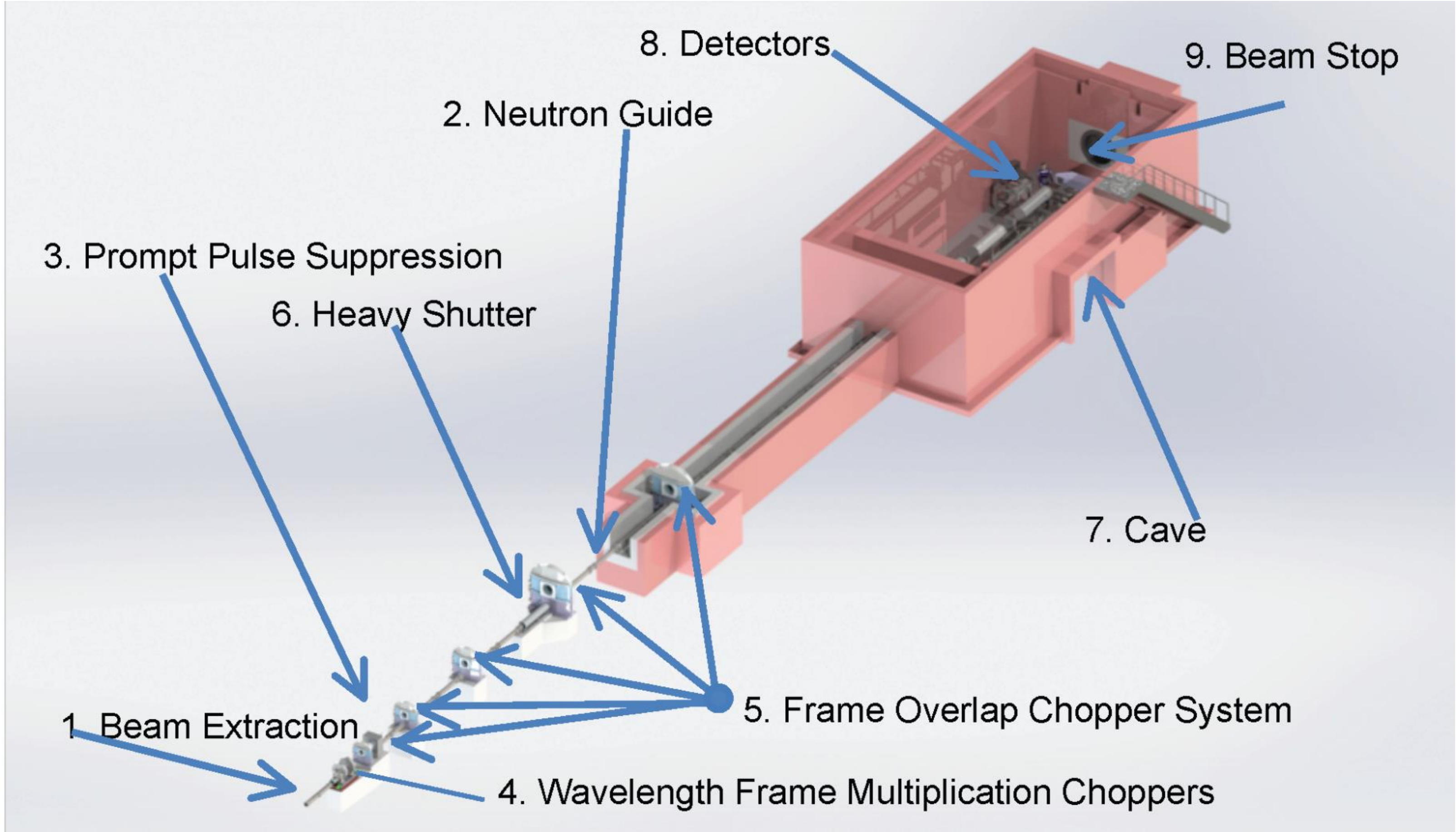

BNC Neutron imaging facilities

Budapest Research Reactor (10 MW)

NORMA

RAD

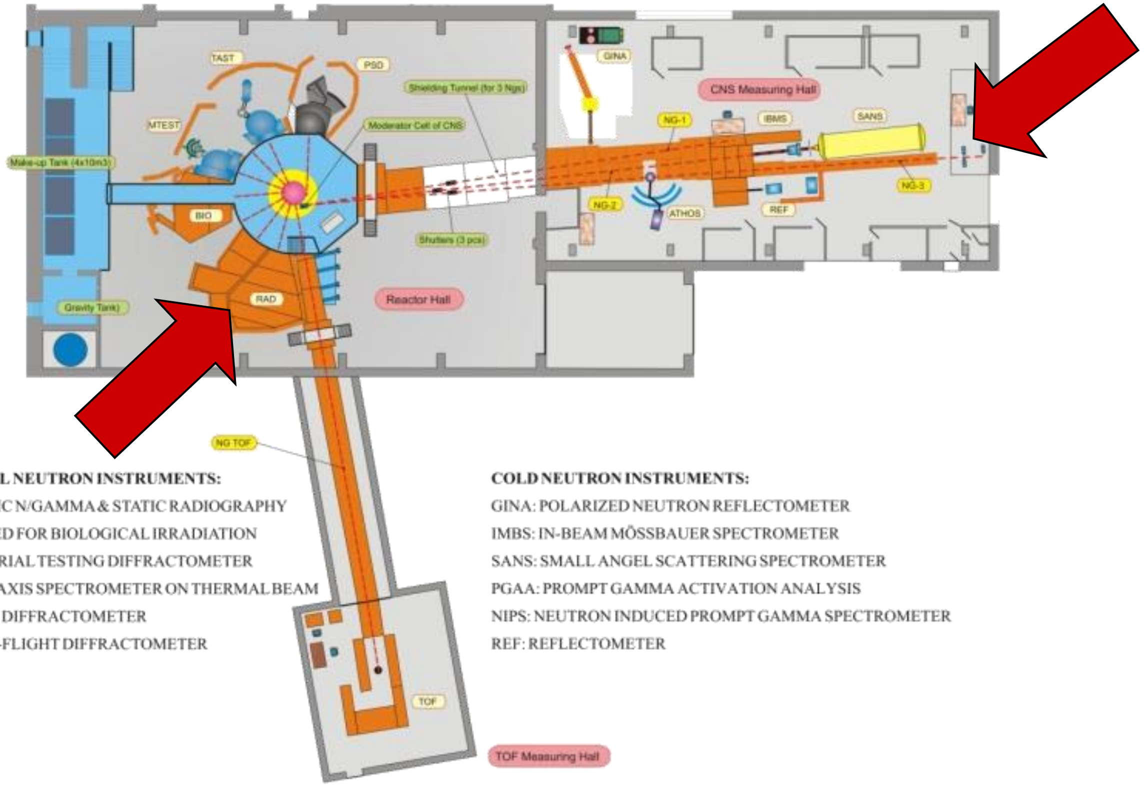

TRADITIONAL NEUTRON INSTRUMENTS:
RAD: DYNAMIC N/GAMMA & STATIC RADIOGRAPHY
BIO: PORT USED FOR BIOLOGICAL IRRADIATION
MTEST: MATERIAL TESTING DIFFRACTOMETER
TAST: TRIPLE AXIS SPECTROMETER ON THERMAL BEAM
PSD: POWDER DIFFRACTOMETER
TOF: TIME-OF-FLIGHT DIFFRACTOMETER

COLD NEUTRON INSTRUMENTS:
GINA: POLARIZED NEUTRON REFLECTOMETER
IMBS: IN-BEAM MÖSSBAUER SPECTROMETER
SANS: SMALL ANGEL SCATTERING SPECTROMETER
PGAA: PROMPT GAMMA ACTIVATION ANALYSIS
NIPS: NEUTRON INDUCED PROMPT GAMMA SPECTROMETER
REF: REFLECTOMETER

RAD @ BNC

Primary aperture to screen distance: 463 – 539 cm
Flux: 4.6 – 3.38 × 10^7 cm^{-2} s^{-1}
L/D = 170 – 195
Diameter: 195 – 230 mm
$\Phi_{subCd}/\Phi_{epi} = 52$

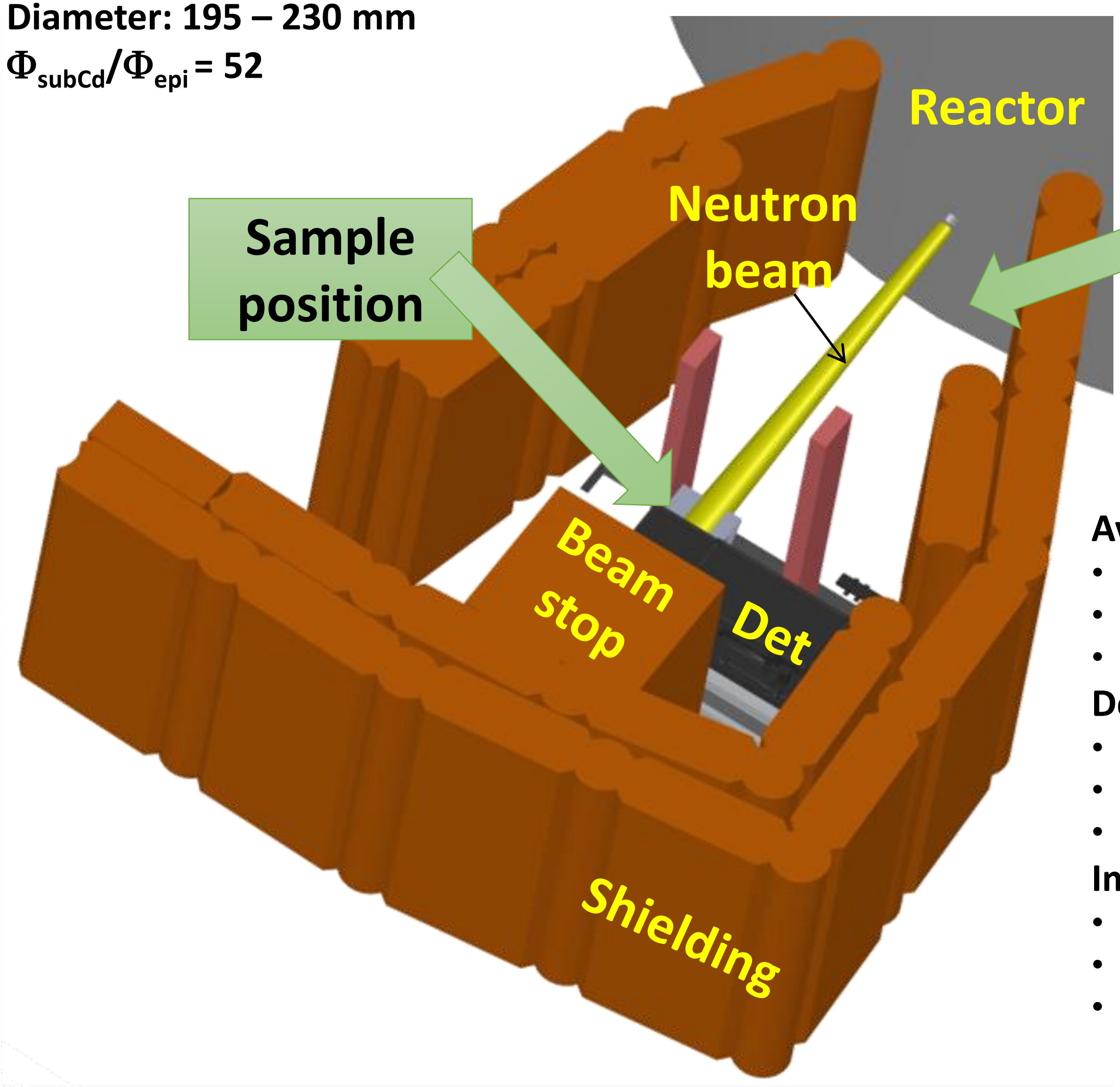

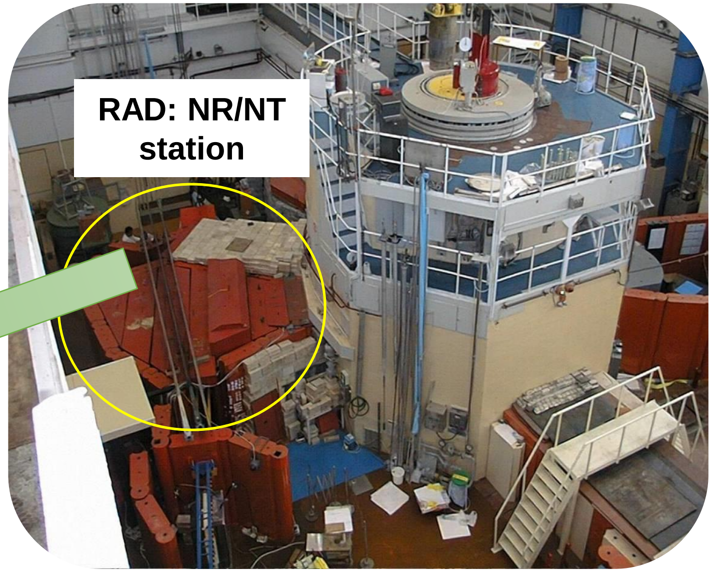

Available modalities:
- Thermal neutron
- Gamma beam: ~ 8.5 Gy/h
- X-ray tube: 25-225 keV, max. 10 mA

Detector options:
- 16-bit 4 Mpx sCMOS camera
- Highly sensitivity TV-camera
- Image plate

Imaging options:
- Radiography or Tomography of larger objects
- Small FOV, better resolution
- (Sapphire filter to get rid of fast neutrons)

Neutron, X-ray imaging at RAD

- static imaging:
  - radiography and tomography based on digital sCMOS camera (Andor Neo 5.5)
  - neutron: Li^6F/ZnS, Gadox; X-ray: Gadox; gamma-ray: NaI(Cs) crystal

- dynamic imaging:
  - radiography based on low-level-light analog TV camera (Vidicon tube) and digi

- different field of views:
  - 250×250 mm^2 (Sigma 50mm)
  - 100×100 mm^2 (Nikon 105mm)
  - 40×40 mm^2 (Nikon 300mm)

  - 60-250 μm spatial resolution
  - 1-35 s temporal resolution

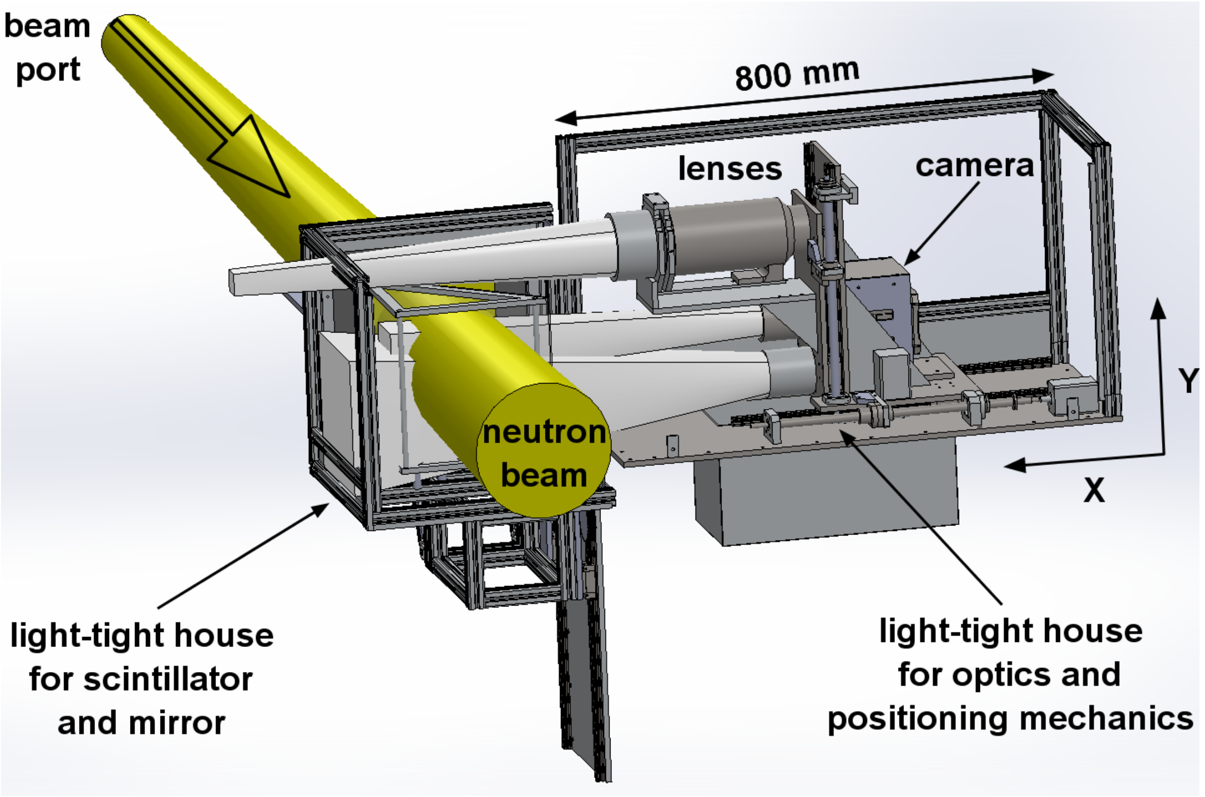

Neutron Optics and Radiography for Material Analysis (NORMA) with cold neutrons

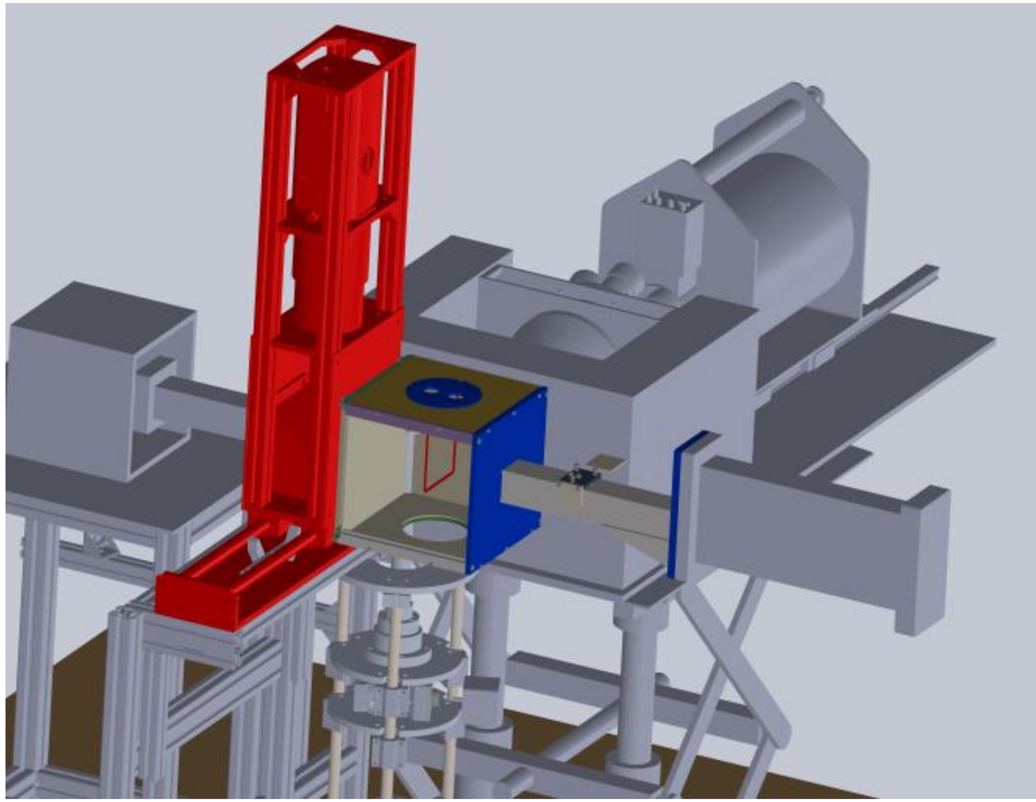

Combination of local element analysis by prompt gamma activation analysis

and

structure analysis by neutron radiography/tomography

Unique instrument

Commissioned in 2012 at the cold neutron guide hall

Flux: 2.7×10^7 cm^{-2} s^{-1}
Resolution: 230 μm
Field of view: 40x40 mm
L/D ratio: 233

Variable L/D ratio at NIPS-NORMA

- Higher L/D through less D's:
  - Changeable primary apertures at the end of the neutron guide
  - Available sizes: 550 mm^2 (25×22 mm^2), 121.54 mm^2 (Ø12.44 mm), 9.95 mm^2 (Ø3.54 mm)
  - L/D values measured by Gd-foil edge method: 233, 500, 1800

- More uniform neutron flux distribution using scatterers:
  - Changeable graphite scatterer sheets upstream to primary apertures
  - Available thicknesses: 3 mm, 2 mm and no scatterer in the beam

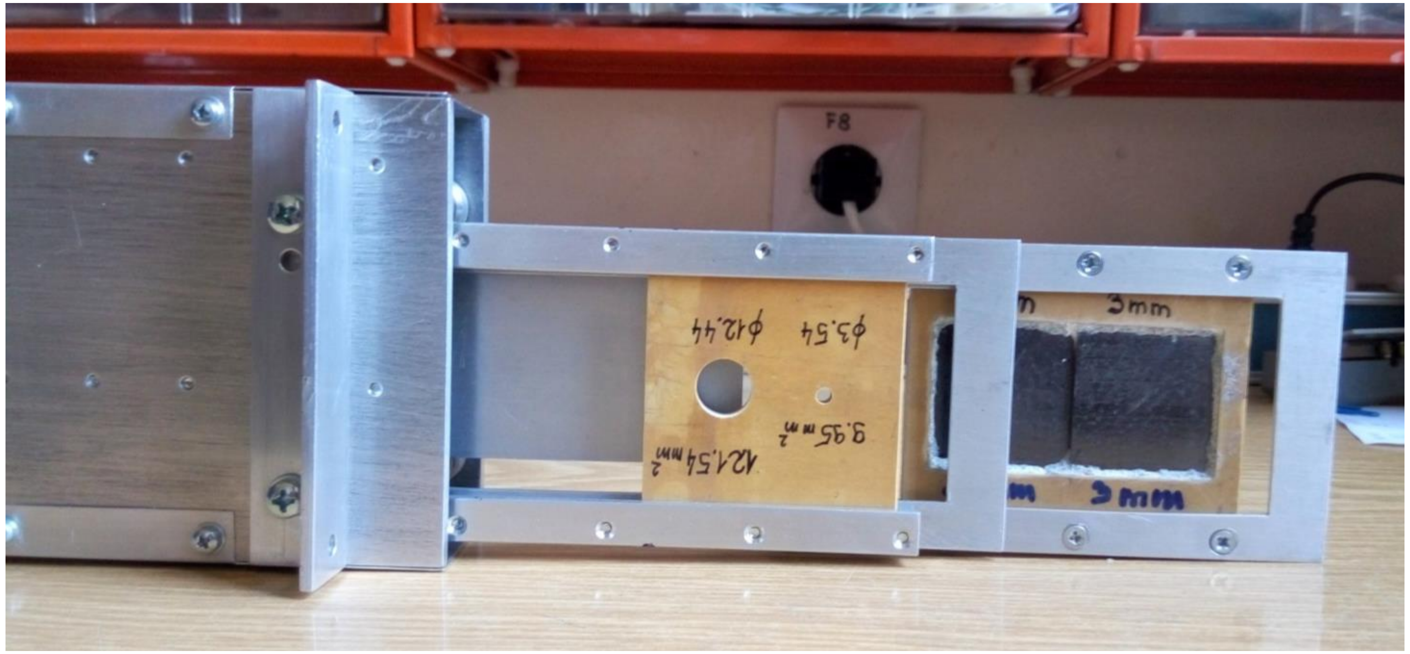

Variable L/D ratio at NIPS-NORMA

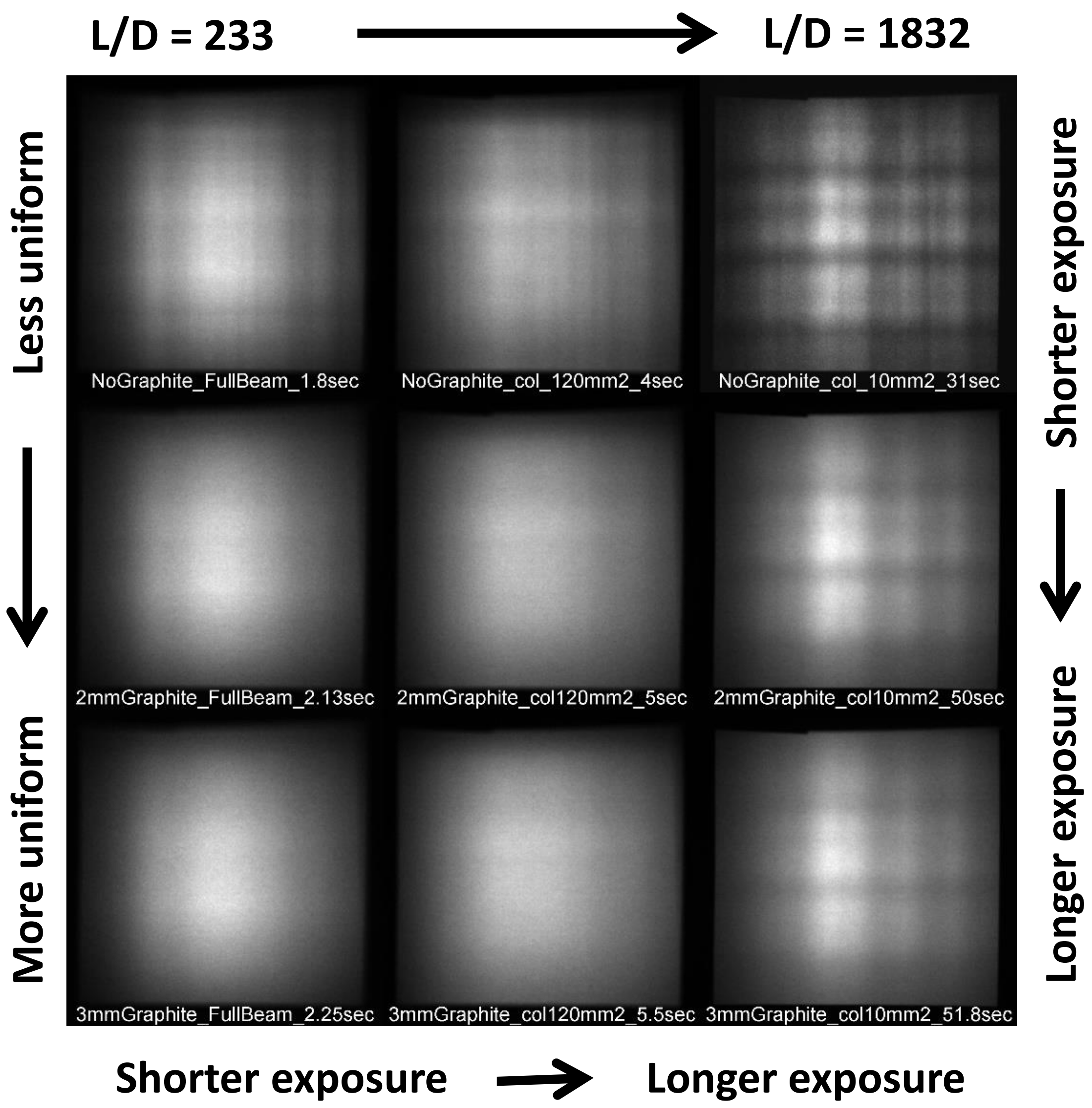

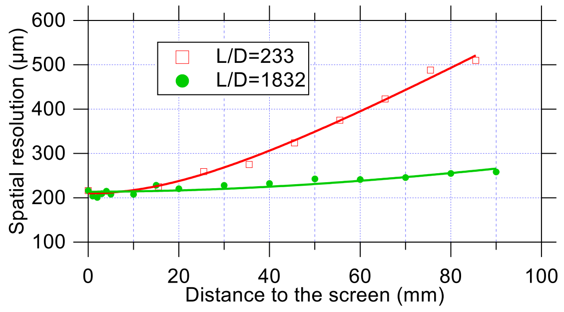

- Advantages:
  - Better spatial resolution farther from the screen (tomography of larger objects!)
  - More uniformly irradiated field of view
- Disadvantages:
  - Longer exposure times

Applications

Breakdown of use

Which methods are used mostly in present applications?

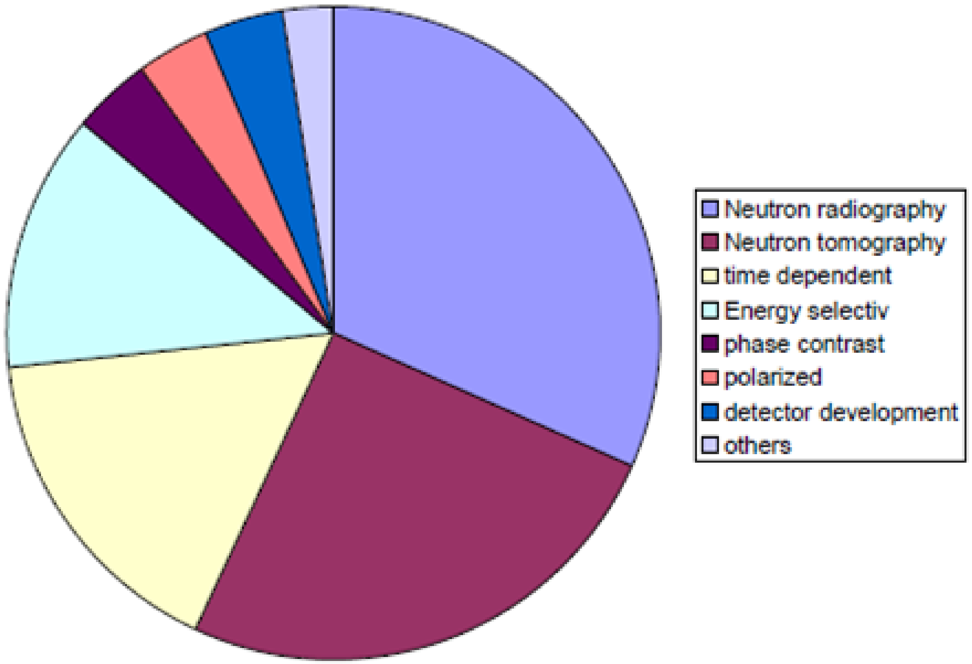

What are the specific requests for the improvement of the existing facilities?

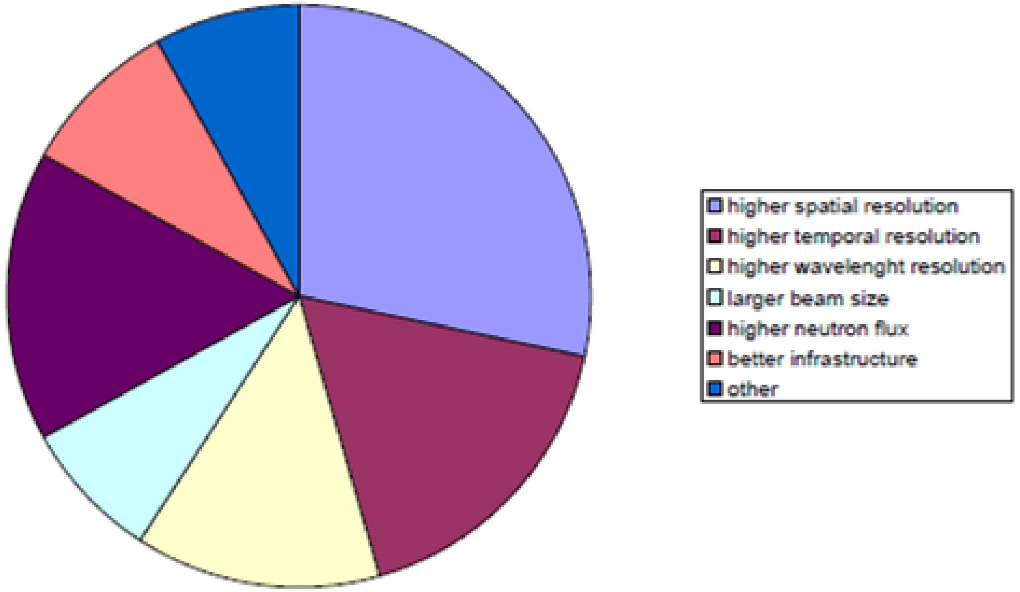

http://europeanspallationsource.se/sites/default/files/nius_2012.pdf

Applications: science + industry

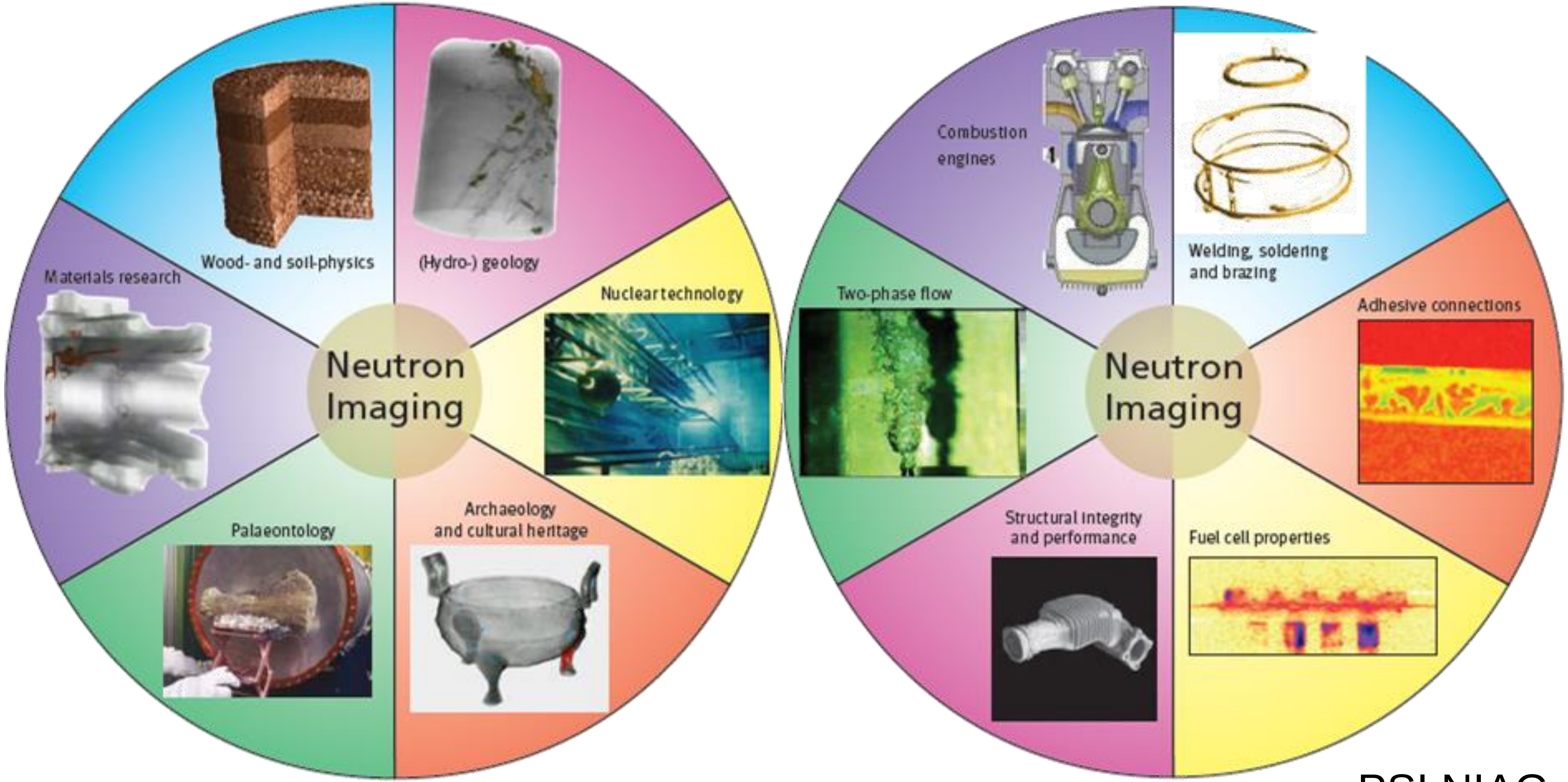

PSI NIAG

Proof of meteoritic origin of mankind's earliest (?) iron artefacts, 3200 BC, by neutron and X-ray techniques

A predynastic cemetery was excavated near Gerzeh by **G.A. Wainwright** and **J.P. Bushe-Fox** in **1911**

Principal Proposer: Thilo Rehren – UCL London

Iron beads at NORMA

- to be determined the nature of the iron from which these earliest iron beads are made - can we demonstrate that they are meteoritic in origin, as has been speculated based on their early date?
- All three artefacts have a central hole along their long axis, not visible during visual inspection due to their corrosion. It demonstrate that the beads were made from rolled iron sheet, with areas of overlapping metal visible at the centre of the seam UC10740.
- This would have required repeated hammering with intermittent annealing.

Properties of The Petrie Museum of Egyptian Archaeology, London

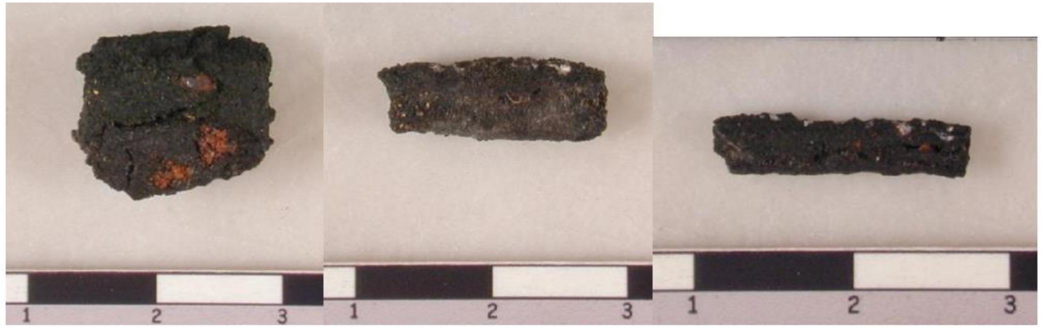

Fig. 1: Beads UC10738 (left), UC10739 (centre) and UC10740 (right). Scale in cm.

One of the beads had been analysed in the 1920s and found to contain about 7.5 wt% Ni

Rehren et al, Journal of Archaeological Science **40** (2013) 4785-4792

Mankind's earliest iron beads were the very first images of NORMA

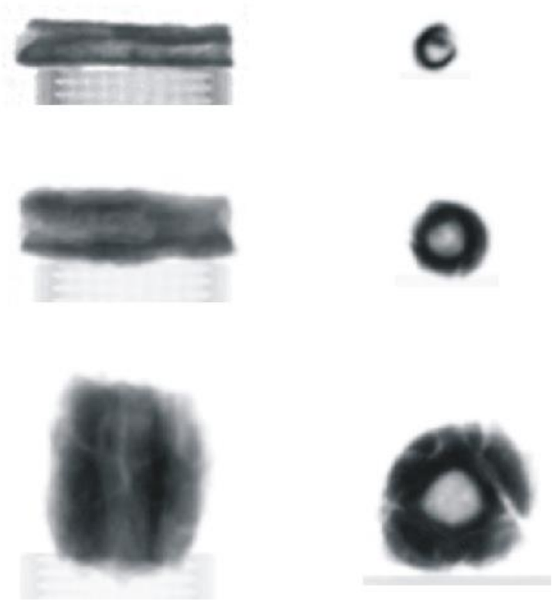

Egyptian Vase from the Pharao age

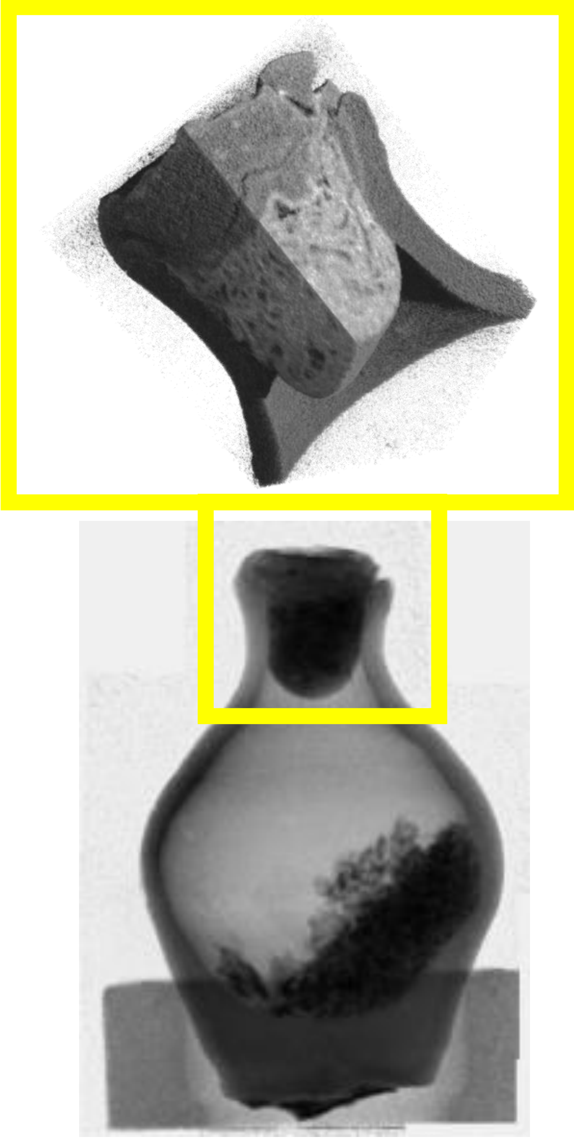

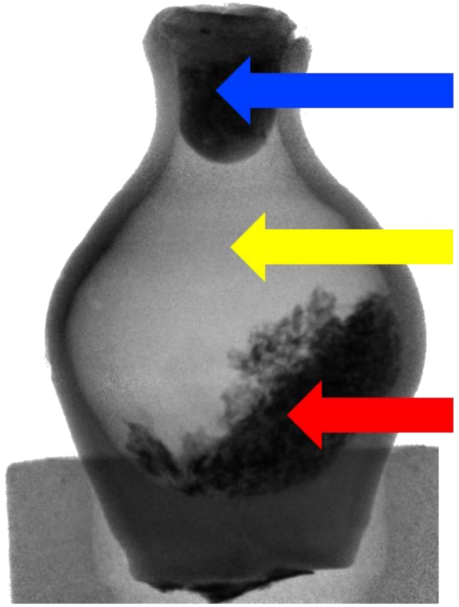

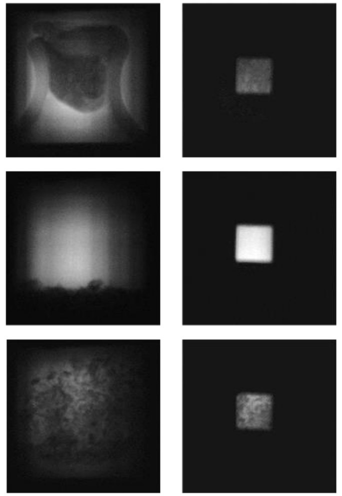

Full beam

10×10 mm^2 beam for PGAI

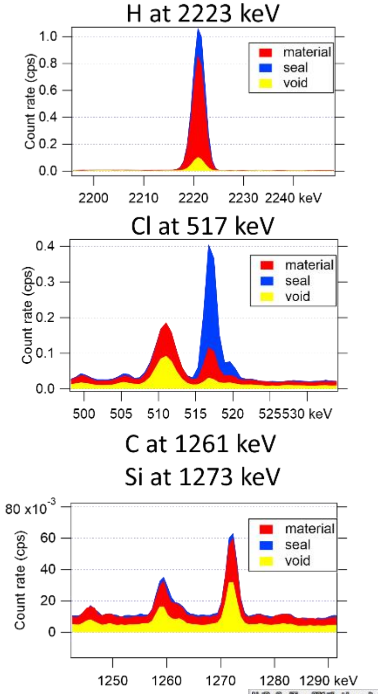

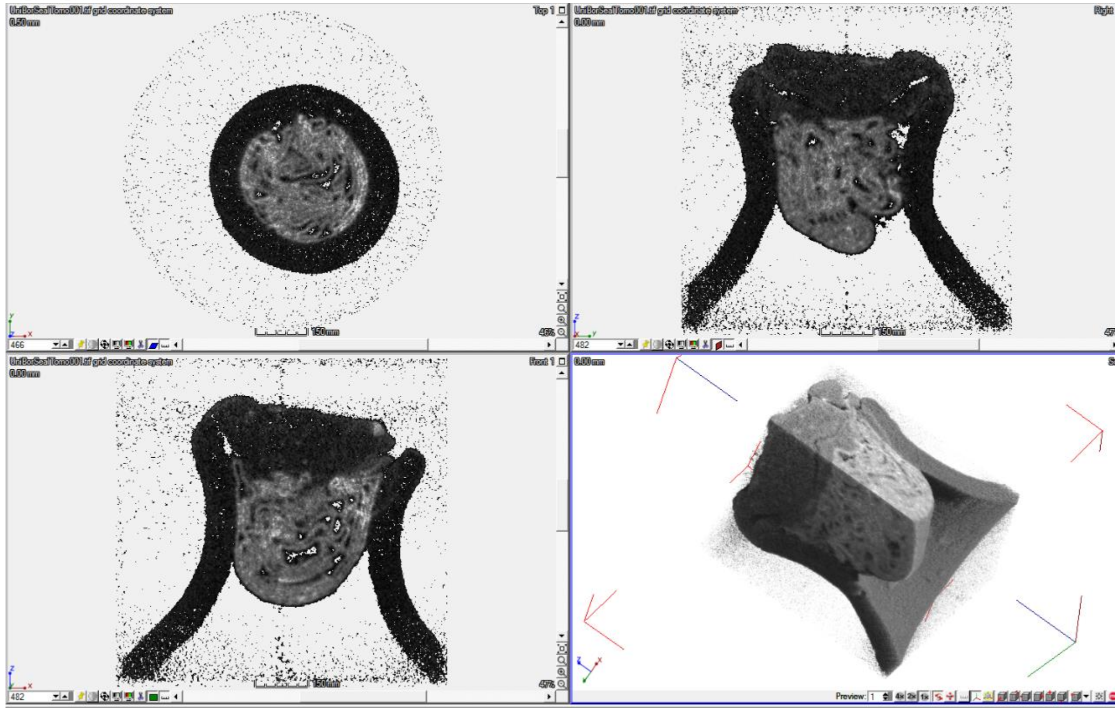

E. Abraham et al, Appl. Phys. A (2014) 117:963–972
DOI 10.1007/s00339-014-8779-3

Bronze Monkey - Visualization of regions with

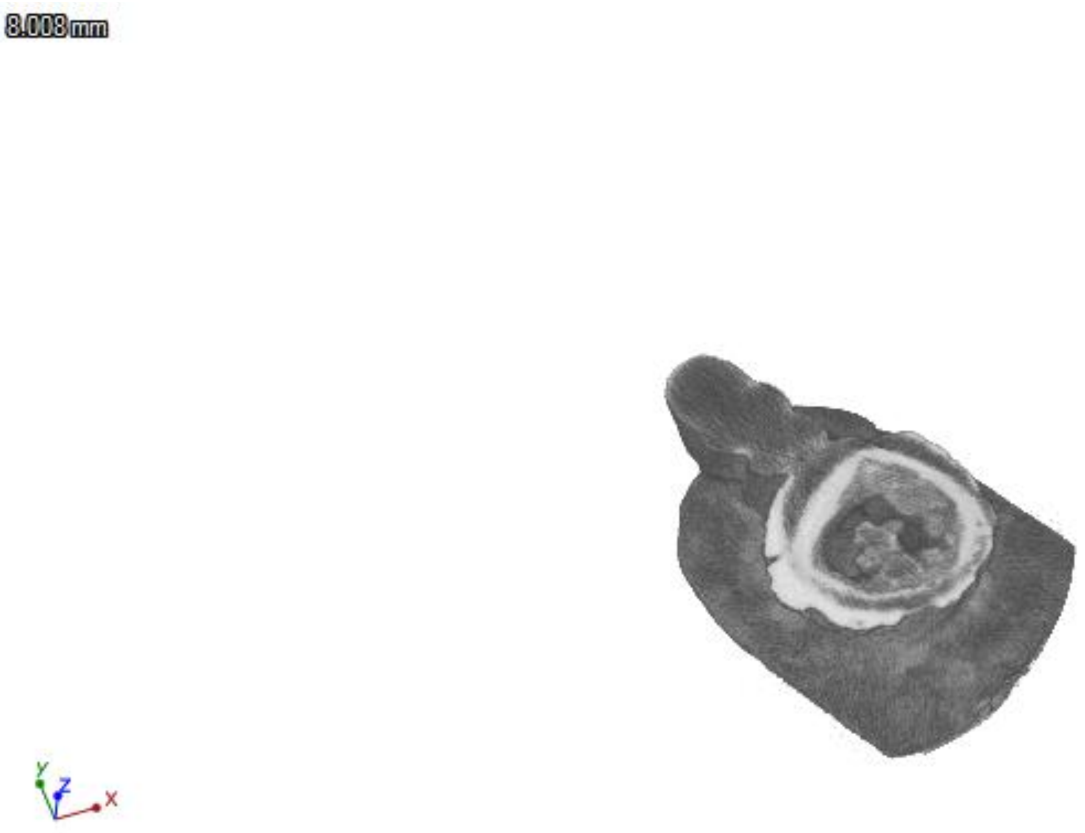

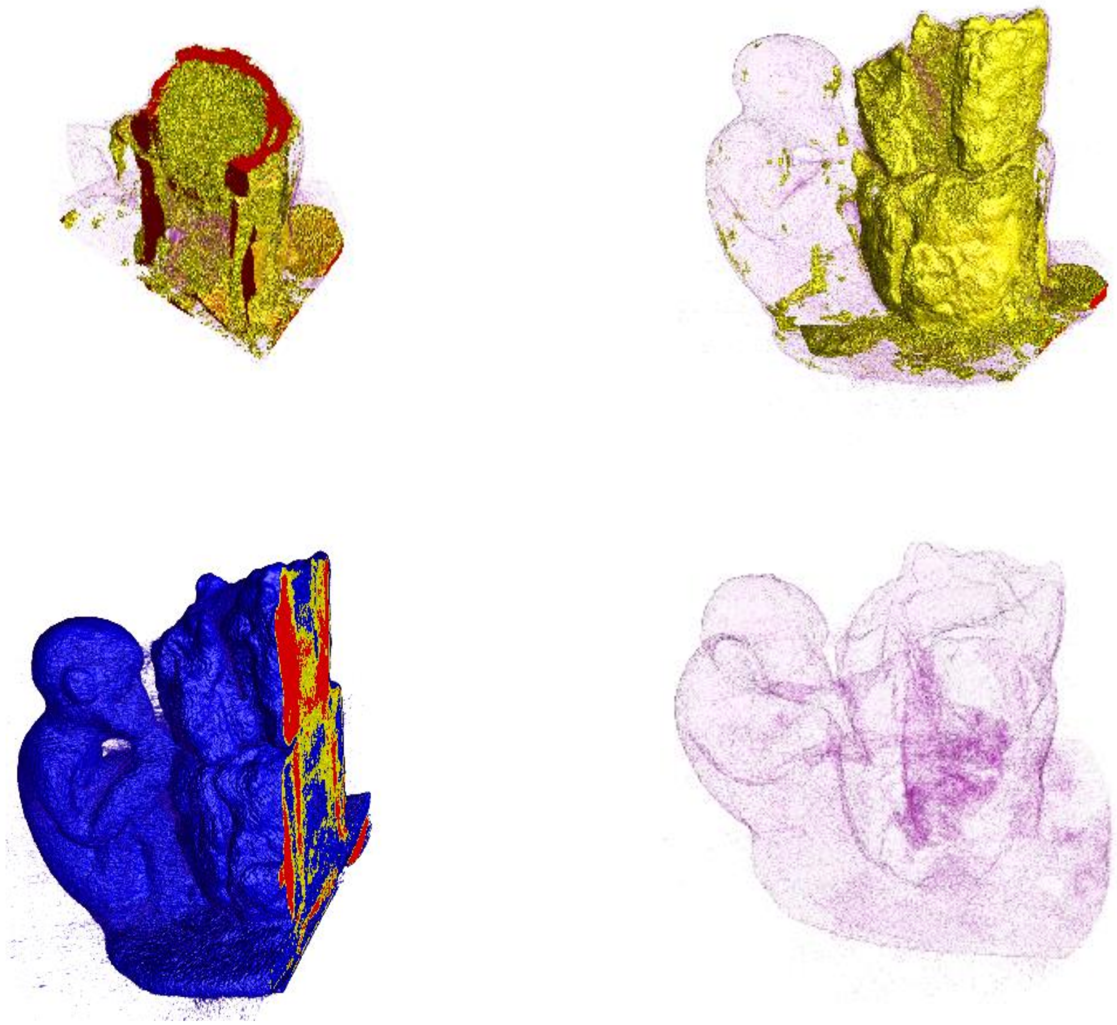

B. Maróti et al, J Radioanal Nucl Chem (2017) 312:367–375

Cultural heritage – Early Iron Age bronze shield

Gábor Tarbay, Hungarian National Museum

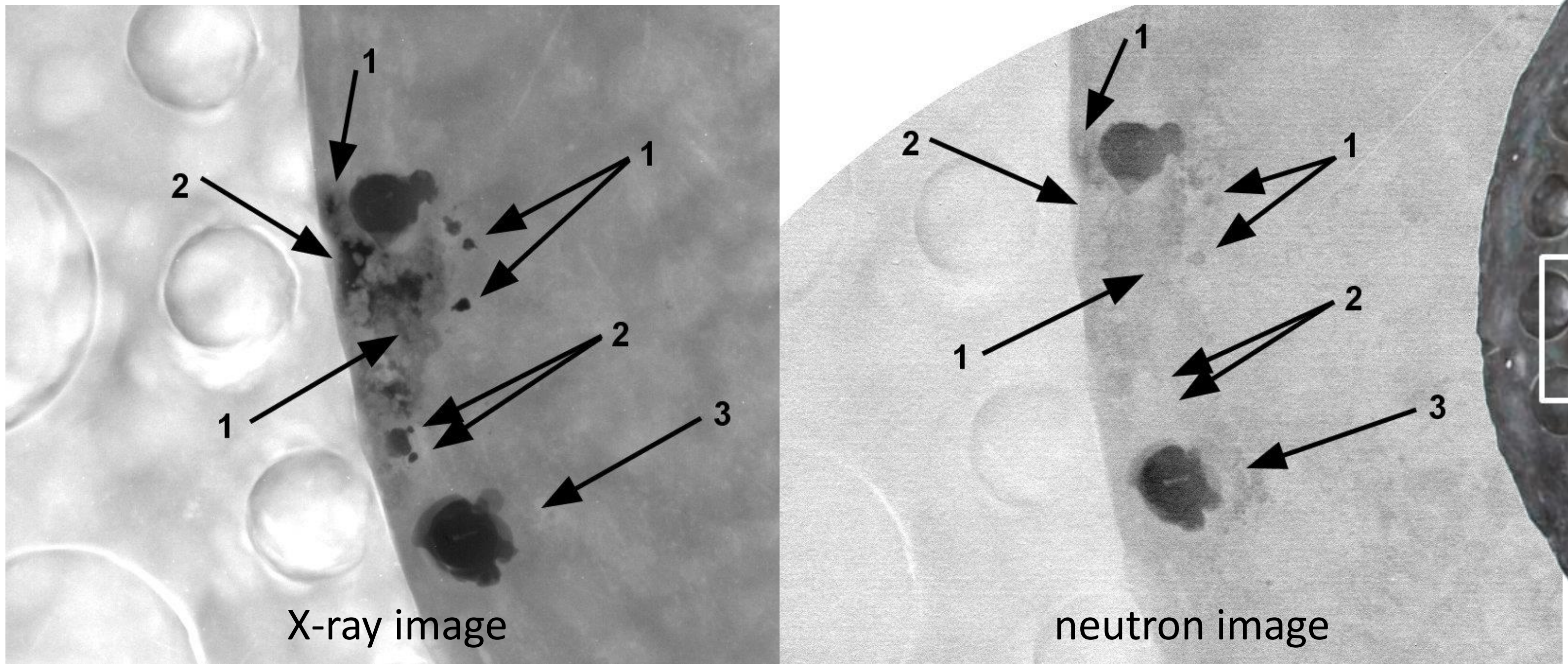

Do we see contrast? Cases if:

1. X-ray – yes, neutron – yes: e.g. bronze (rivet fragments)
2. X-ray – yes, neutron – no: high atomic number (e.g. lead)
3. X-ray – no, neutron – yes: low atomic number (e.g. organic)

A bronze spearhead (Inv. nr.: HNM 75.1893.1200)

Gábor Tarbay, Hungarian National Museum

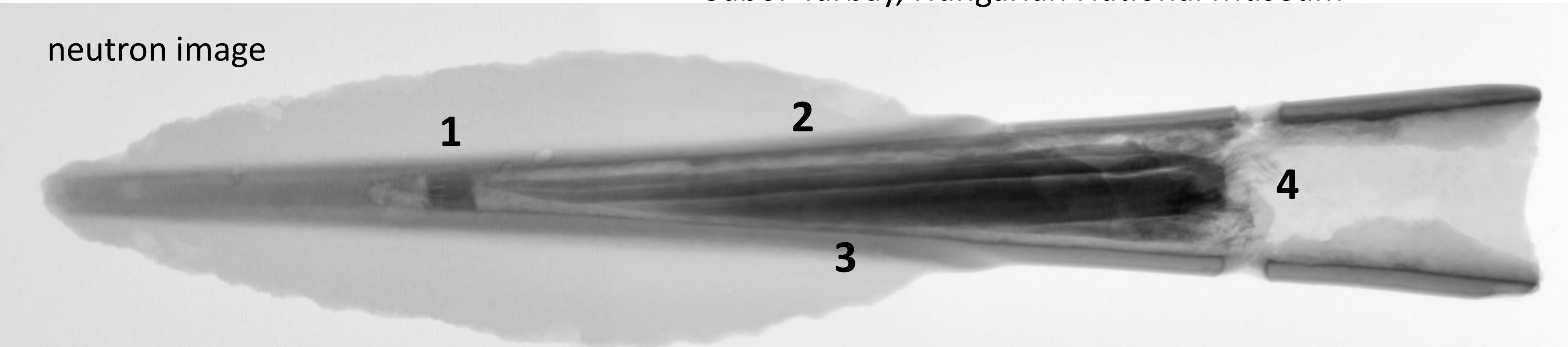

- **Hollow is filled with different materials**
- **Not seen in the X-ray images → organic**

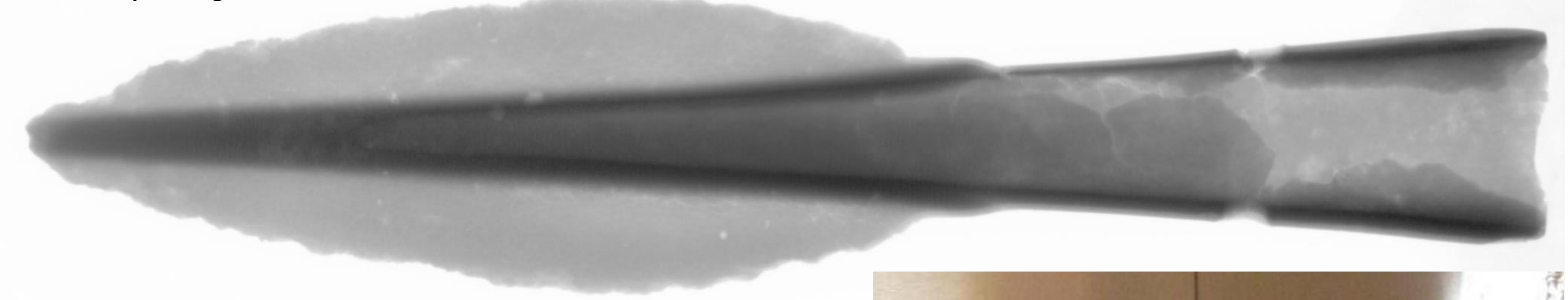

1. small fibrous-like material
2. a sharp, long and slim wand
3. next to 2 a similar but thicker wand
4. around the bottom of wands a fibrous-like substance

Bimodal imaging of a snail shell

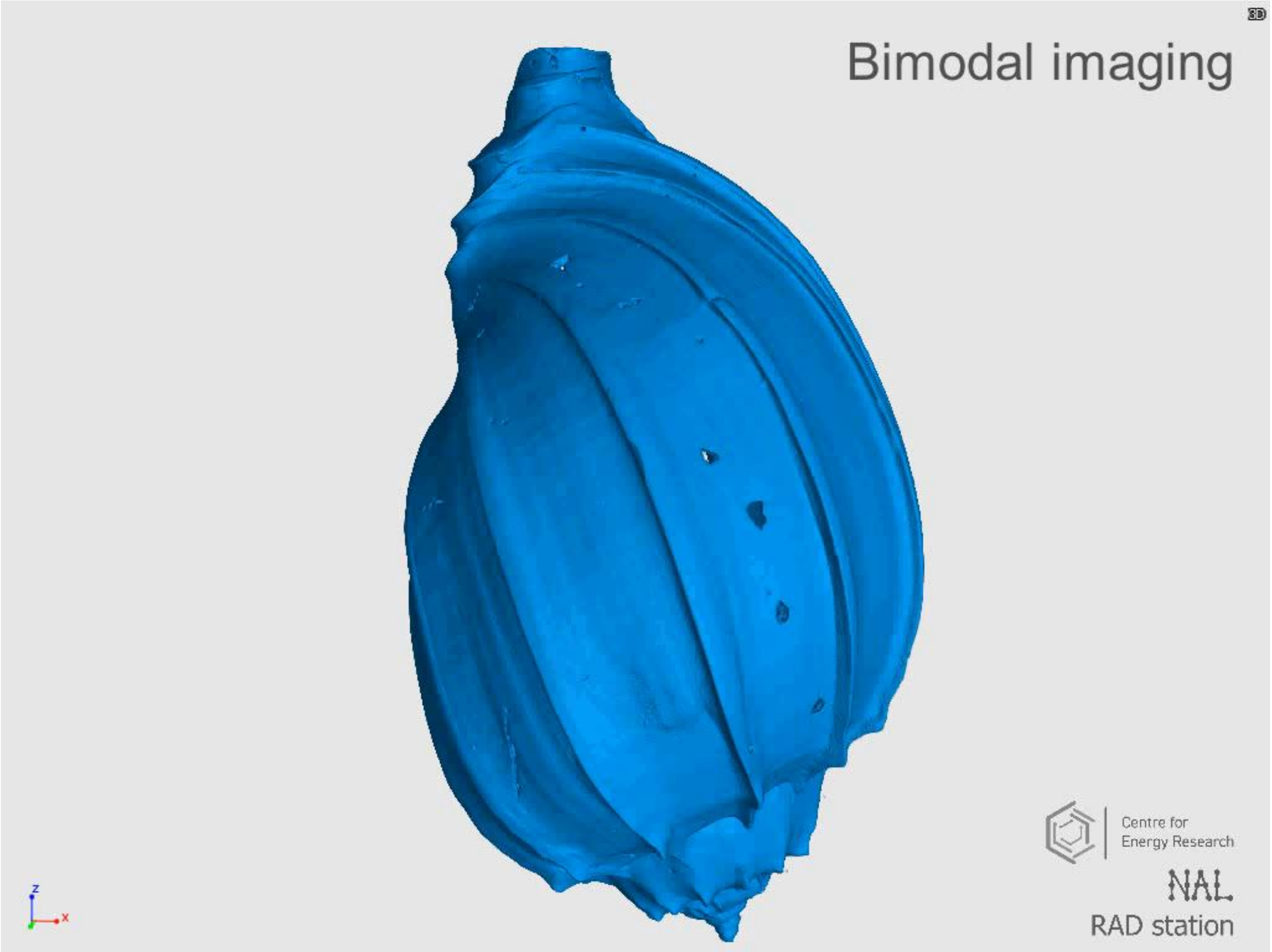

Neutron activation Autoradiography (NAAR)

Example: Panczyk et al., INCT – Warsaw

IRRADIATION	MEASURE	SENSITIVITY	APPLICATIONS
Uniform cold / th neutron field	Delayed γ "2D image"	High: trace elments (Cu, Mn, Fe, Hg)	paintings, pigments

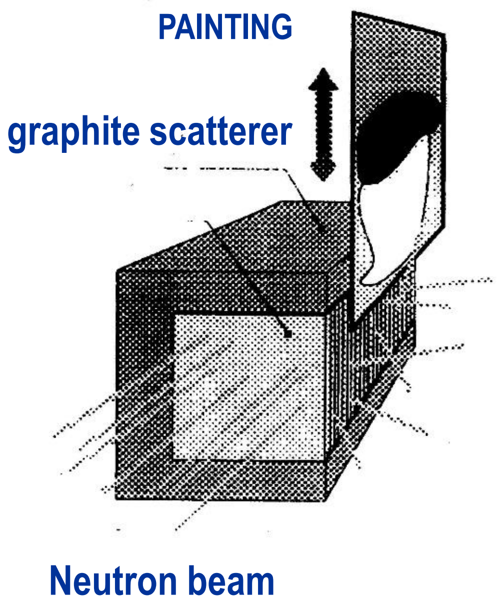

NAAR system at '*MARIA*' reactor, Warsaw

J. Tintoretto (1519-1594)
„Portrait of a Venician admiral"

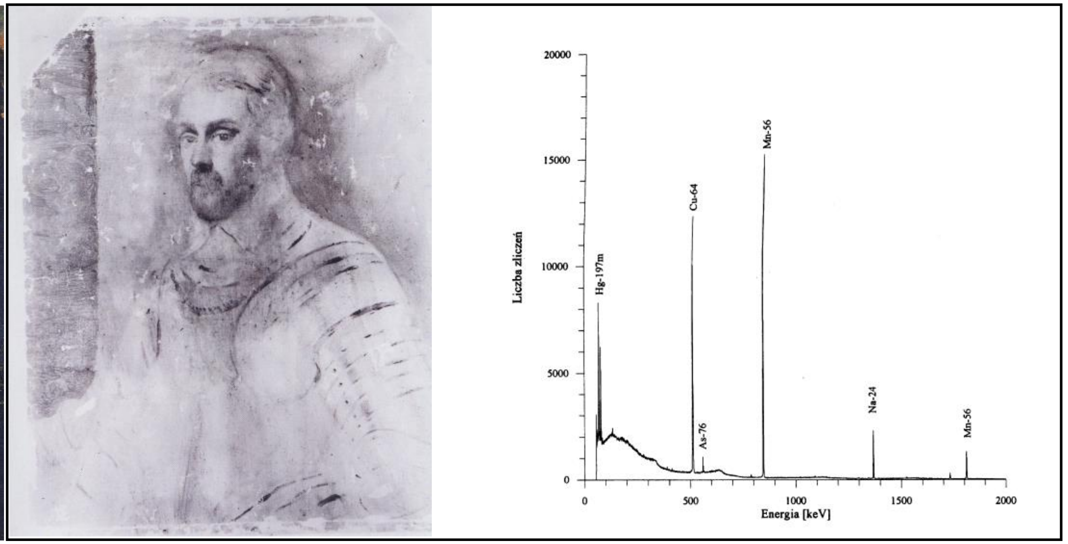

Autoradiograph, 12 min after irradiation. Irradiation time: 3h. Blackenning mainly due to **^{56}Mn** and **^{64}Cu**

Centre for Energy Research

Non-destructive reverse engineering of internal

Budapest Neutron Centre

Excavation kit – a plastic dinosaur skeleton within gypsum

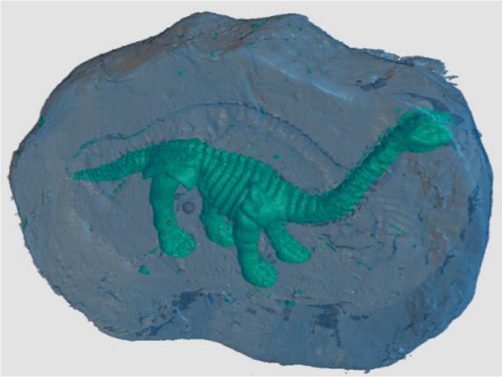

2. Segmentation of the tomogram

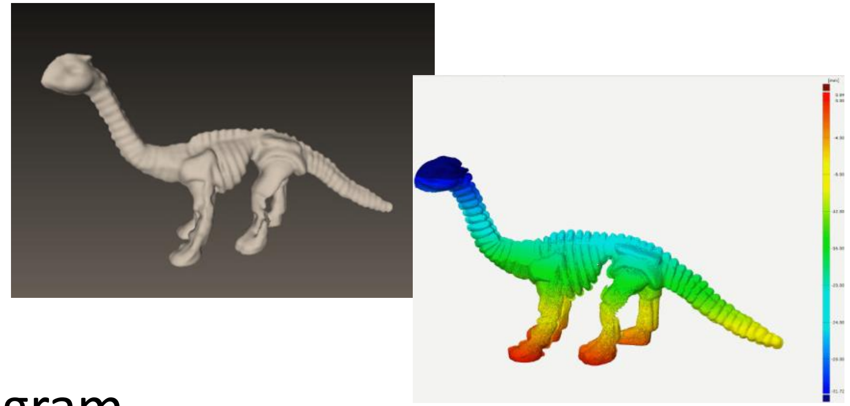

3. Engineering analysis of the segmented dinosaur model

1. Surface – 3D scan

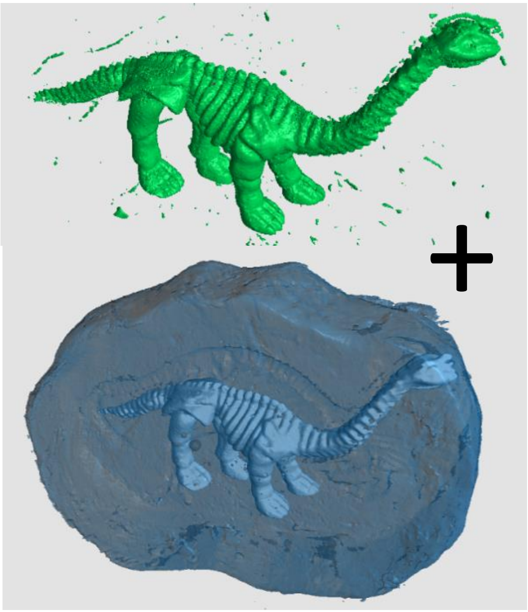

4. 3D-printed dinosaur model

Pore volume distribution based on the NT

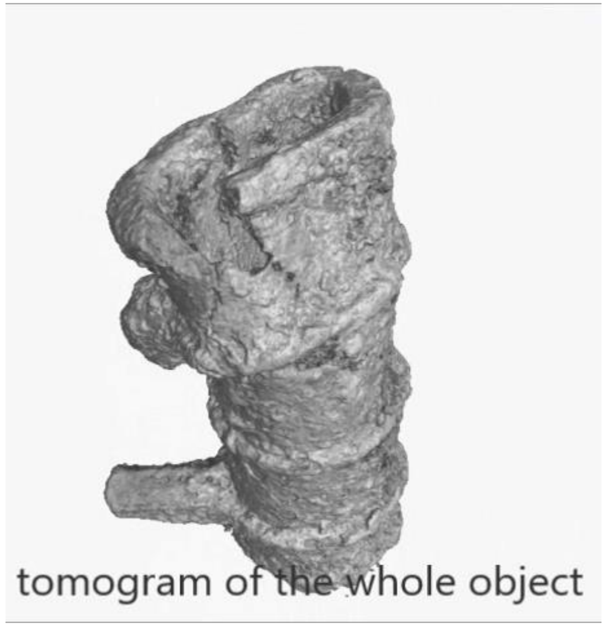

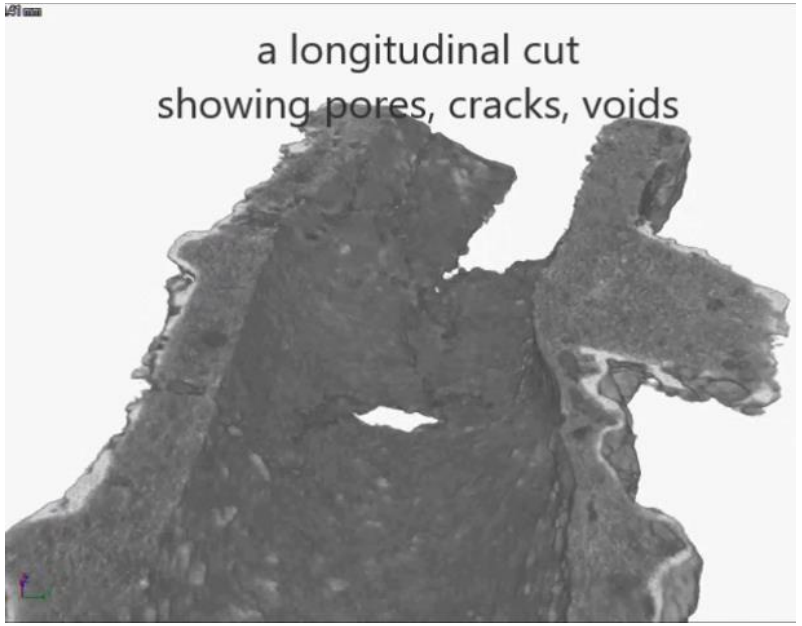

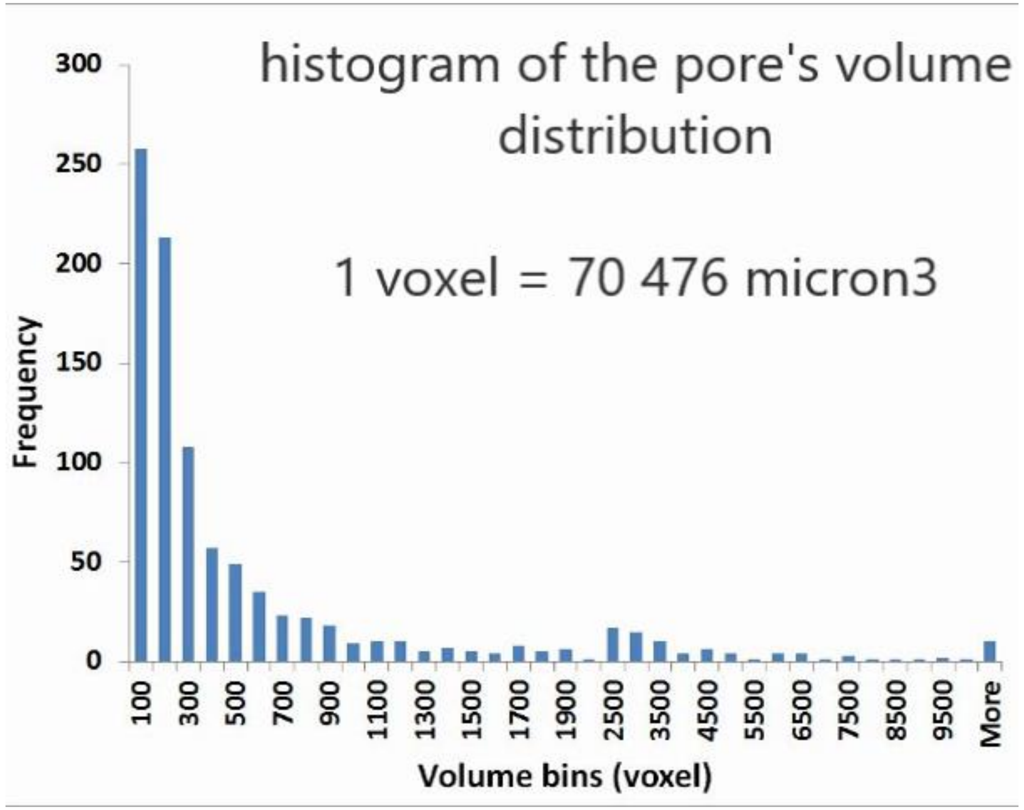

X-ray and neutron radiography, tomography – foams

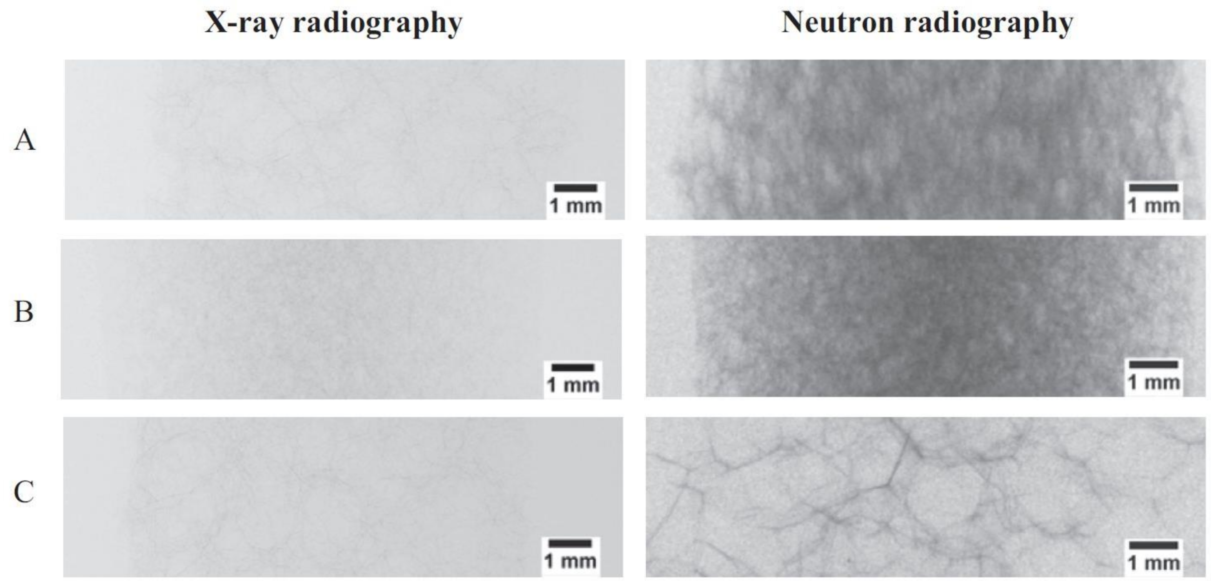

'ig. 4. X-ray (left) and neutron (right) radiograms of polypropylene (A and B) and polyethylene (C) foams.

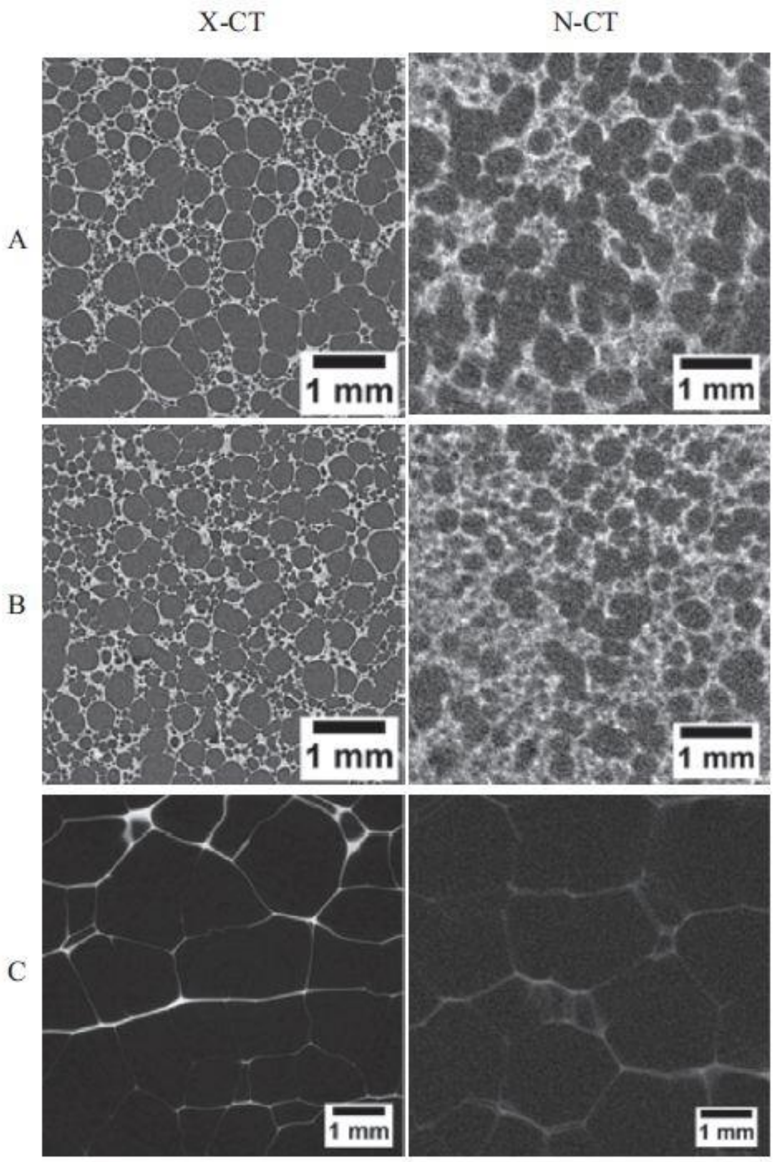

Fig. 6. Tomographic sections of the different types of foams studied.

Pore size distribution, wall thickness distribution

E. Solórzano et al., Nuclear Instruments and Methods B 324 (2014) 29–34

Hawaii basalt – visualization of air bubbles

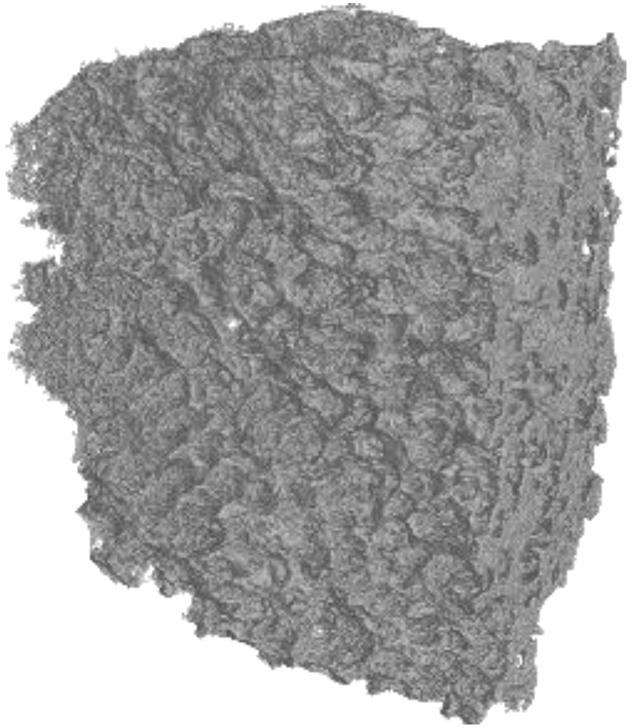

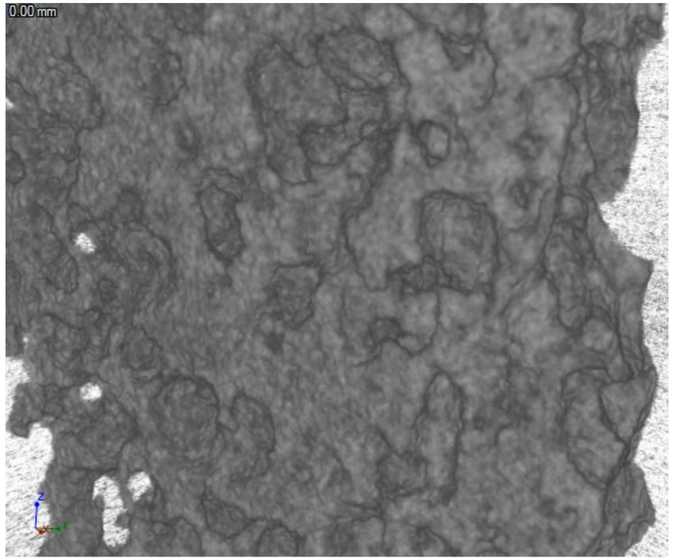

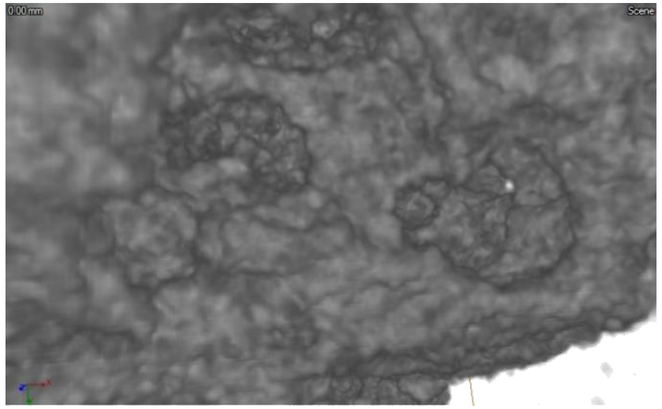

Sandstone with oil

Neutron Tomograph

Red is high neutron attenuation
Red indicates very high H conc.

Image has had low attenuation regions subtracted

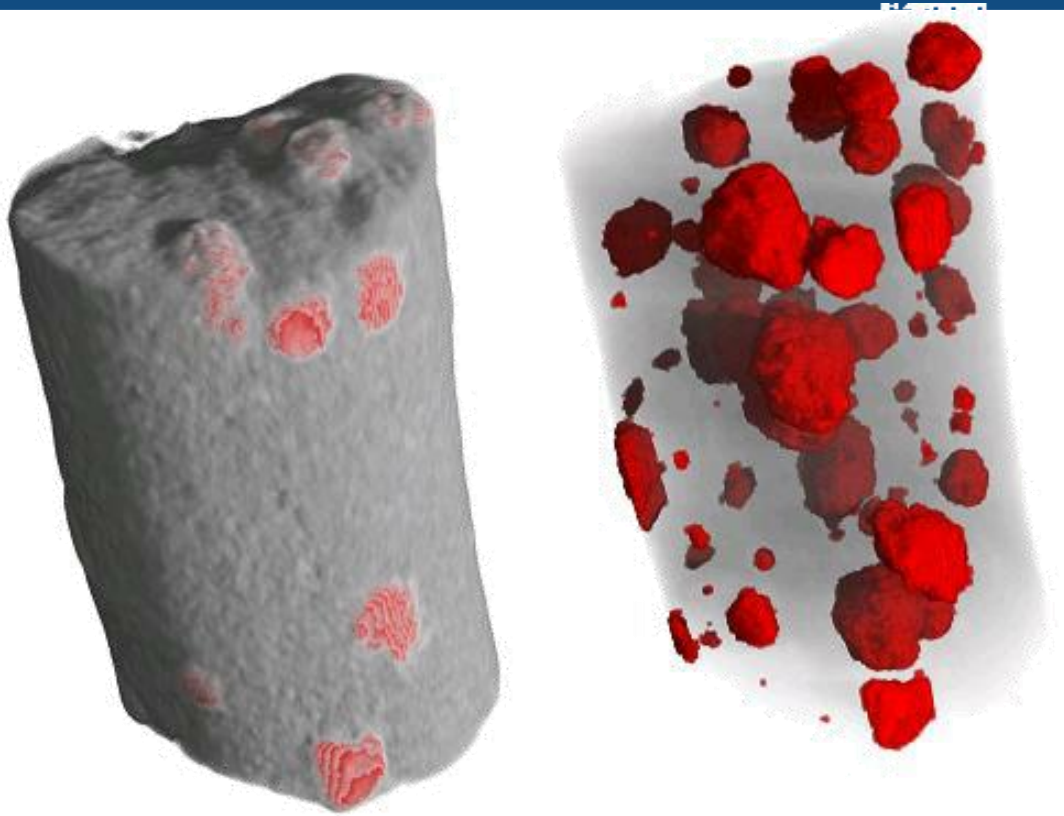

X-ray Tomography

Left: Tomograph of core surface
Right: 3D perspective with low X-ray attenuating material subtracted
Red indicates zones of high density

NOTE: X-RAY IMAGE SHOULD REPRESENT THE OPPOSITE TO NEUTRON IMAGE.
THUS: Neutron "sees" hydrocarbon; X-ray "sees" matrix

Centre for
Energy Research

Lapis lazuli – visualization of heterogeneities

Budapest
Neutron Centre

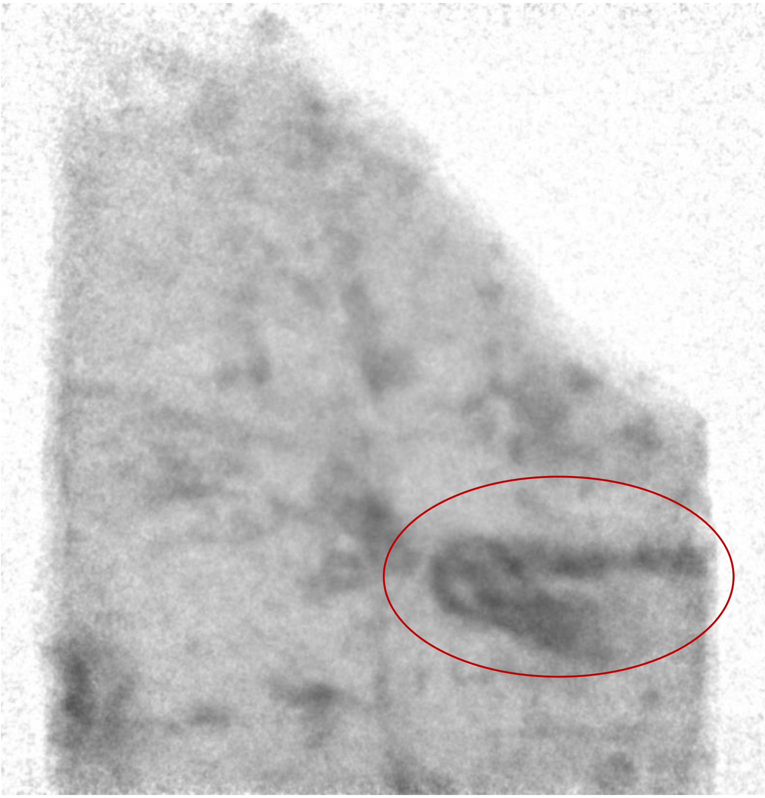

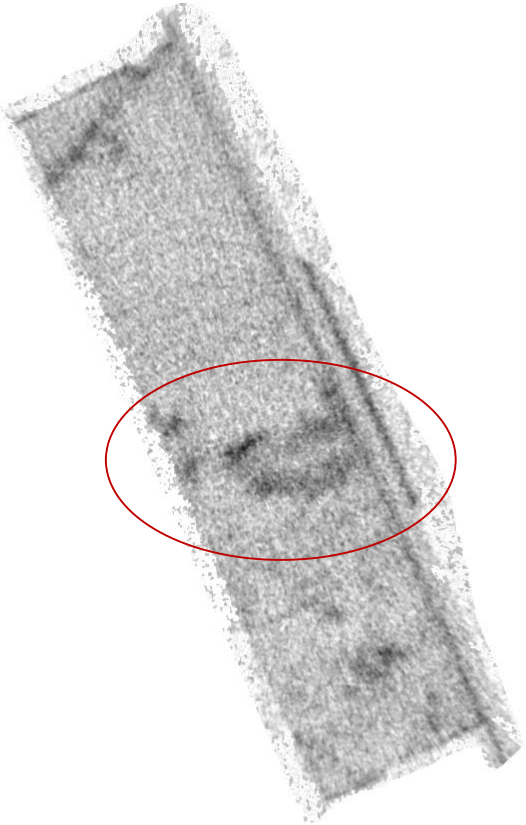

Engineering – Virtual cuts / real fracture face

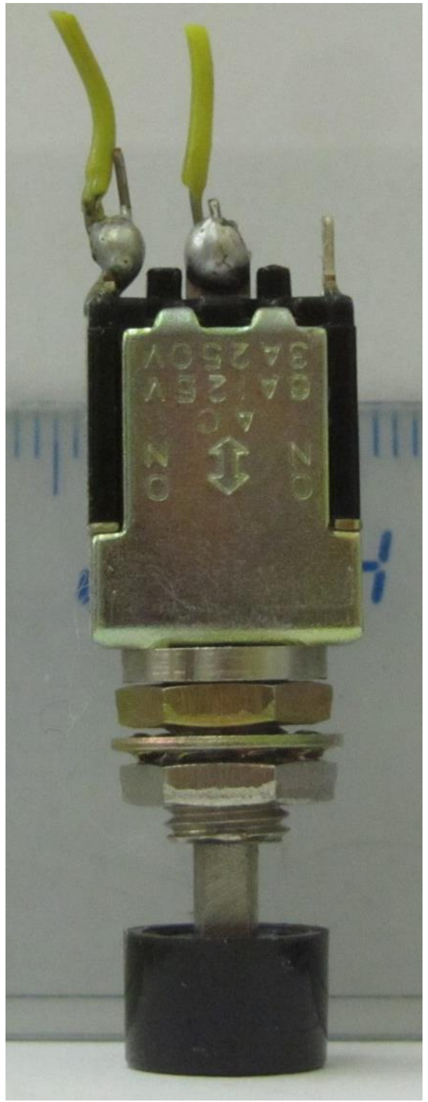

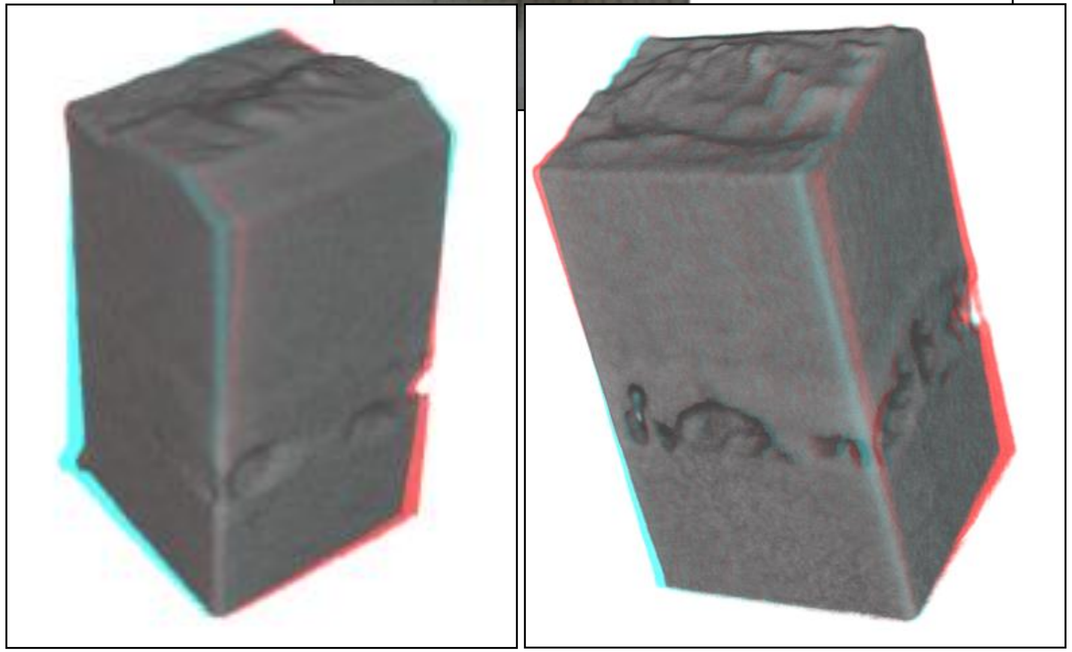

S3D (stereoscopic 3D) visualization

Turbine blade inspection – visualization of casting template remains

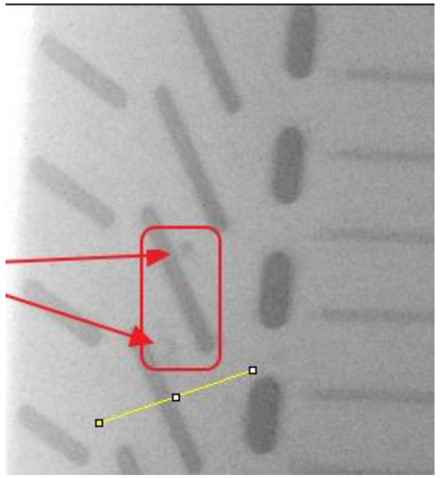

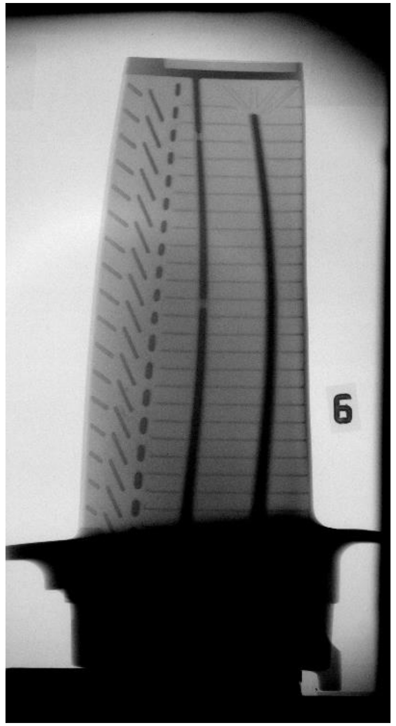

Images from DNR vs. NORMA

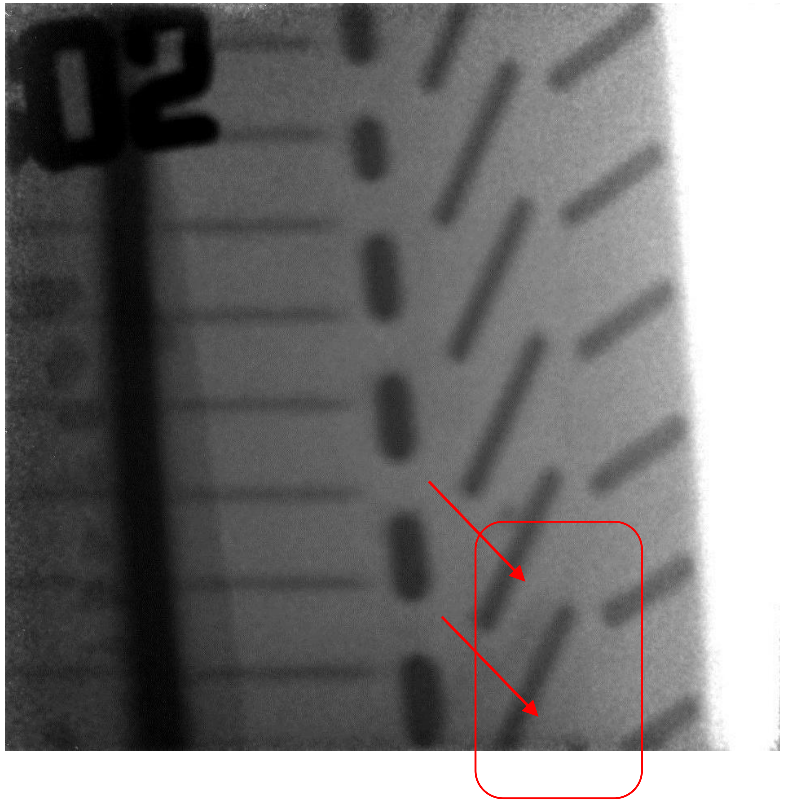

Contrast enhancement with a Cd-solution

Secondary hydriding – Zr fuel rod cladding

$$\frac{n_H}{n_{Zr}} = \frac{\frac{A_H}{t_H}}{\frac{A_{Zr}}{t_{Zr}}} \frac{\sigma_g(E_{Zr})}{\sigma_g(E_H)} \frac{\varepsilon(E_{Zr})}{\varepsilon(E_H)} \frac{f(E_H)}{f(E_{Zr})}$$

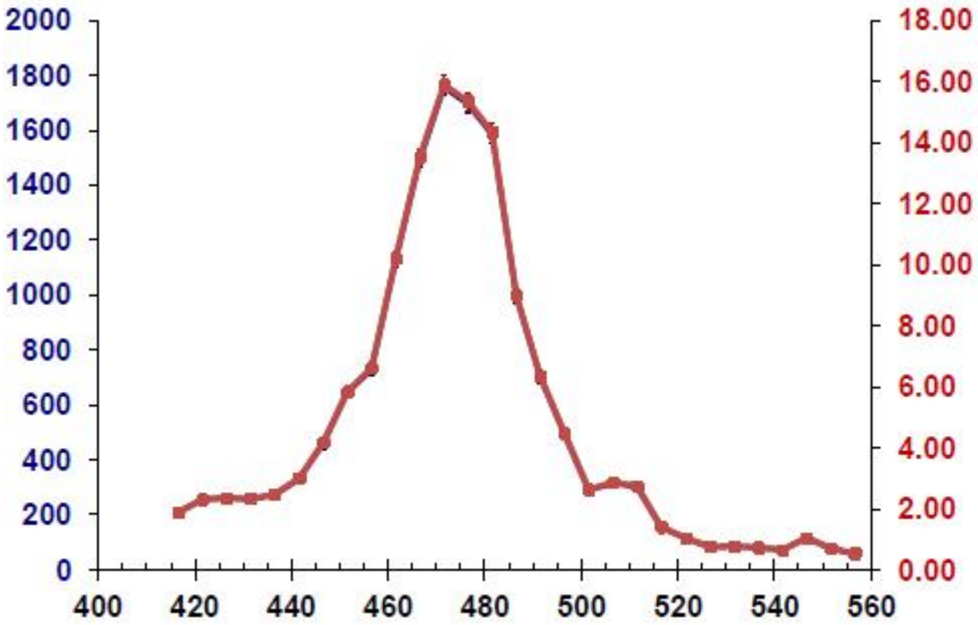

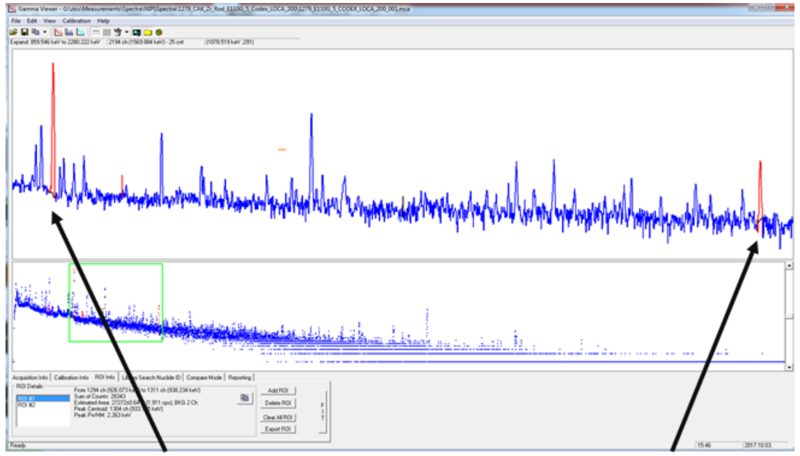

Zr peak @ 935 keV

H peak @ 2223 keV

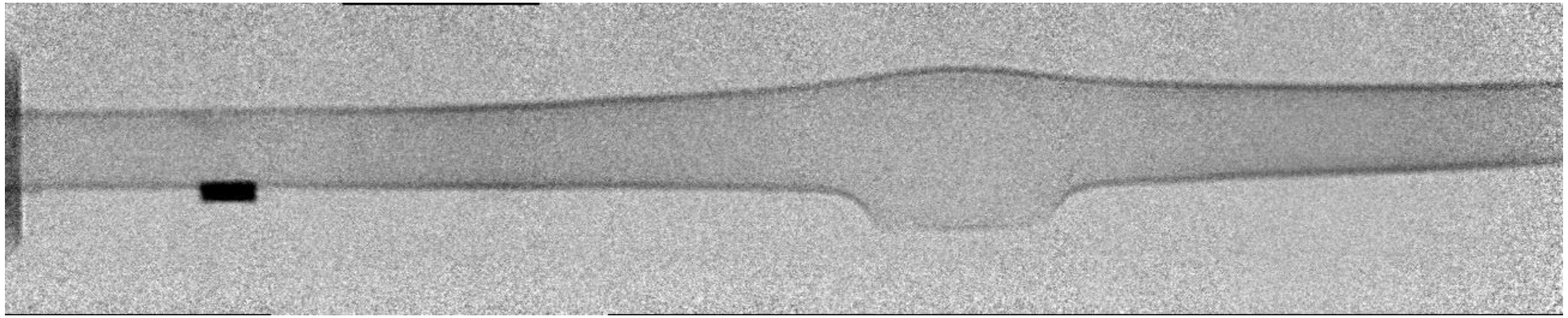

- Process leading accidental situation in NPPs: loss of coolant accident (LOCA)
- NR: H-distribution in Zr fuel rod cladding around the burst

Mi-24 military chopper rotor blade

- 19 sectors,
- 9,85 m long,
- 700 mm wide,
- 65 mm thick,
- total weight 115 kg

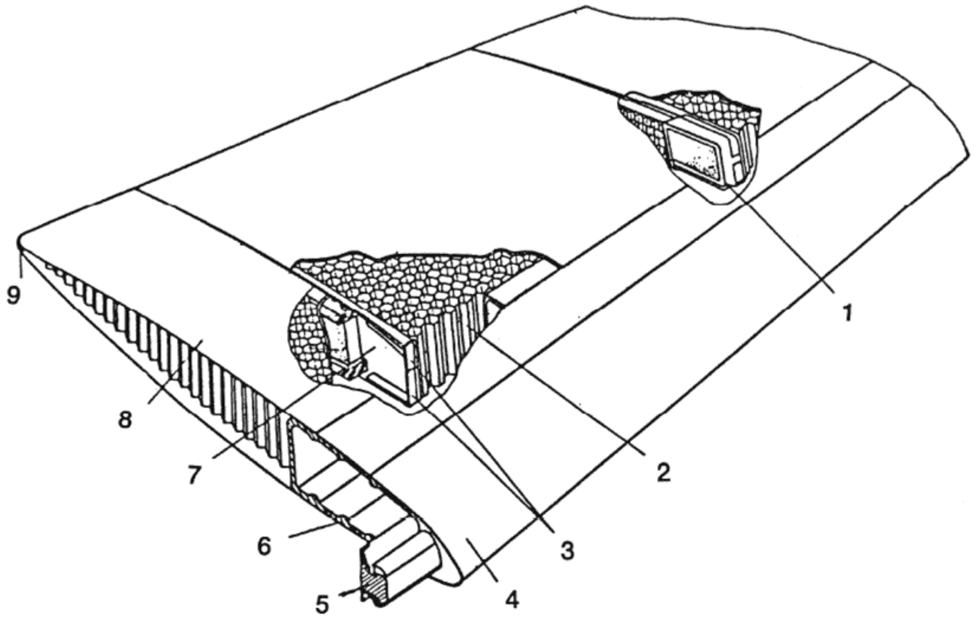

Teljes forgószárnylapát száraz NR képe (a)

Teljes forgószárnylapát nedves NR képe (b)

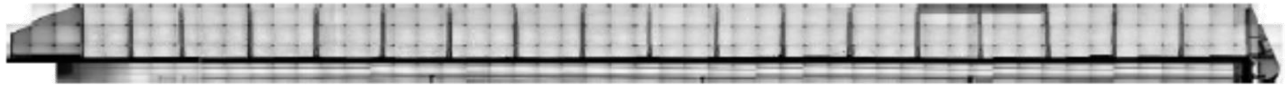

Teljes forgószárnylapát nedves XR képe (c)

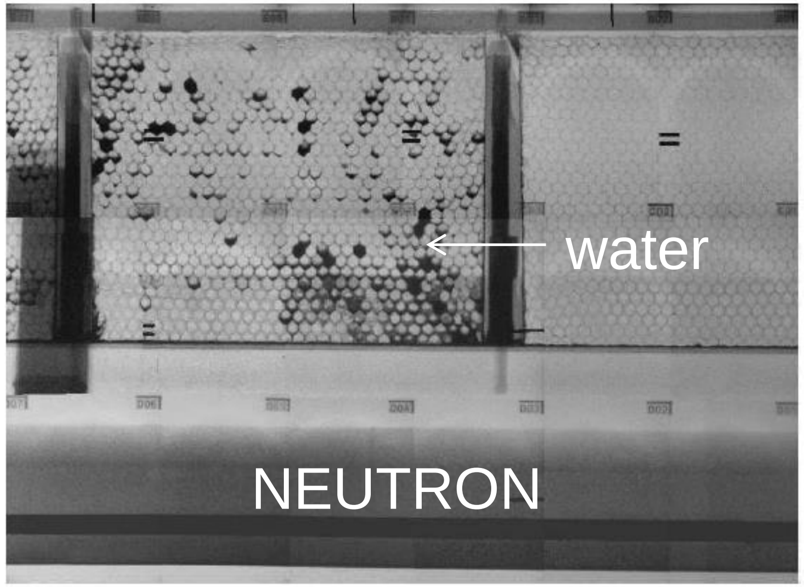

Balasko, M., Svab, E., Molnar, Gy., & Veres, I. (2005). Classification of defects in honeycombcomposite structure of helicopter rotor blades. Nuclear Instruments and Methods in Physics Research, 542A, 45-51

Balasko, M., Veres, I., Molnar, Gy., Balasko, Zs., & Svab, E. (2004). Composite structure ofhelicopter rotor blades studied by neutron and X-ray radiography. Physica B: Condensed Matter, 350(1-3), 107-109

Industrial Quality control

- Macroscopic objects

welding of metals

- Micro-tomography: FOV 27×27 mm^2, 1:1 Lens
- Pixel size 9 µm, 10 µm Gadox scintillator, Scan times 15-20 h

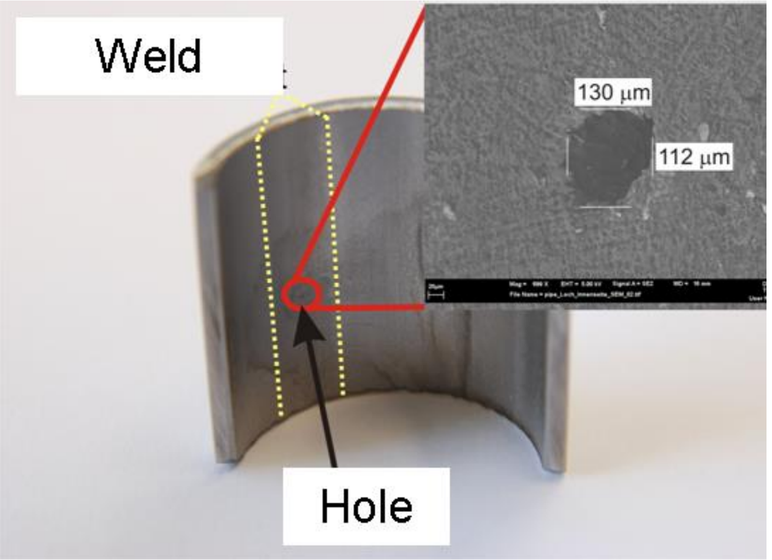

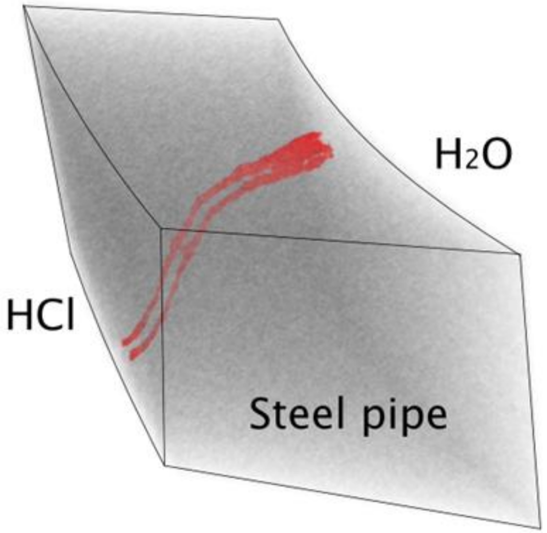

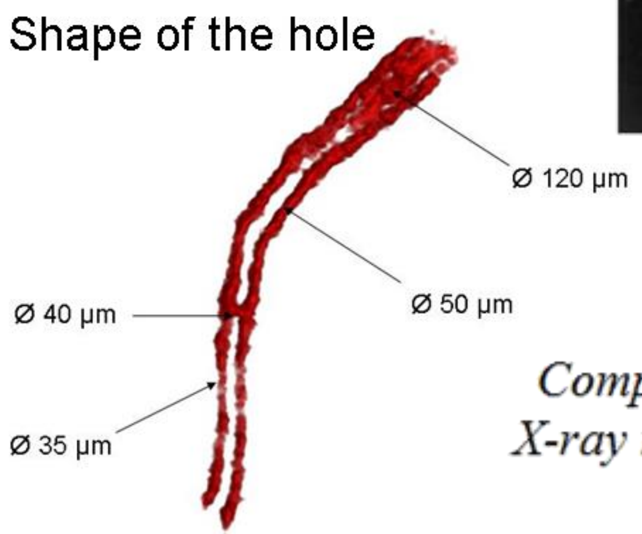

Quality control of explosive devices for space applications

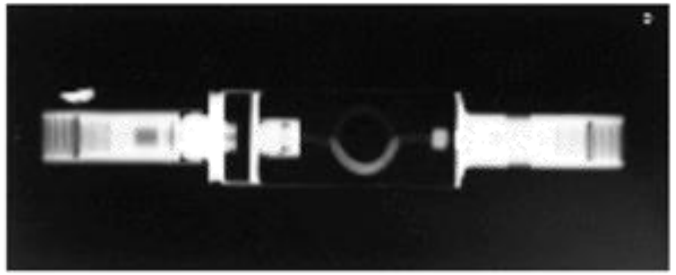

Comparison of neutron radiography and X-ray radiography of an ARIANE cartridge fuse (DASSAULT-AVIATION)

Quality assurance - Damage assessment of ball bearings

- 100Cr6 high-carbon chromium steel, organic grease -> problem for X-rays
- Unexpected damage observed during use of a double row bearing, due to insufficient lubrication
- Before taking it apart for further studies (e.g., diffraction), the exact geometry can be recorded
- Collaborator: Rogante Engineering Office, Italy

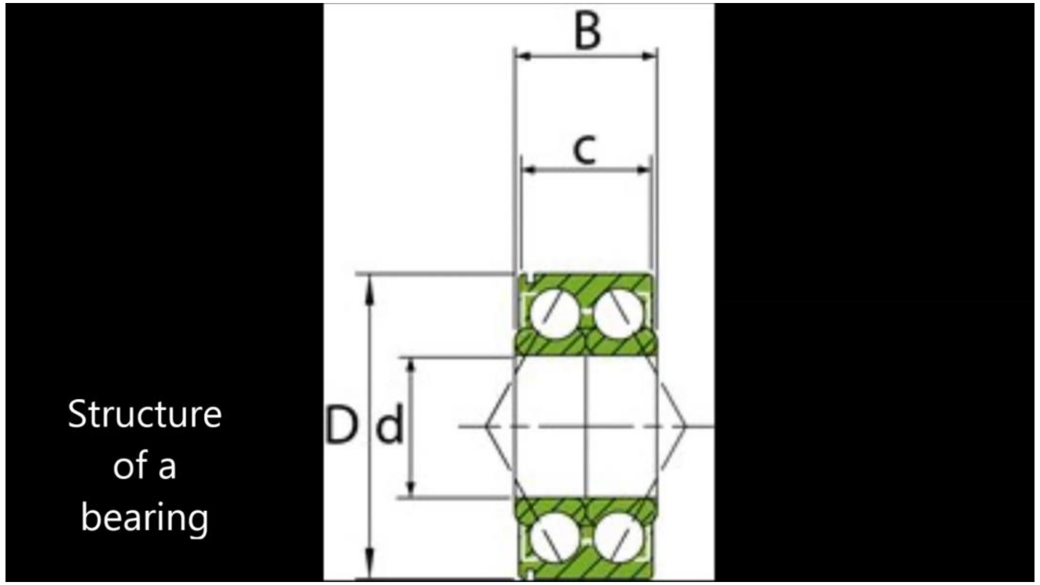

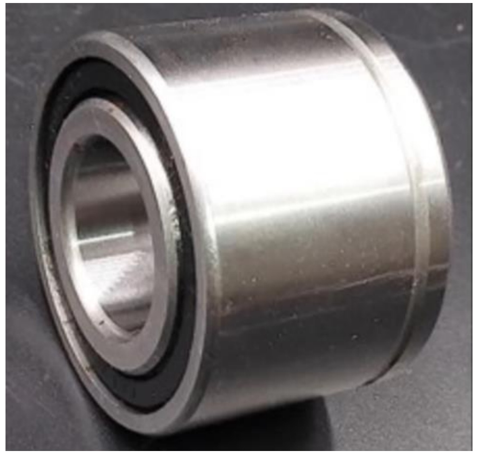

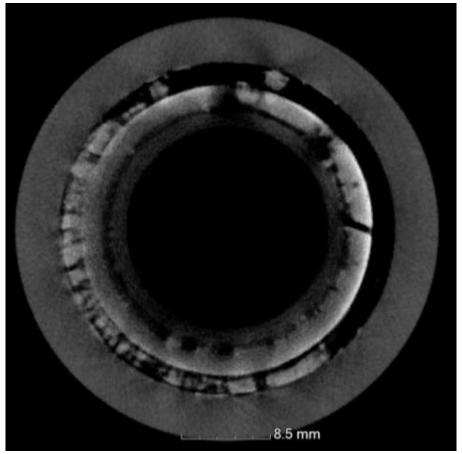

M. Rogante, Z. Kis, L. Szentmiklósi: Neutron imaging of Double-Row Ball Bearings Made of 100Cr6 High Carbon Chromium Steel for Automotive Application, International NR Newsletter No. 18 February 2023, p 11-13 http://www.isnr.de/images/nr_newsletter/NR18.pdf

Probing local density via neutron imaging

- Spray-dried refractory carbide and metal powder mixtures, containing tungsten carbide, is compacted and sintered during the production of conventional **cutting tool inserts**

- The friction between the pressing tool and the powder results in **density gradients in the powder compact**, and uneven shrinkage during sintering

- **To validate the finite element simulation** of the pressing procedure, the density gradients in the powder compacts must be **measured with a high spatial resolution**.

- Since **Tungsten** has a high atomic number, it is **hard to penetrate with X-rays and even cold neutrons**.

- Calibration of the neutron attenuation vs. thickness using homogeneous pellets

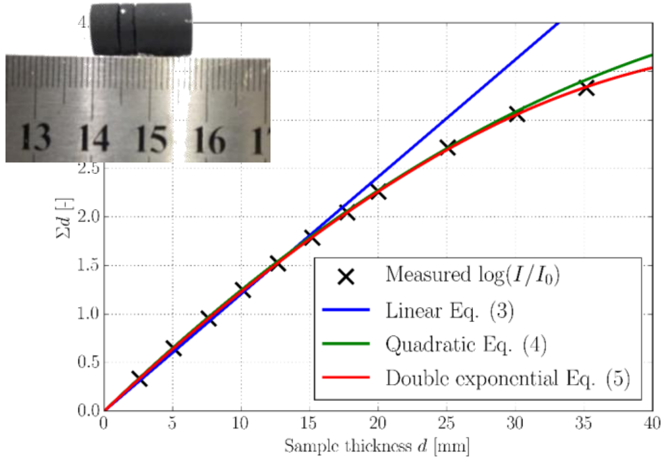

Insert manufacturing

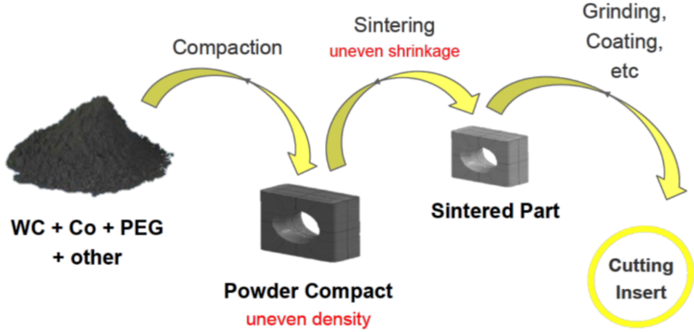

https://www.youtube.com/watch?v=0QrynzJ_lZ4

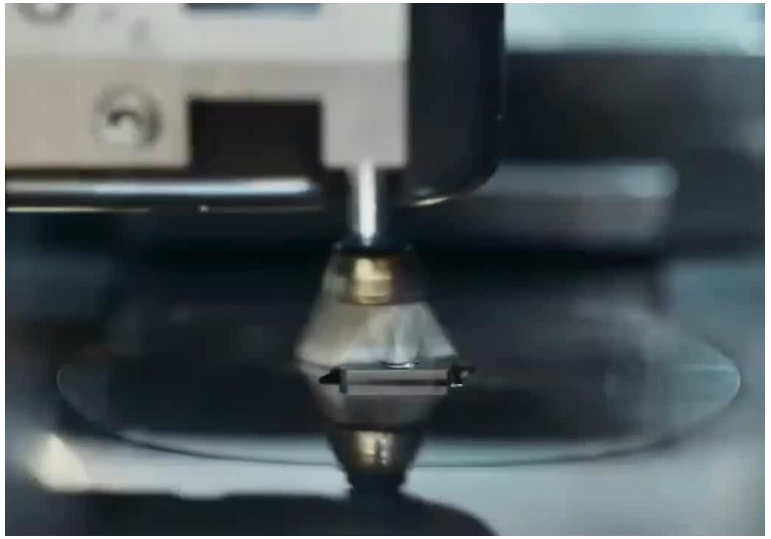

Experimental vs. calculated density

- Finite element simulations and experimental imaging results are in close agreement

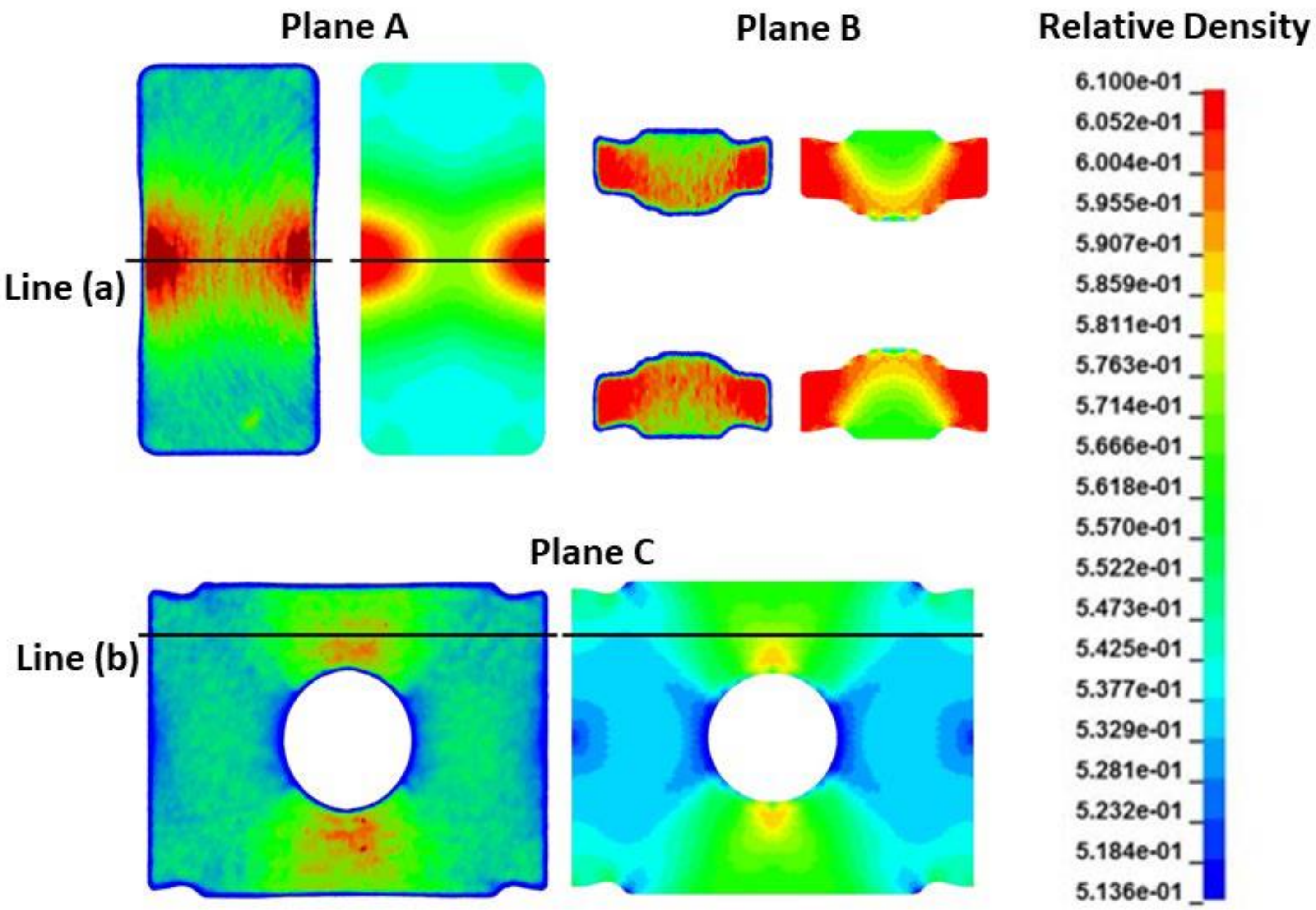

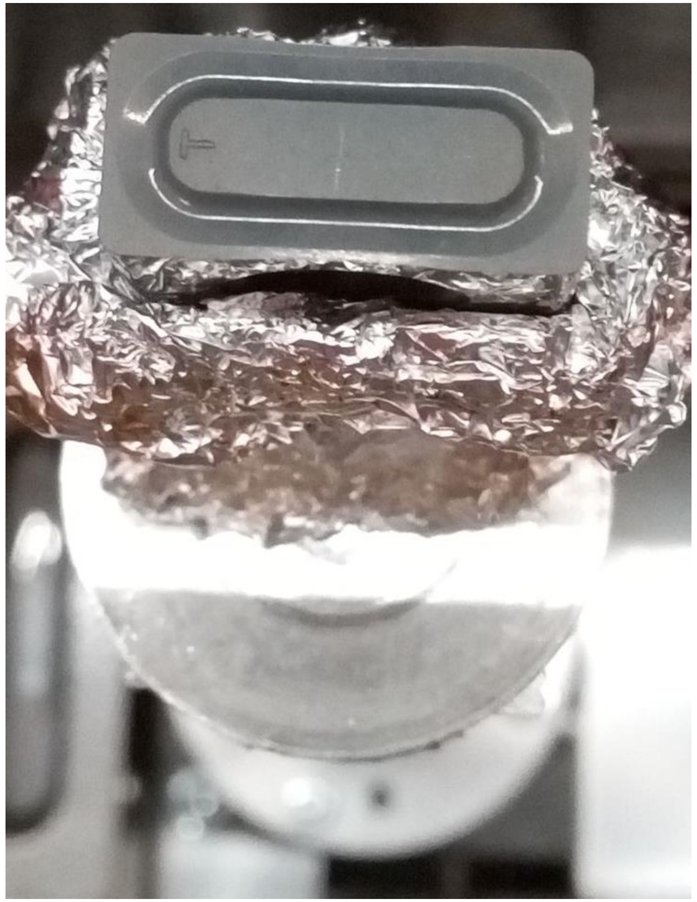

Hjalmar Staf, Zoltán Kis, László Szentmiklósi, Bartek Kaplan, Erik Olsson and Per-Lennart Larsson, Determining the density distribution in cemented carbide powder compacts using 3D neutron imaging, Powder Technology **354** 584-590 (2019)
DOI: 10.1016/j.powtec.2019.06.033

a) 50, b) 75,
c) 100, d) 150,
e) 200 keV X-ray beam

f) thermal neutron beam

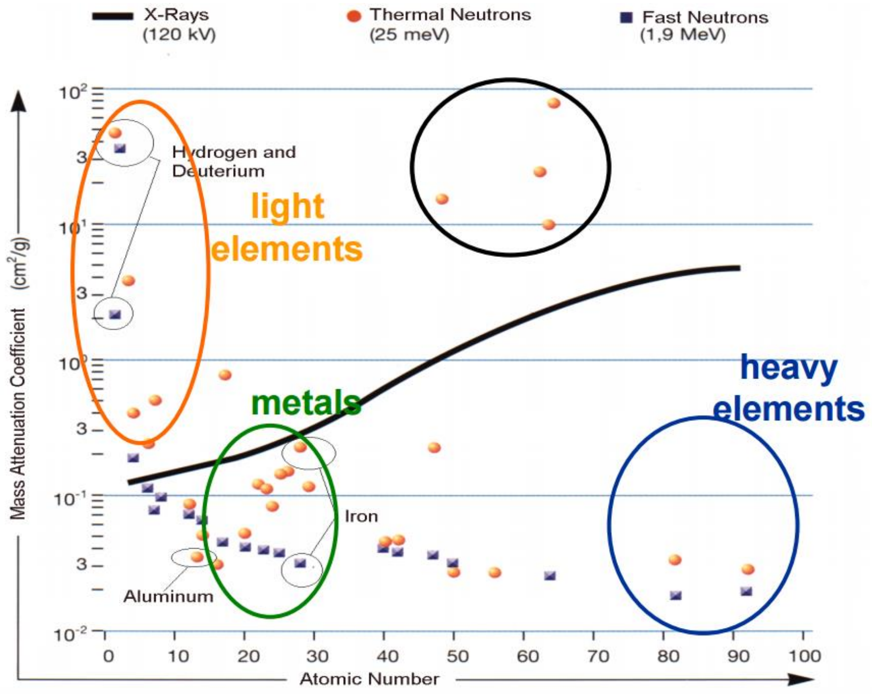

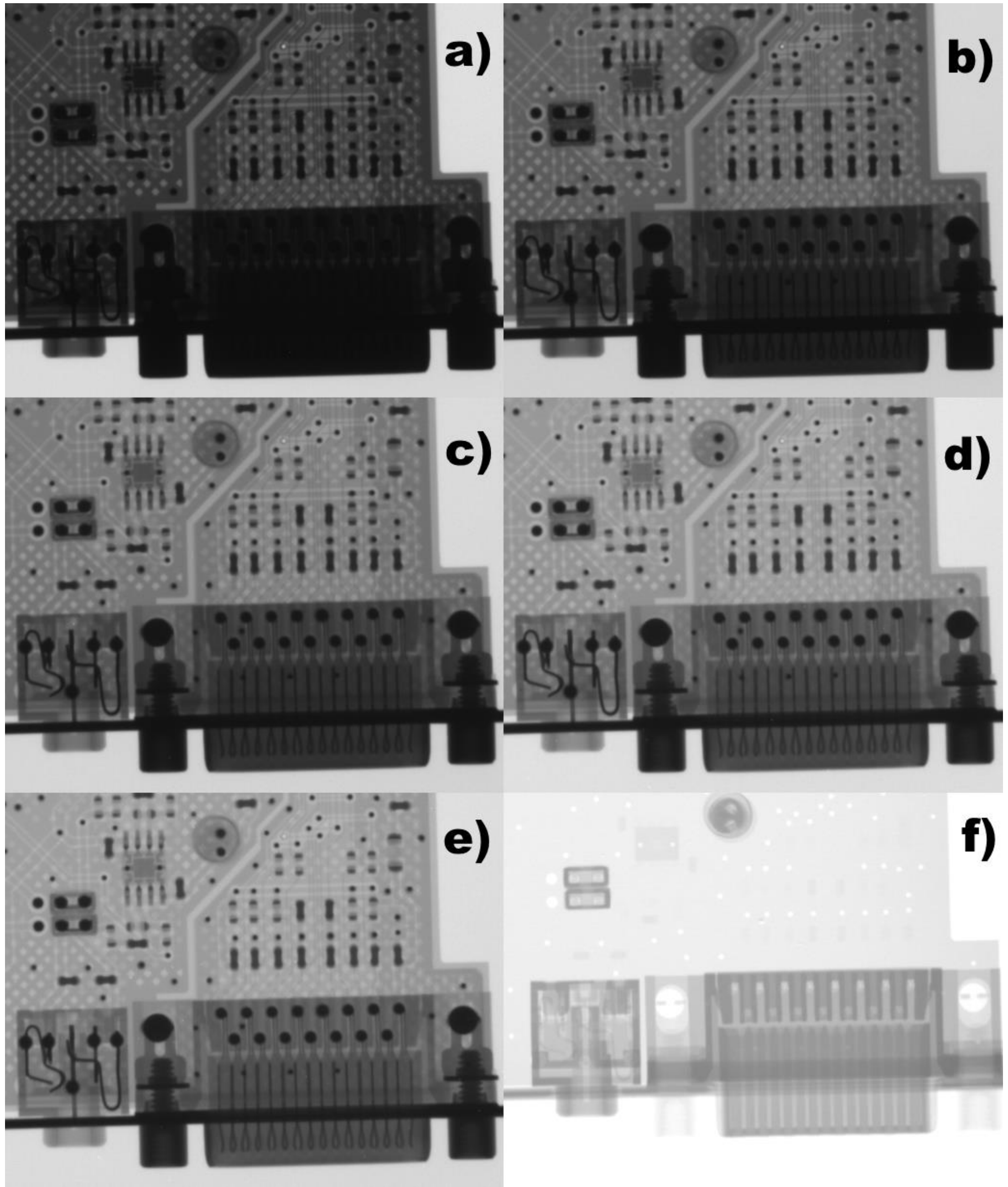

Composite Image segmentation

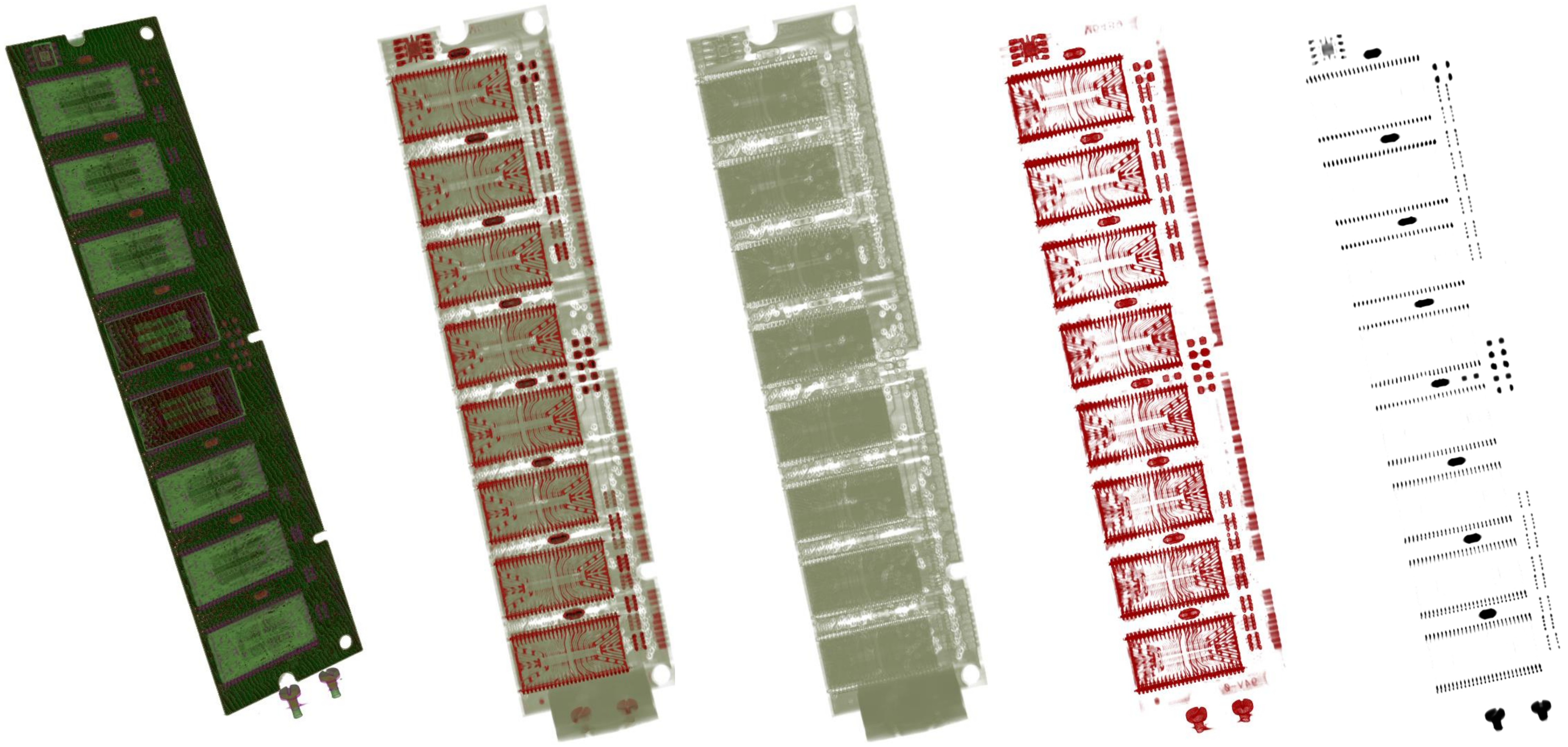

Cell phone in 3D

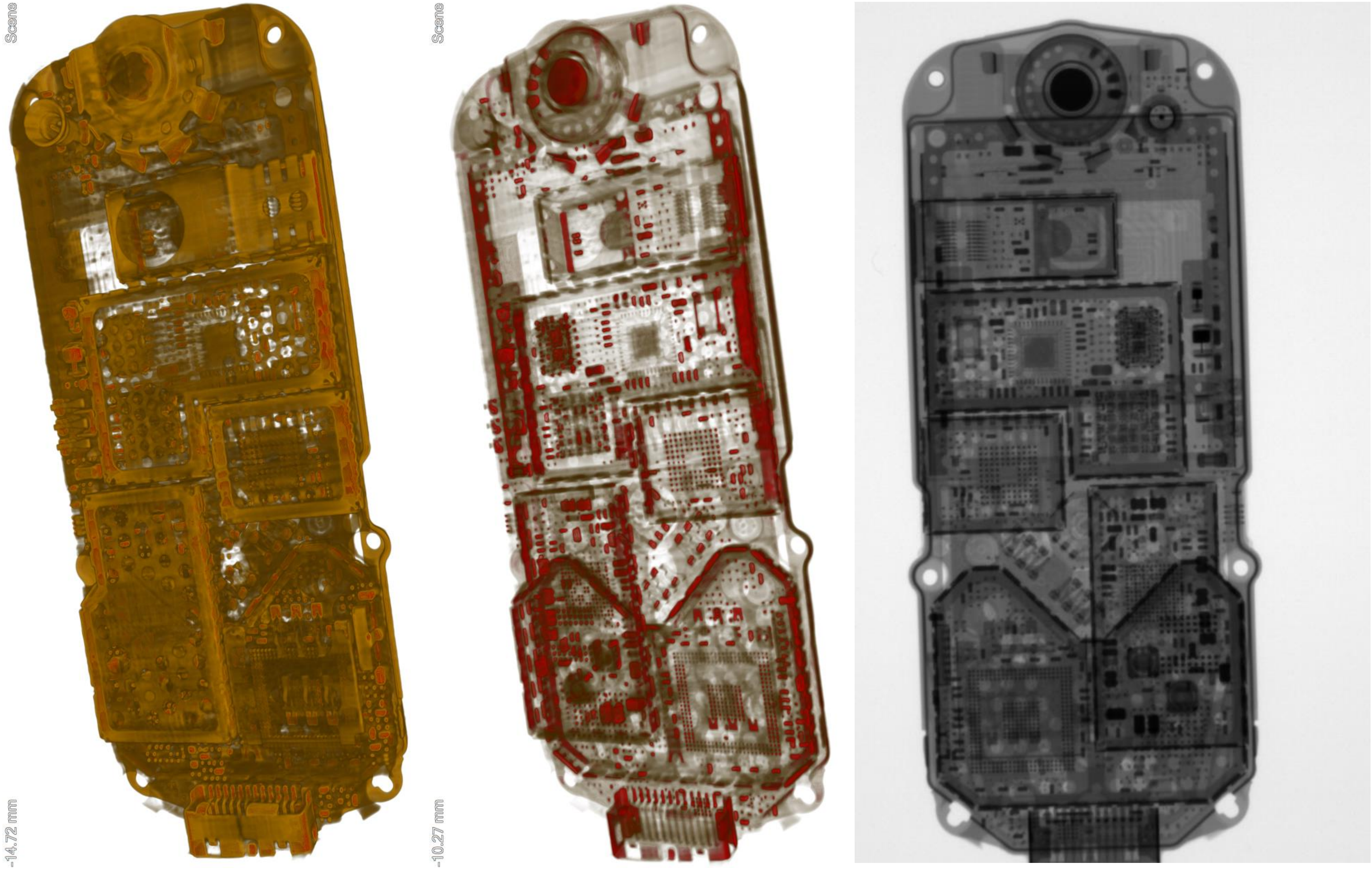

Centre for
Energy Research

Water uptake of construction materials

Budapest
Neutron Centre

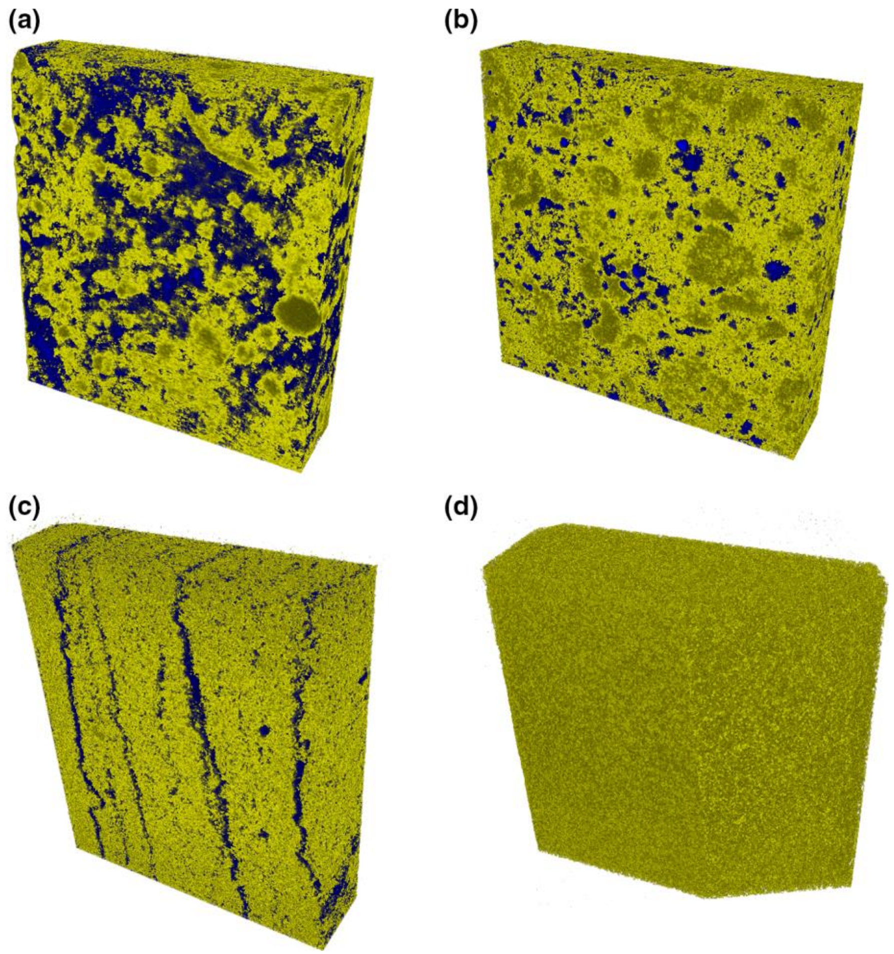

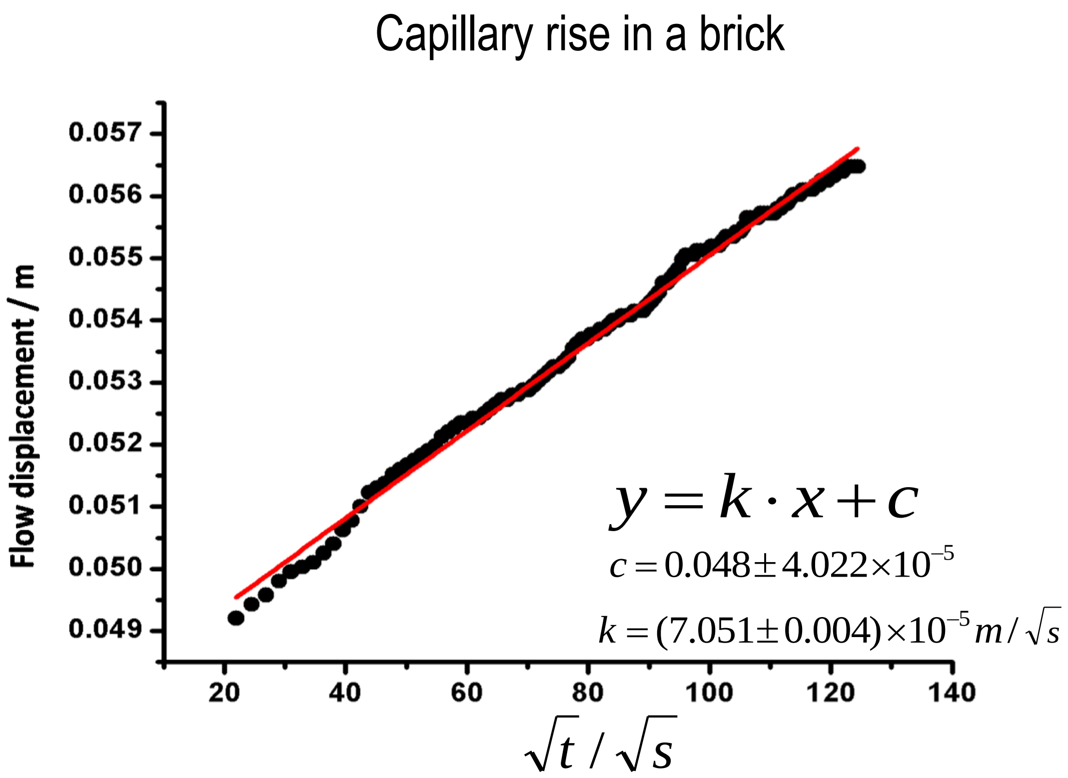

Z. Kis, F. Sciarretta, L. Szentmiklósi: Water uptake experiments of historic construction materials from Venice by neutron imaging and PGAI methods, Materials and Structures (2017) 50:159 DOI 10.1617/s11527-017-1004-z

Time-resolved imaging

High-speed imaging of very fast, singular processes requiring several thousand frames per second

Example: Gun shot - hardly feasible for neutrons!

Problems:

- the number of neutrons/photons in one time window becomes very low, below the detector noise
- in classic detectors, the number of detector pixels that can be read out in one time window becomes very small, drastically decreasing resolution

But: New detectors are becoming fast enough (see below), the neutron flux is the main limiting factor!

Stroboscopic imaging of very fast but repetitive processes

Example: Fuel injection / oil flux in a combustion engine

Advantage:

- the number of neutrons/photons in one time window is still very low, but many exposures of the same time window of the periodic process may be accumulated on the detector before read-out, thus increasing the available intensity

Disadvantage:

- Only one time window of the periodic process can be recorded in one sequence, the periodic process has to be recorded in a sequence of many consecutive time window accumulations, sacrificing most neutrons.

Physical limitations

- Available neutron/photon flux in a time window
- Decay time of scintillation light
- readout speed and gating time of the detector (if applicable)

Real-time neutron imaging

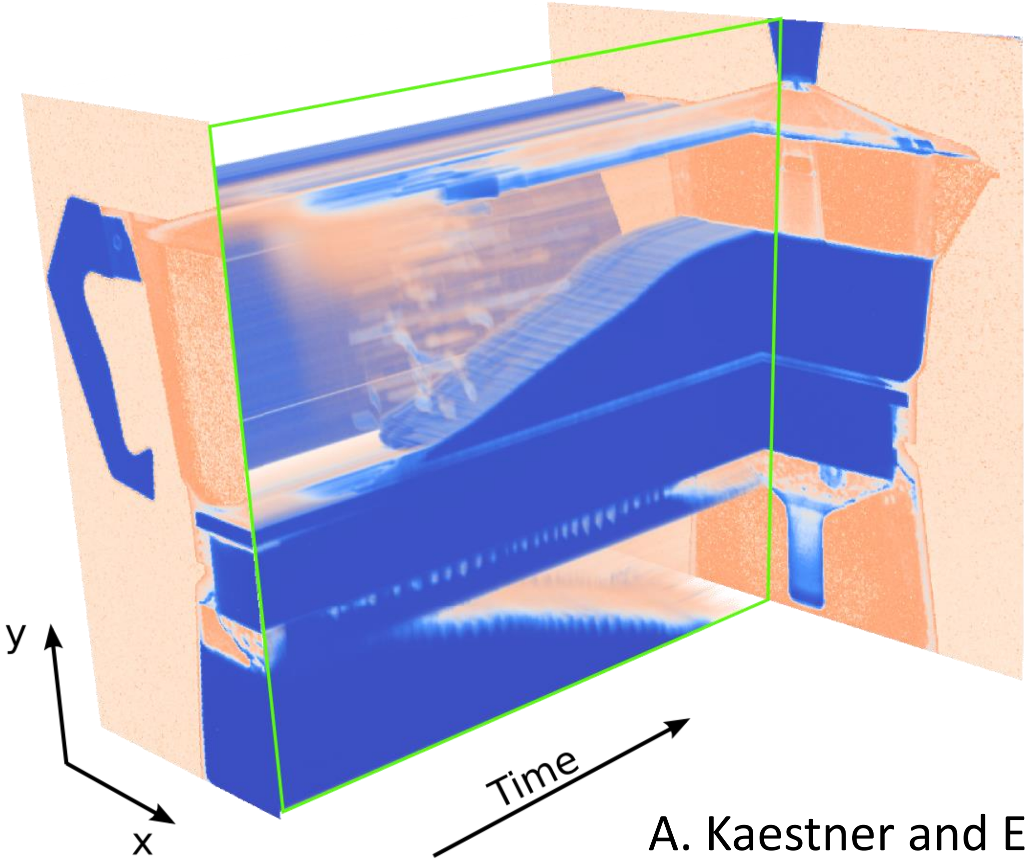

A. Kaestner and E. Lehmann, IAEA TM on Regional RR Users' Networks: advances in neutron imaging, 26-29 Nov. 2012, Jakarta, Indonesia

In situ (dynamic) radiography@ RAD

- Real-time visualization of an engineering object
- p,T,v parameters external controlled
- ANCARA – experimental loop to study the behaviour of SCW
- For an improved efficiency of future energy production

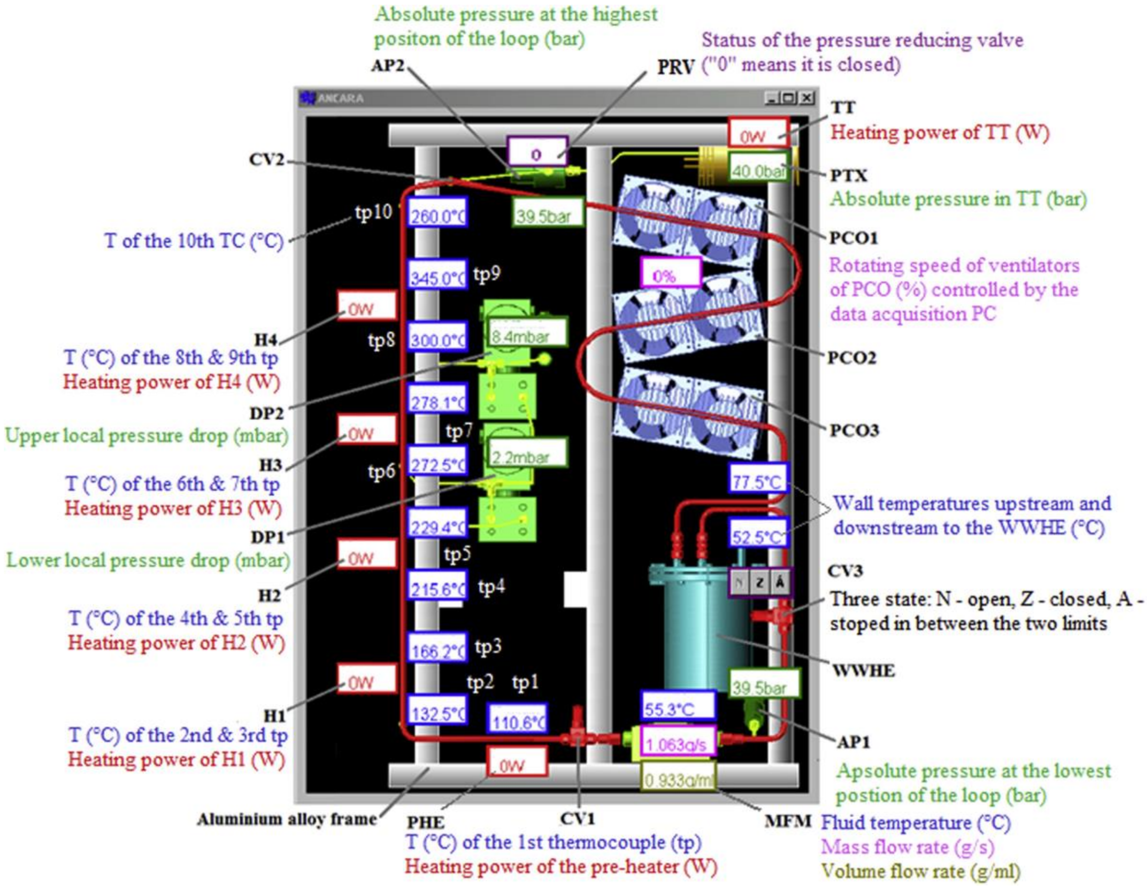

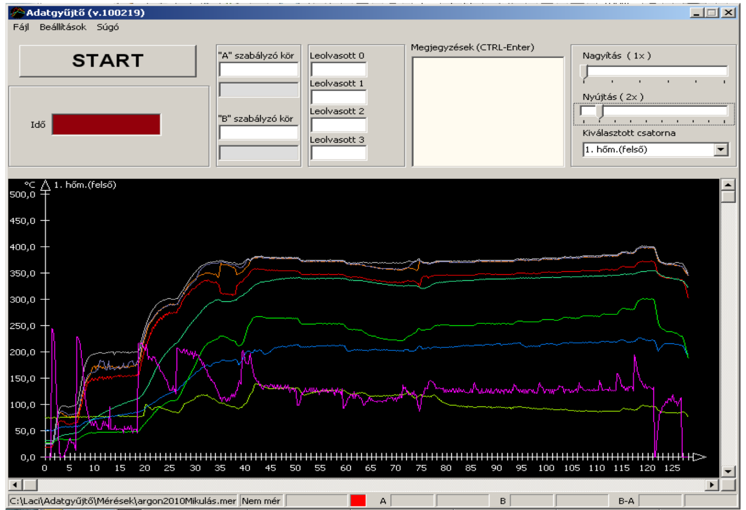

M. Balaskó, L. Horváth et al, Physics Procedia 43 (2013) 254 – 263

Attila Kiss, Márton Balaskó, László Horváth, Zoltán Kis, Attila Aszódi, Experimental investigation of the thermal hydraulics of supercritical water under natural circulation in a closed loop, Annals of Nuclear Energy, 100 (2) 2017, 178-203,DOI: 10.1016/j.anucene.2016.09.020.

Supercritical water @ RAD

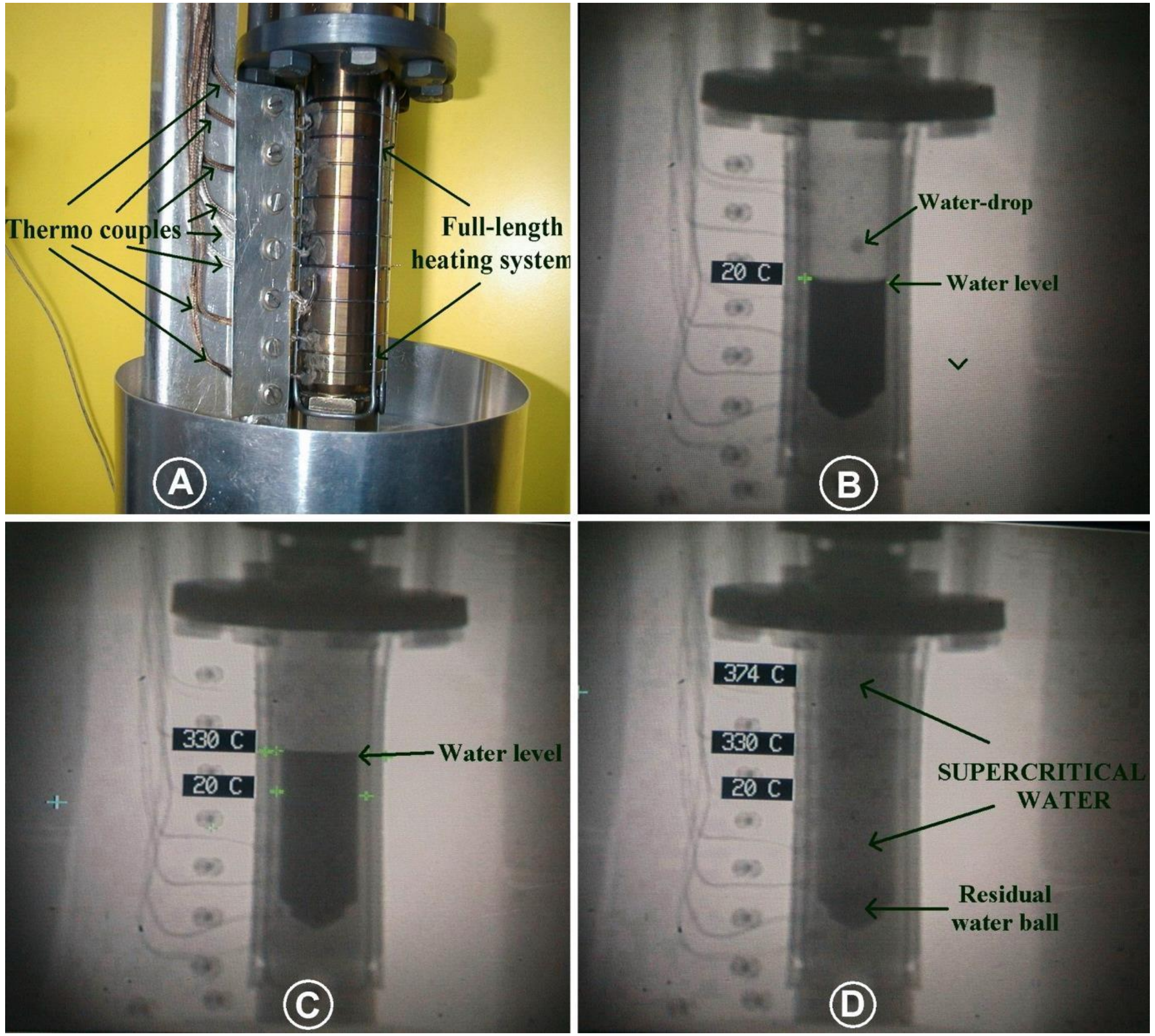

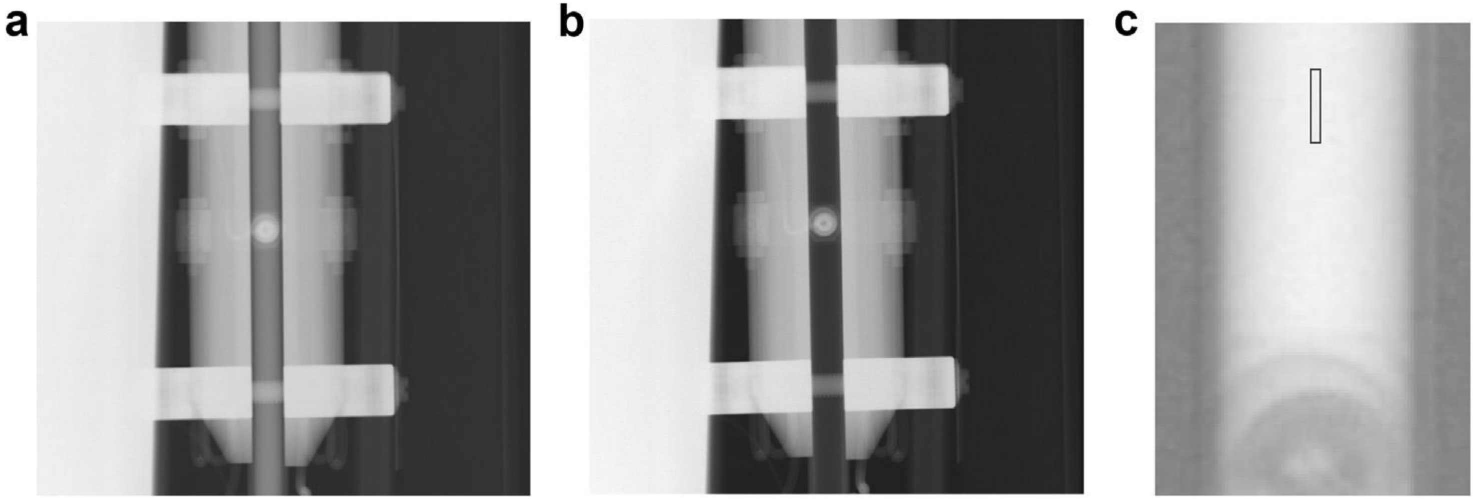

A. Kiss, Annals of Nuclear Energy 100 (2017) 178–203

Fuel cell in situ @ RAD

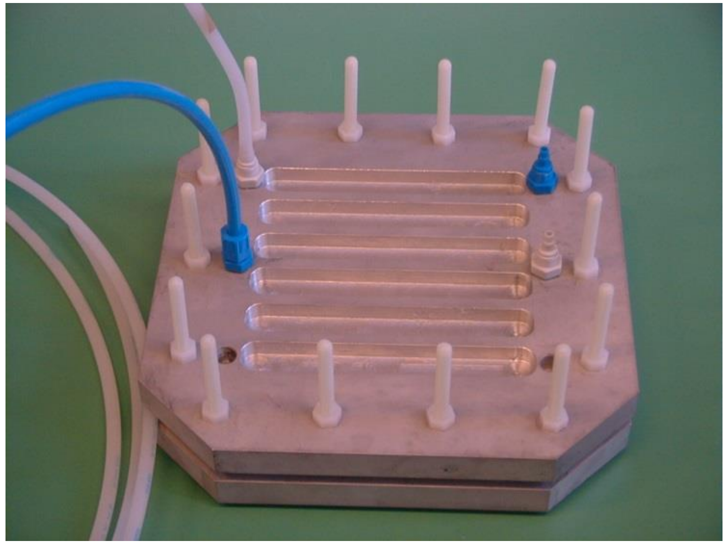

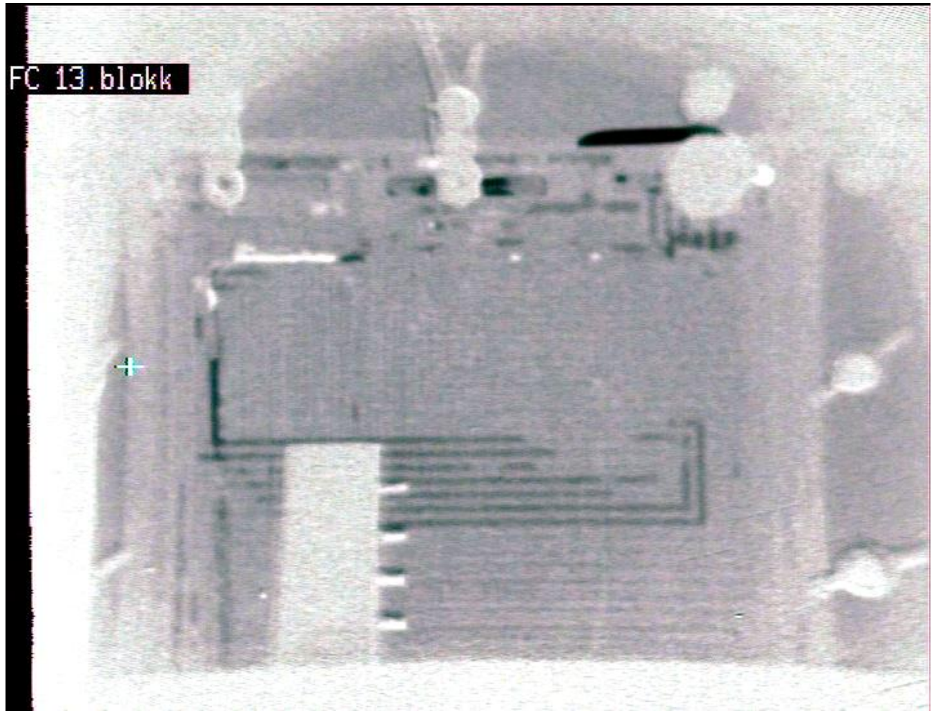

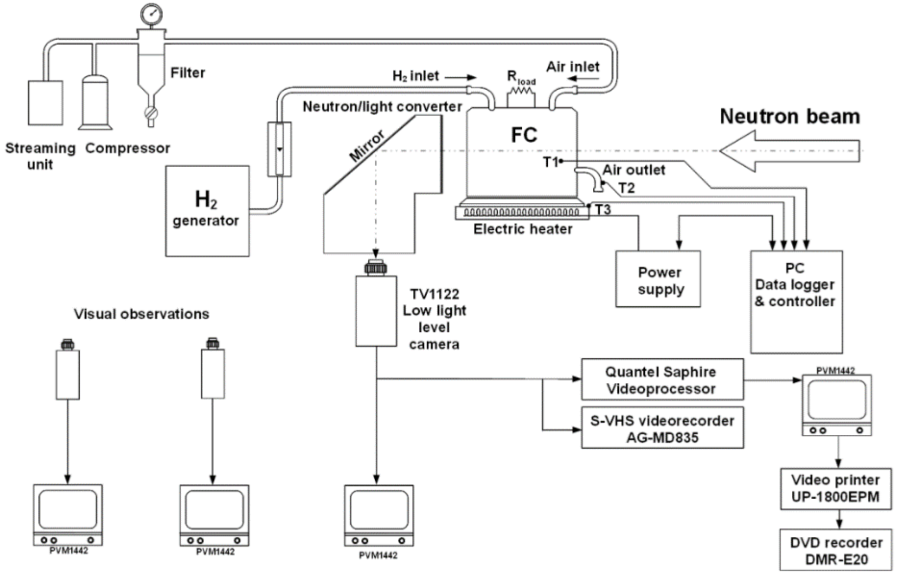

Gas formation during charge cycle of Li ion

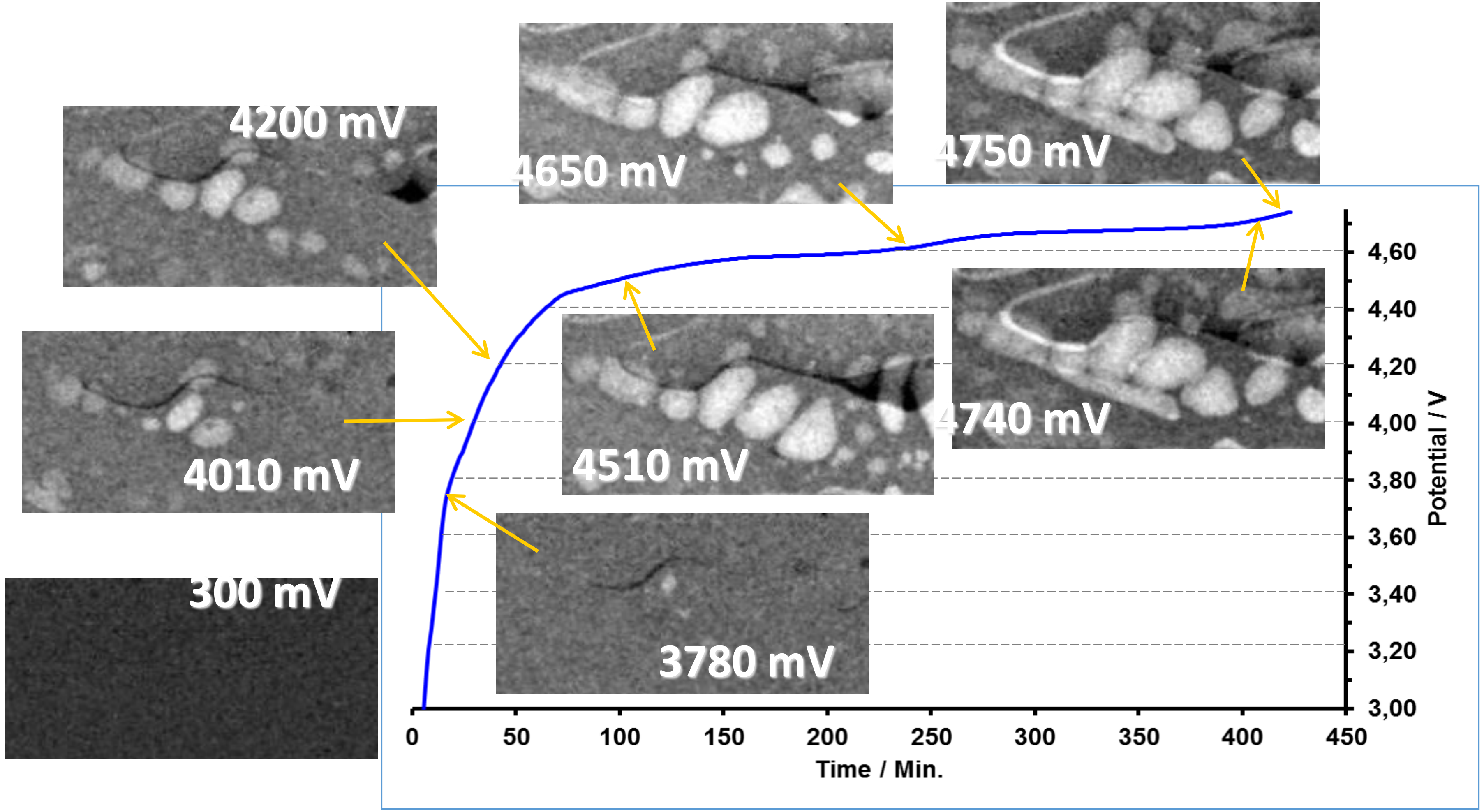

H. Sommer

Stroboscopic imaging – repetitive image acquisition

- The camera is triggered by an event in the process
- Many short time exposures accumulated per frame
- Cyclic processes can be faster than real-time imaging
- Different positions can be reached by delay

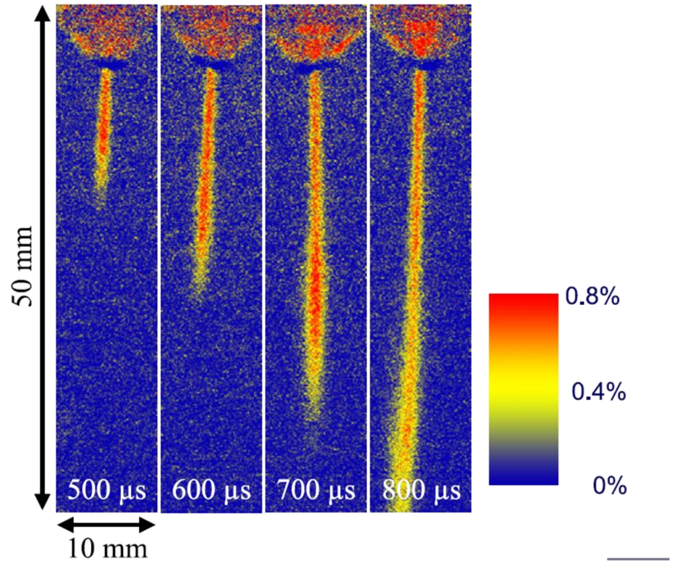

Common-rail diesel
injector nozzle

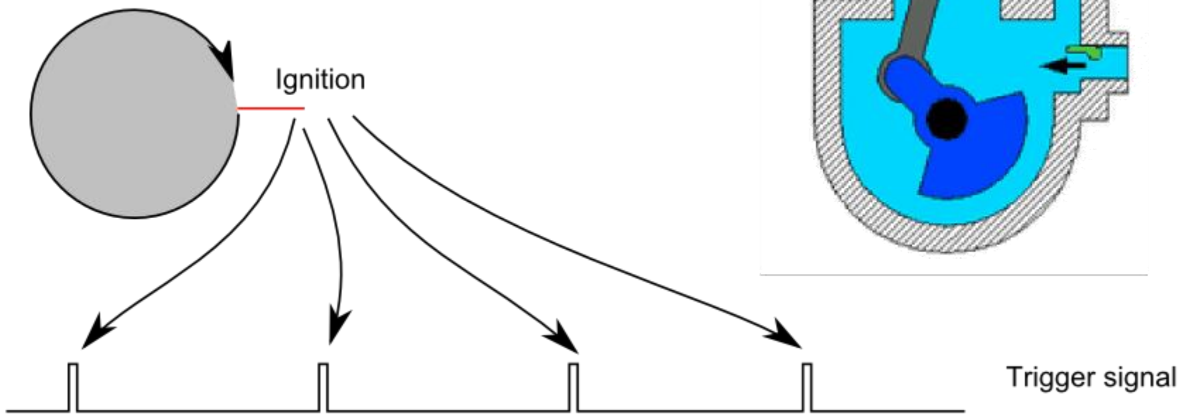

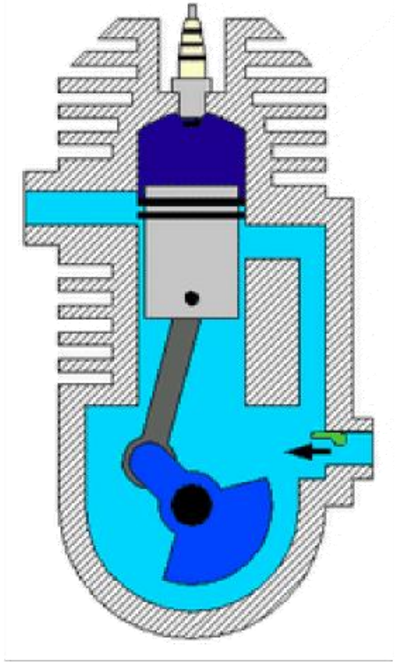

Centre for Energy Research

Chainsaw engine – movie @ ICON, PSI

Budapest Neutron Centre

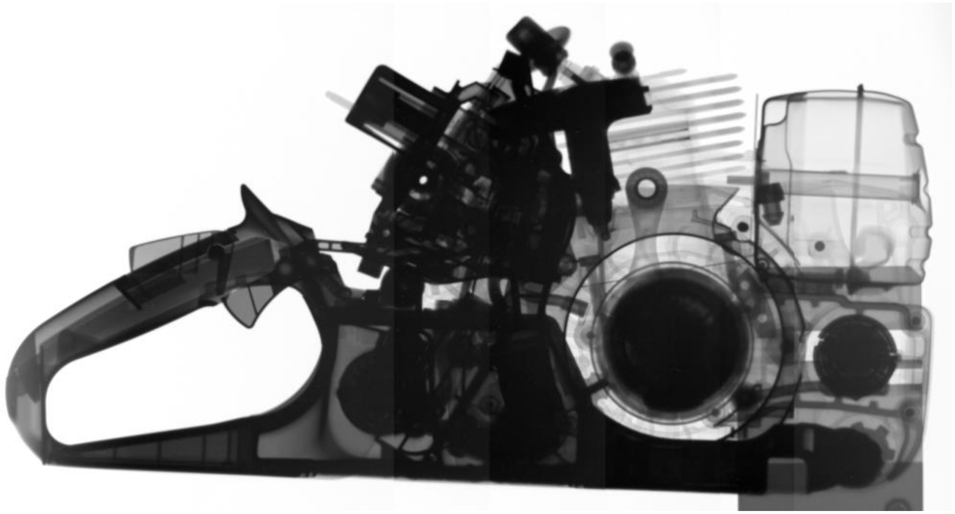

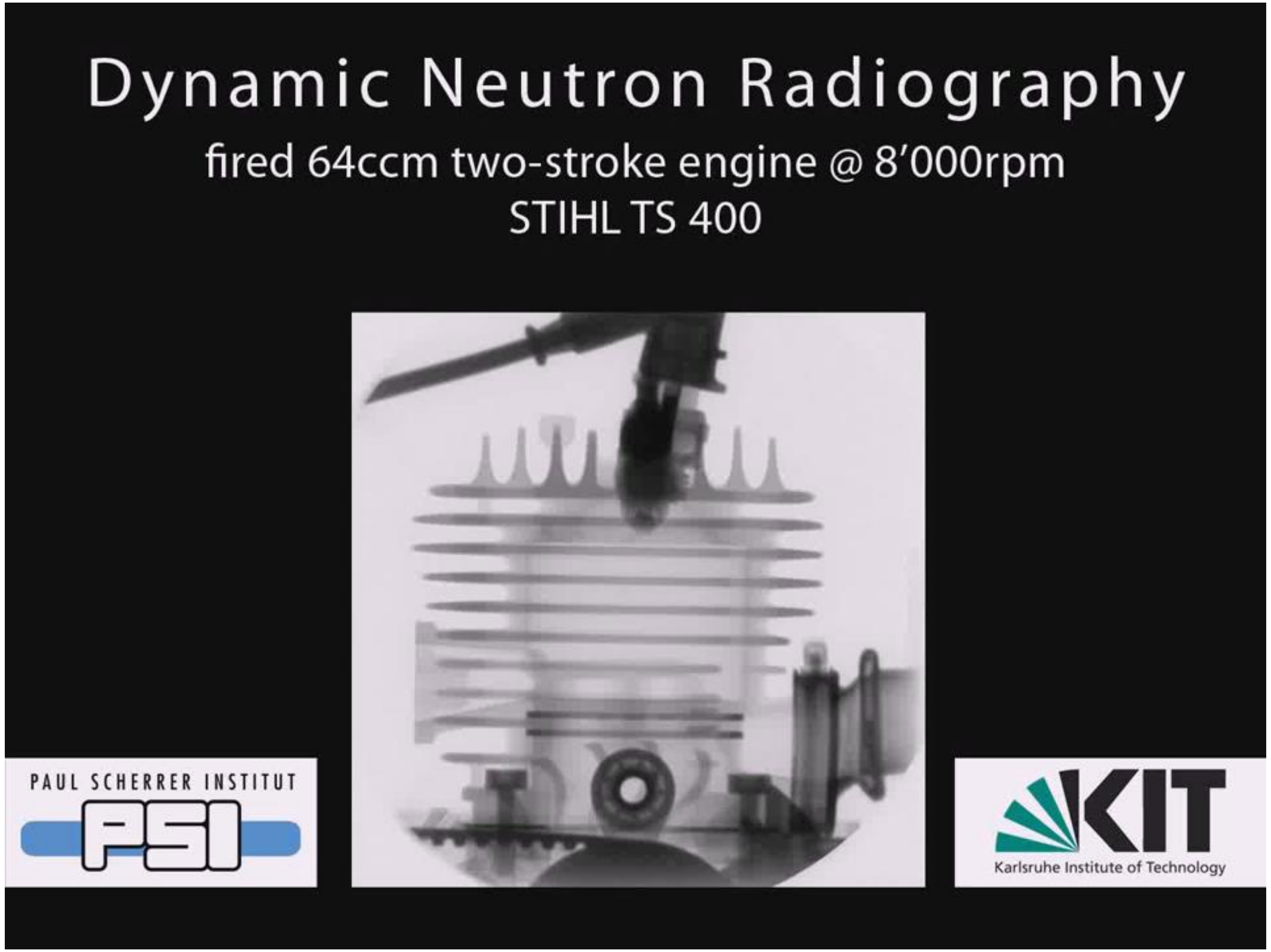

- Fired two-stoke engine running idle at 3000 RPM
- 40 frames created from 32 images each.
- 1 ms exposure time/frame

Energy-selective imaging

The contrast can be adjusted by selecting different wavelenghts

Photo **Neutrons** **Monochromatic Neutrons** **Polychromatic**

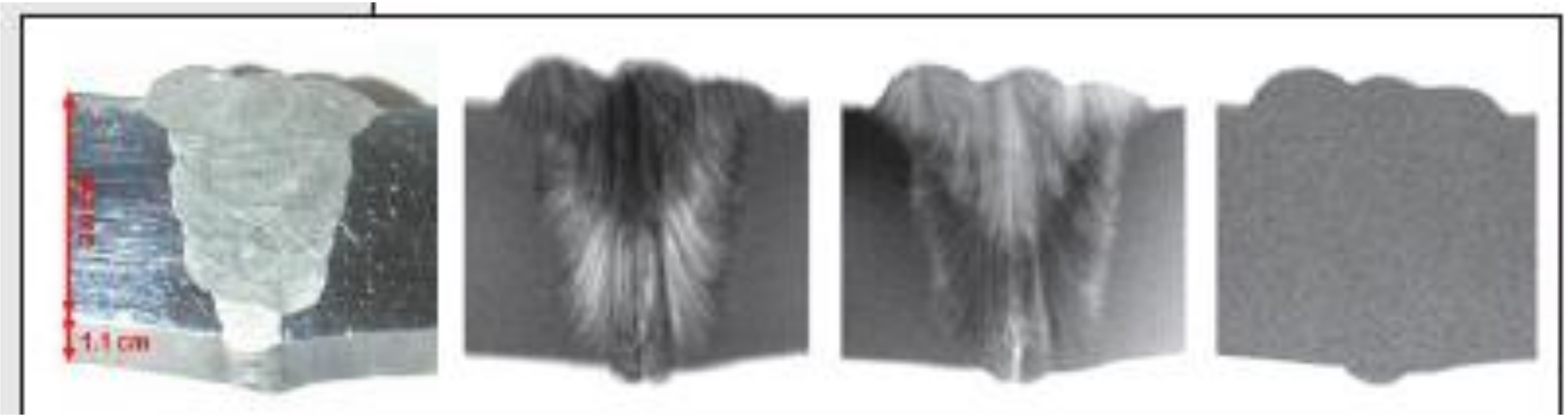

Phase contrast imaging

Neutrons act as waves; due to wave-particle dualism neutrons can also be described by matter waves with a certain wavelength.

In the case of the phase contrast method, one uses the fact that the waves which transverse an object have a different velocity to those which do not, and therefore have a different wavelength.

The resulting displacement of the wave maxima leads to a change of the propagation direction and therefore to an angular change.

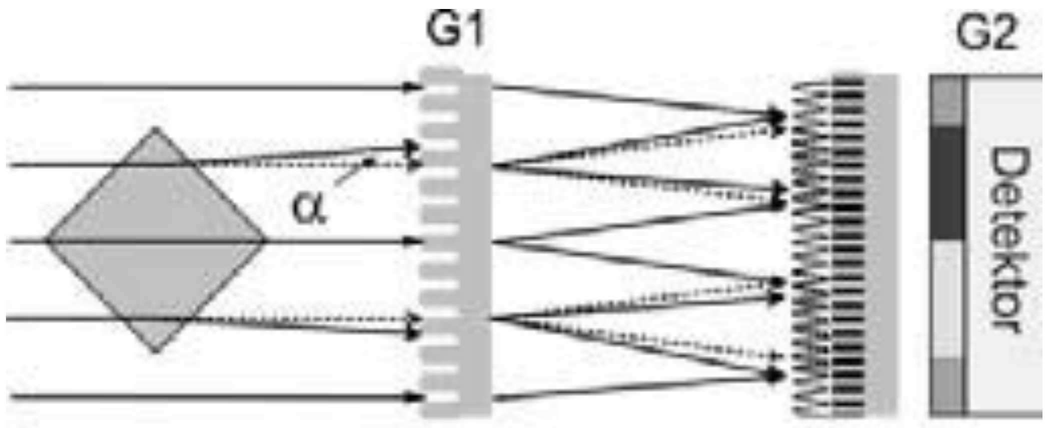

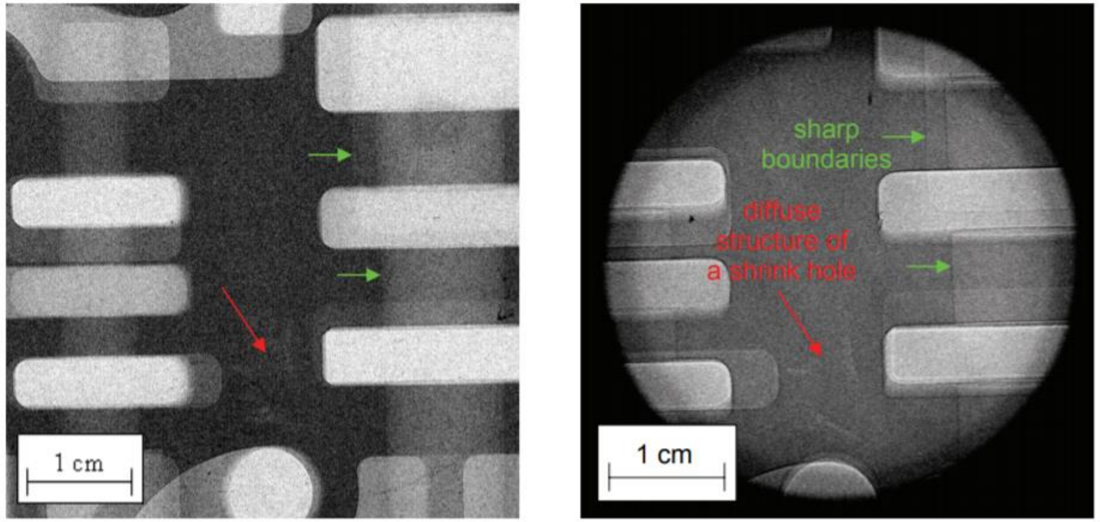

Fig. 3.9: Conventional (left) and phase contrast (right) radiography of a cast aluminum sample with shrink holes. Both radiographs were measured with an image plate that was read out with a pixel size of 50 μm. The exposure time for the absorption based radiograph was 30 s and for the phase contrast image 180 min. The position of sharp edges is much better visible with phase contrast (green arrows) but the visibility of shrink holes is not improved (red arrow).

Klaus Lorenz, FRM II

Imaging of magnetic field with polarized neutrons

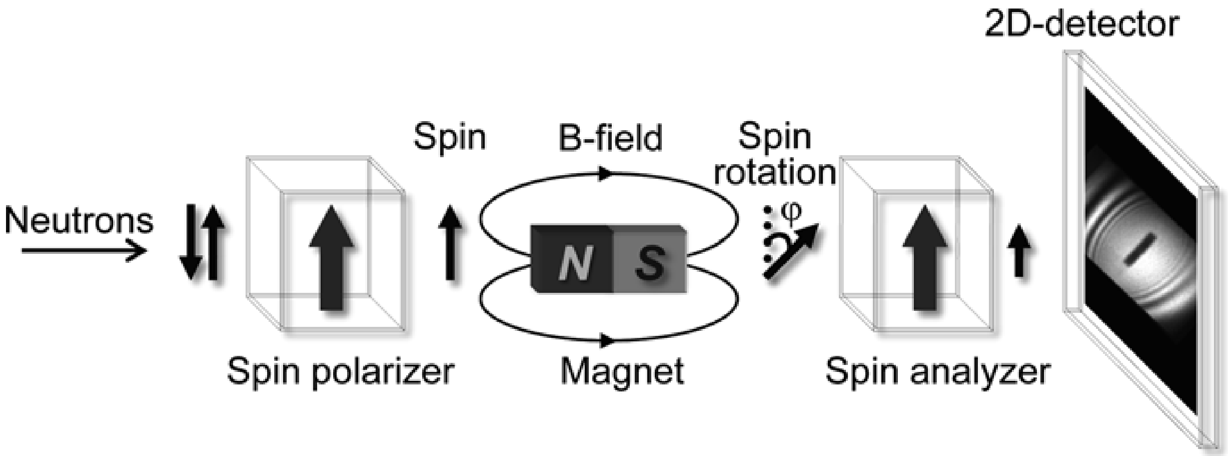

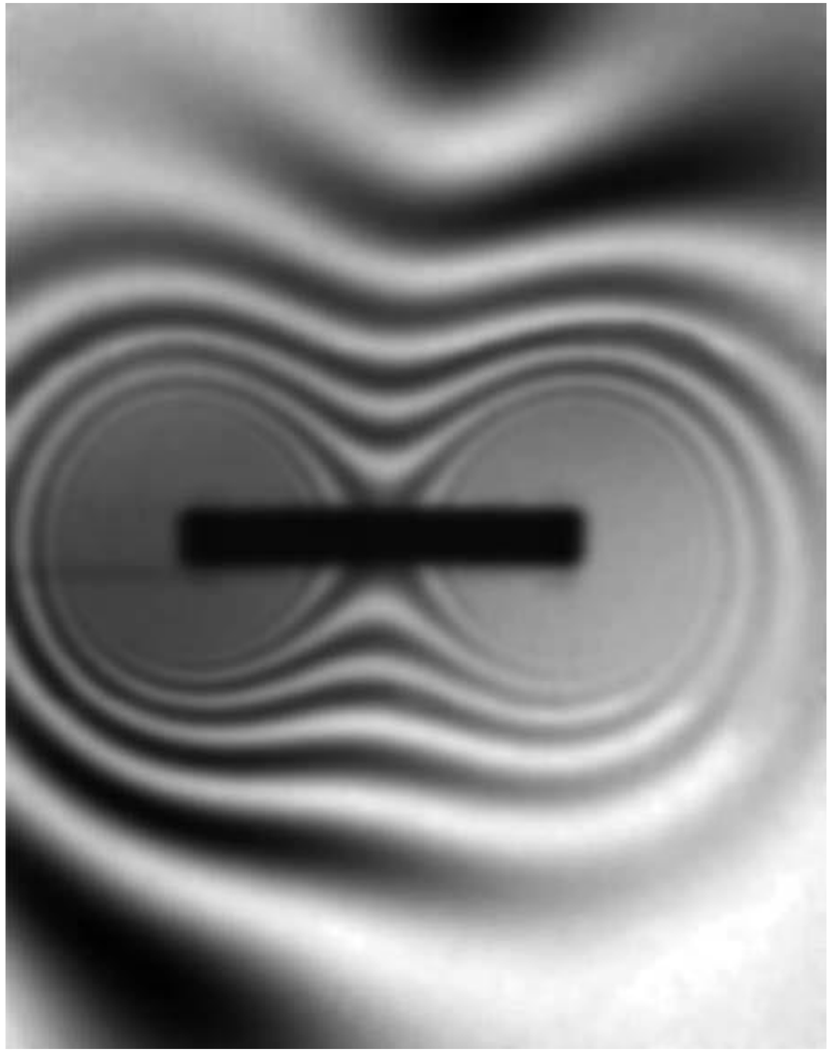

A radiograph showing the field lines surrounding a bar magnet. The magnetic field decreases in strength with distance from the magnet, resulting in a series of maxima and minima, where the beam polarization is sequentially parallel or antiparallel to the analyzer.

Very close to the magnets (where the field is strongest) the field lines are too close together to be spatially resolved
(N. Kardjilov)

Conclusions

- Neutron imaging is a popular and capable tool in nondestructive material testing
- 2D/3D Images with 10-200 μm resolution
- Contrast scatters substantially by elements
- User facilities operated at large neutron centres

- BNC: RAD and NORMA

Thank you for your attention!